



CZECH TECHNICAL UNIVERSITY IN PRAGUE

FACULTY OF MECHANICAL ENGINEERING

Dynamic analysis of satellite telescope front door

Diploma thesis

Study program: Aeronautics and Astronautics

Field of study: Aerospace Technology

Thesis supervisor: Ing. Jaromír Kučera

Bc. Matěj Stejskal

I. OSOBNÍ A STUDIJNÍ ÚDAJE

Příjmení: **Stejskal** Jméno: **Matěj** Osobní číslo: **419792**
Fakulta/ústav: **Fakulta strojní**
Zadávací katedra/ústav: **Ústav letadlové techniky**
Studijní program: **Letectví a kosmonautika**
Studijní obor: **Letadlová a kosmická technika**

II. ÚDAJE K DIPLOMOVÉ PRÁCI

Název diplomové práce:

Dynamická analýza dvířek dalekohledu družice

Název diplomové práce anglicky:

Dynamic analysis of satellite telescope front door

Pokyny pro vypracování:

- Pro vypracování proveďte následující:
- 1) popis mise, funkce zařízení, popis designu
 - 2) tvorba a popis MKP modelu
 - 3) vibrační zkoušky vývojového modelu
 - 4) experimentální modální analýza vybraných uzlů vývojového modelu
 - 5) ladění parametrů MKP modelu na experimentální data
 - 6) statická a dynamická analýza MKP modelu
 - 7) výpočet únosnosti konstrukce dvířek na základě výsledků analýz
 - 8) výpočet únosnosti šroubových spojů na základě výsledků analýz

Seznam doporučené literatury:

Dle pokynů vědouceho

Jméno a pracoviště vedoucí(ho) diplomové práce:

Ing. Jaromír Kučera, ústav letadlové techniky FS


Jméno a pracoviště druhé(ho) vedoucí(ho) nebo konzultanta(ky) diplomové práce:


Datum zadání diplomové práce: **30.04.2019**

Termín odevzdání diplomové práce: **02.08.2019**

Platnost zadání diplomové práce:



Ing. Jaromír Kučera
podpis vedoucí(ho) práce



Ing. Robert Theiner, Ph.D.
podpis vedoucí(ho) ústavu/katedry


prof. Ing. Michael Valášek, DrSc.
podpis děkana(ky)

III. PŘEVZETÍ ZADÁNÍ

Diplomant bere na vědomí, že je povinen vypracovat diplomovou práci samostatně, bez cizí pomoci, s výjimkou poskytnutých konzultací. Seznam použité literatury, jiných pramenů a jmen konzultantů je třeba uvést v diplomové práci.


Datum převzetí zadání


Podpis studenta

Declaration

I declare that I completed this thesis titled "Dynamic analysis of satellite front door" by myself with supervision of Ing. Jaromír Kučera and with help of literature, which is listed at the end of this thesis.

September 6th 2019, Prague

Bc. Matěj Stejskal

Acknowledgment

I would like to thank Ing. Jaromír Kučera for very good and helpful supervision of my work. I would also like to thank all of the professors who taught me during my studies since without the knowledge they provided I would not be able to complete this thesis. Last but not least I would like to thank my family and friends for their support.

Abstract

Author:	<i>Bc. Matěj Stejskal</i>
Title (CZ):	Dynamická analýza dvířek dalekohledu družice
Title:	Dynamic analysis of satellite telescope front door
Year:	2019
Study program:	Aeronautics and Astronautics
Field of study:	Aerospace Technology
Department:	Department of Aerospace Engineering
Supervisor:	Ing. Jaromír Kučera
Consultant:	Ing. Jaromír Kučera
Bibliographic data:	pages: 86 figures 40 tables 22 appendixes 6
Keywords (CZ):	satelit, družice, koronograf, dvířka, mechanismus, analýza
Keywords:	satellite, coronagraph, spacecraft, structure, mechanism, mechanical, analysis
Abstract (CZ):	Práce se zabývá mechanickou analýzou sestavy Front Door Assembly (FDA), která je součástí kosmické mise PROBA-3. FDA slouží jako dvířka dalekohledu koronografu, který je součástí jedné z družic mise PROBA-3. Analýza se skládá z tvorby MKP modelu, vibračního testování fyzického návrhového modelu, ladění MKP modelu, mechanické analýzy v podobě mnoha MKP simulací a vyhodnocení namáhání dílů a spojů.
Abstract:	The thesis deals with mechanical analysis of a satellite Front Door Assembly (FDA) for PROBA-3 mission. The FDA serves as a door for a coronagraph telescope which is part of one of the PROBA-3 spacecraft. The analysis consist of creation of a FEM model, vibration testing of a physical design model, correlation of the FEM model, mechanical analysis in form of various simulations and evaluation of the loading of the parts and fasteners.

Table of contents

1	INTRODUCTION	5
2	MISSION DESCRIPTION	6
2.1	Formation flying.....	6
2.2	Payload.....	7
2.3	Front Door Assembly.....	9
2.4	Mission profile	9
3	THE PROCEDURE.....	11
3.1	FEM model creation	12
3.2	Preliminary simulations and testing.....	12
3.3	Vibration testing.....	13
3.4	Tuning.....	13
3.5	Coupled analysis	13
3.6	Full simulation	13
4	DESIGN DESCRIPTION.....	14
4.1	Design requirements	14
4.2	FDA design	15
4.3	FDA configurations.....	15
4.4	Materials	16
4.5	Parts and subassemblies description.....	17
5	FEM DESCRIPTION.....	23
5.1	Coordinate system.....	23
5.2	Mesh	24
5.3	Concentrated masses.....	25
5.4	Material properties.....	25
5.5	Modal and Random model.....	26
5.6	Screws	27
5.7	Lid Shaft.....	28
5.8	Pin-puller.....	29
5.9	Touch screw.....	29
5.10	Lid nose	30
5.11	Flange-Tube connection.....	31
5.12	FEM checks	31
6	PRELIMINARY SIMULATION.....	33
6.1	Tightening torques.....	33
7	LID PRELOAD.....	35
7.1	Preload calculation	35
7.2	Preload application and measurement.....	36

8	VIBRATION TESTING	38
8.1	Setup	38
8.2	Accelerometers	39
8.3	Test plan	39
8.4	Settling.....	40
8.5	The testing.....	41
8.6	Key failure.....	47
8.7	Results.....	48
8.8	Conclusion	48
9	EXPERIMENTAL MODAL ANALYSIS.....	49
9.1	Test setup	49
9.2	Measurements	50
10	FEM MODEL TUNING.....	54
10.1	Locations	54
10.2	Parameters	56
10.3	Method.....	57
10.4	The procedure and simplifications	58
10.5	Results.....	59
11	MECHANICAL ANALYSIS.....	60
11.1	Modal analysis	60
11.2	Random simulation.....	63
11.3	Quasi-static simulation	66
11.4	Static simulation	67
11.5	Stress evaluation.....	67
11.6	Screw forces evaluation	68
12	THREADED FASTENERS.....	69
12.1	Loads.....	69
12.2	Calculation	70
12.3	Results.....	78
13	CONCLUSION	80
	LITERATURE	81
	SYMBOLS	82
	ABBREVIATIONS.....	84
	FIGURES	85
	APPENDIXES.....	86



1 Introduction

The goal of this thesis is to describe a process of a mechanical analysis of a satellite's subassembly called Front Door Assembly (FDA), which is part of the PROBA-3 mission.

The PROBA-3 mission will launch two separate satellites, which will fly in a formation with a very high precision creating almost a kind of rigid structure in orbit. The mission will mainly serve as a formation flying technology demonstration, preparing the space industry for the use of formation flying in the future. The second purpose of the mission is an observation of the Sun with a large coronagraph. One of the satellites will be an occulter, creating a shadow for the second satellite carrying the coronagraph telescope.

The FDA serves as a door on the coronagraph telescope. It will protect the optics from particles and light on the ground as well as in the orbit, where it will be able to open and close repeatedly and therefore cover and uncover the telescope as desired.

The mechanical analysis of a spacecraft structure is a very complex process and especially when it is a mechanism like the FDA. The main goal of such analysis is to prove that the design is capable to withstand the severe vibrations that occur during the launch of the satellite.

This thesis goes through that process by describing creation of a FEM model, vibration testing of a physical design model, correlation of the FEM model, mechanical analysis in form of various simulations and finally evaluation of the loading of the parts and fasteners.



2 Mission description

The PROBA-3 (Project for On-Board Autonomy-3) mission is mainly devoted to the in-orbit demonstration of precise formation flying techniques and technologies for future ESA missions. Two satellites will fly in a precise configuration forming a “large rigid structure” in orbit to prove formation flying technologies. The mission will also serve as qualification for the equipment used onboard the formation flying satellites and the technology will be demonstrated to TRL 9 (Technology Readiness Level 9). The development, design, implementation and validation principles for formation flying will continue to be established for future formation flying missions. In addition to technology demonstration, the mission will carry a scientific payload in form of solar coronagraph instrument.

2.1 Formation flying

There are two different approaches for control of the configuration. First one is Ground-based control in which the GNSS (Global Navigation Satellite System) data are sent to the ground control center that will command the satellites to adjust their attitude and position in the formation. Ground-based control is used for configuration with distance between the satellites in order of kilometers and with intervals between the adjustment maneuvers ranging from weeks to months.

The second approach of control and the one actually used in PROBA-3 mission is Autonomous formation flying in which the satellites communicate with each other, broadcasting the data about their relative positions and using the Attitude and Orbit Control System (ACOS) to maneuver into the adequate configuration. This approach is applicable for formations with smaller distances between the satellites that require autonomous and more frequent adjustment of orientation and position.

There are three types of formations:

a) Trailing – In this formation all the satellites share the same orbit and follow each other at a certain distance. This type is used in the PROBA-3 mission.

b) Clusters – The satellites fly close to each other on different orbits and those orbits are defined in a specific way so the satellites remain in a cluster

c) Constellation – Is a formation which provides coverage of the entire Earth. The satellites fly on many different orbits and there is a certain number of satellites on each orbit. Both the orbits and the number of satellites on them is designed to achieve the coverage of the entire Earth. The best example of constellation is GPS.

2.2 Payload

PROBA-3 will fly ASPIICS (Association of Spacecraft for Polarimetric and Imaging Investigation of the Corona of the Sun) as the primary payload, which uses the formation flying to form a very big coronagraph capable of producing a nearly perfect eclipse allowing to observe the corona closer to the rim than ever before.

Flying first in the formation is the Occulter Spacecraft (OSC) which is about 200kg and its main function is to block the sun and create an artificial eclipse for the other satellite. It achieves that with a 1400mm occulting disc facing away from the Sun.

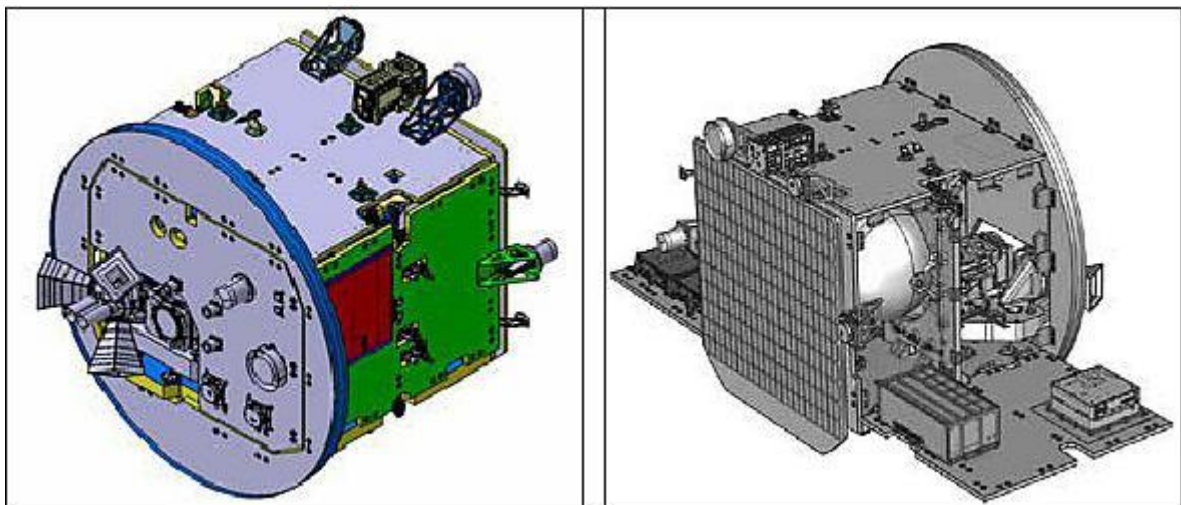


Figure 2.1 – External (left) and internal (right) view of Occulter Spacecraft [1]

The second satellite is the Coronagraph Spacecraft (CSC) and will fly approximately 150m behind the Occulter Spacecraft and is about 340kg. It will carry a telescope pointing directly at the Occulter Spacecraft and observe the corona of the Sun. Most of the formation flying systems will be on this satellite and it will be responsible for majority of the maneuvers.

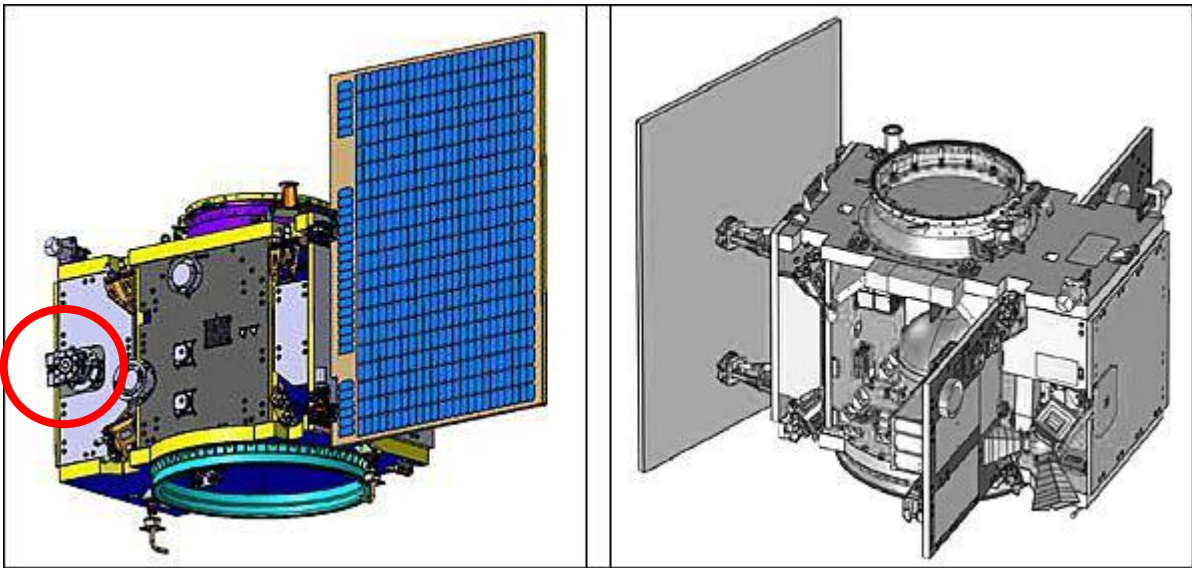


Figure 2.2 - External (left) and internal (right) view of Coronagraph Spacecraft [1]

Thanks to this configuration the Coronagraph system (ASPIICS) will be the first coronagraph to cover the range of radial distances between 1.08 and 3 solar radii and thus providing observation conditions close to those during a total solar eclipse and without effects of the Earth's atmosphere. This will provide more understanding of processes in the solar corona, processes leading to coronal mass ejections and space weather.

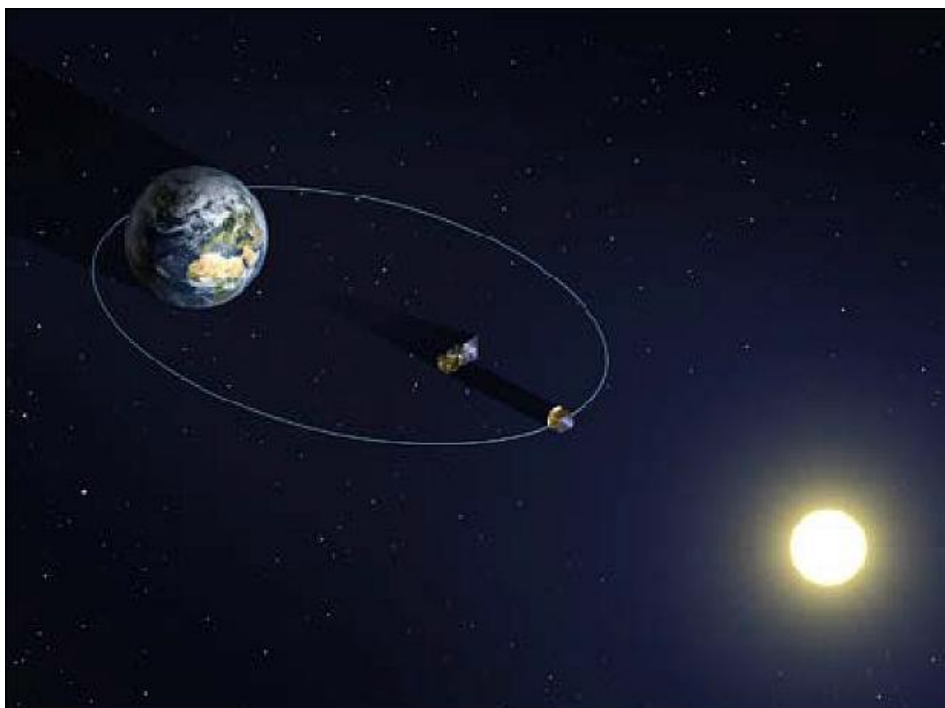


Figure 2.3 - Illustration of the PROBA-3 mission [1]



2.3 Front Door Assembly

The Front Door Assembly (FDA) which is the main subject of this thesis is a subsystem of the Coronagraph system which is designed to protect the telescope optics from contamination on the ground and during launch. It will be able to open and close in orbit, so it can also protect the optics from contamination during some flight operations and protect the internal parts of coronagraph from thermal loads. The position of the FDA on the Coronagraph Spacecraft is marked with a red circle in Figure 2.2.

2.4 Mission profile

The PROBA-3 mission consists of three main phases which are shortly described below.

2.4.1 a) Launch and Early Orbit Phase (LEOP) – 2 days

The mission begins with the two satellites being launched together with the OSC mounted on top of CSC. This configuration is called STACK. After STACK separates from the launcher it will perform maneuvers to stabilize itself and when it is stable the CSC solar panel will deploy. After this deployment the STACK will maneuver again to gain desired attitude relative to the Sun, stabilize again and begin commissioning of certain systems. Some actions in this phase are guided from the ground.

2.4.2 b) Commissioning – 2 months

In the next phase, the STACK gets separated and both CSC and OSC start flying independently. The separation of the satellites leaves them with some relative drift. Maneuvers computed on the ground are then performed to stop the drift and put the satellites on the safe relative orbit. In this safe relative orbit, the satellites are less than 1km apart and without the need to be controlled while still remaining in a safe configuration. In this configuration, some actions will be commanded from the ground while commissioning of systems and preliminary calibration of alignment will be performed.

2.4.3 c) Nominal Operations – about 22 months

After commissioning of all systems, the satellites will enter the main operation phase which is the Formation Flying Phase and the satellites become completely autonomous. In this phase, the coronagraph observations are performed and so are the rigid formation demonstration maneuvers. These operations are only performed in the apogee (60 530km) since the formation cannot be maintained during the perigee (600km) passage because the relative dynamic perturbations are very high in the perigee and maintaining of the formation would be very fuel inefficient. The data transfer takes place during the perigee passage. The orbital period is 19,7 hours and the rigid formation is maintained for 6 hours in the apogee arc. At the end of this phase, PROBA-3 will be decommissioned and waiting for its passive re-entry to the Earth's atmosphere.

The nominal orbit during this phase may be seen in Figure 2.4 along with some of the requirements for the relative positioning of the OSC and CSC.

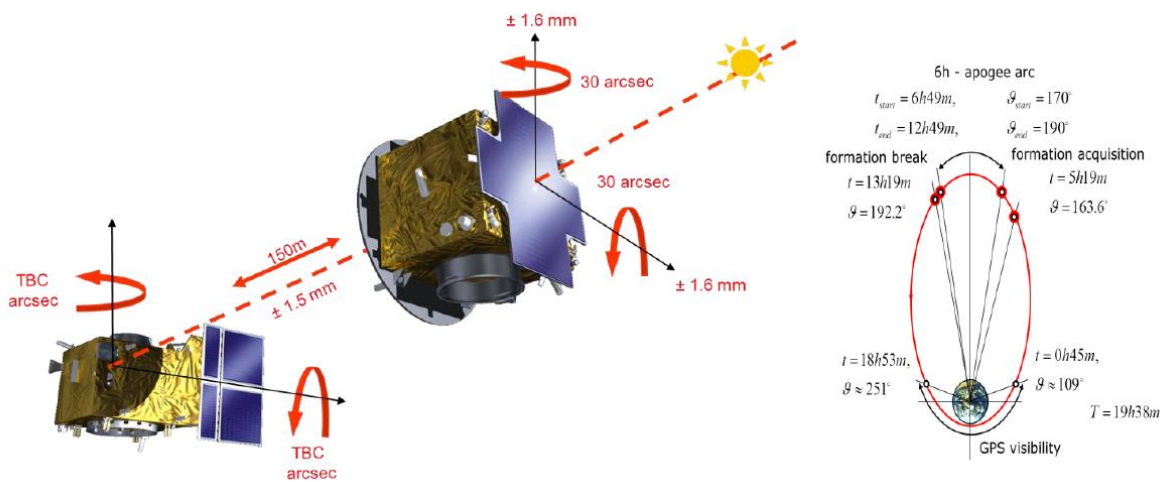


Figure 2.4 - Formation requirements (left) and nominal orbit (right) [1]

3 The procedure

The mechanical analysis of the Front Door Assembly (FDA) is a very complex and iterative process. At the beginning of the procedure, is a mechanical Design Model (DM) and the first approximation of the loading spectra. In the end, is a fully analyzed Flight Model (FM). There are many steps and loops between those stages as shown in Figure 3.1. Those loops make the process highly iterative which could be very time consuming and it is up to the management of the project to decide how many iterations should be done and how accurate should the models and the computations be. Not all the iterations will be covered in this thesis since there was a lot of design iterations and changes based of various reasons, discussions, and computations. The whole procedure is shortly summarized in this chapter.

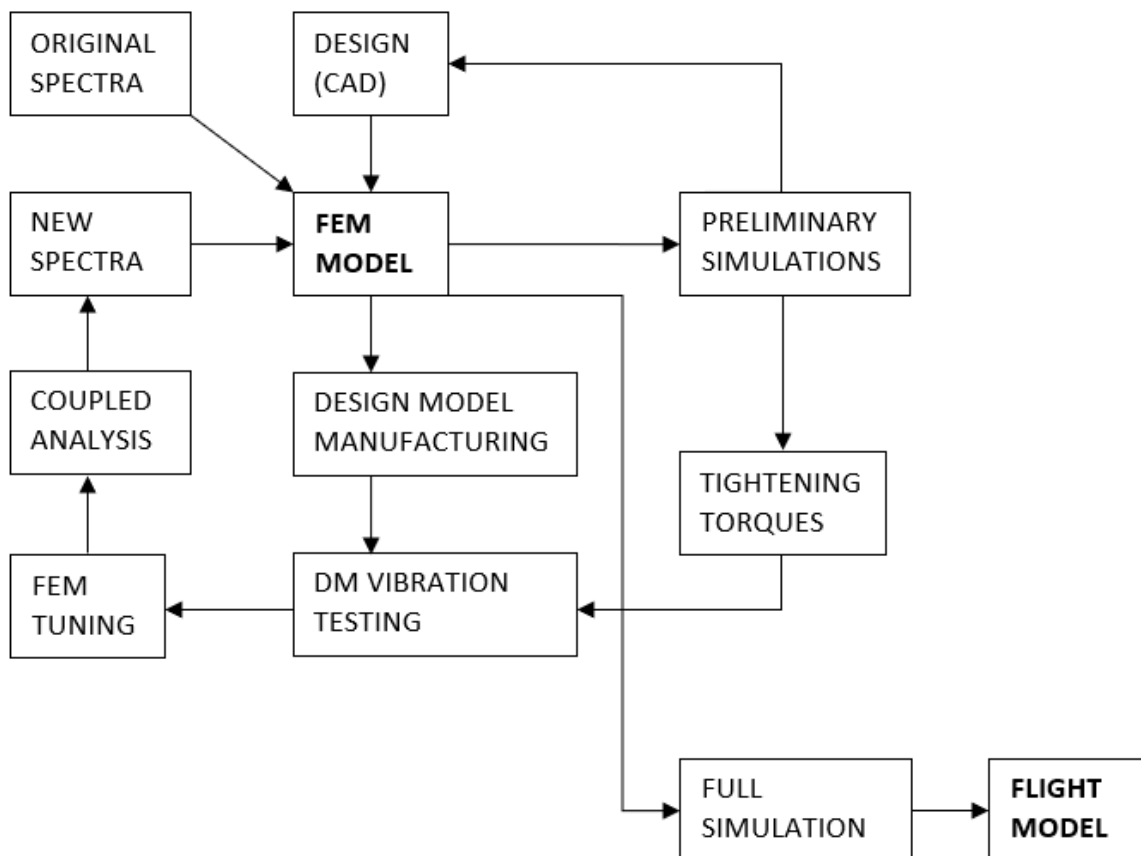


Figure 3.1 - FDA mechanical analysis flowchart



3.1 FEM model creation

As mentioned before the procedure begins with the DM CAD model provided by the designer and made based on previous iterations, testing, and calculations. Some preliminary calculations show that this design should be very close to the final one.

The first step is the creation of the FEM model as described in Chapter 5. There will be two different versions of this model. One for modal analysis and tuning and one for the external loads analysis. Differences between those models are also described in Chapter 5. Material and physical properties such as Young's modulus or density are based of the design. The stiffnesses of the bolted joints are calculated based on the properties of the real screws:

$$k = \frac{A E}{l} \left[\frac{N}{mm} \right] \quad (3-1)$$

Where A is the minimal cross-section of the screw, E is the Young's modulus of the screw's material, l is the effective length and k is the tensile stiffness of the screw. These stiffnesses will be the main subject of the FEM model tuning.

3.2 Preliminary simulations and testing

Before the very time-consuming tuning process and manufacturing of the physical DM begins, some preliminary simulations are run on the FEM model. Resonance search is performed to find if the first natural frequency of the assembly is high enough and preliminary random simulation is performed using the original random loading spectra provided by the contractor based on the preliminary coupled analysis. If the results of the preliminary simulations are not satisfactory the design needs to be changed before further actions are made.

If the design shows acceptable results the parts are manufactured and the physical DM is assembled. The tightening torques for the bolted joints are needed for the assembly. Those are calculated as shown in Chapter 12 with forces evaluated from above described preliminary random simulation done in Chapter 6.



3.3 Vibration testing

The vibration testing of the DM is then performed including resonance search and random vibrations. Results from resonance search are used for tuning the FEM and random responses show if the physical model is able to withstand the loads. This step is described in Chapter 8.

3.4 Tuning

The very long process of tuning the FEM model begins after the vibration testing. The tuned parameters are mainly the stiffnesses of the bolted joints and also Young's moduli. Dozens of tuned parameters and long computation time makes the process very time-consuming and not suitable for automatization. More about this process may be found in Chapter 10.

3.5 Coupled analysis

After the FEM model is tuned to an acceptable quality it is sent to the contractor for new coupled analysis which gives new random loading spectra. Coupled analysis is basically a random vibration simulation of the whole satellite with the tuned FDA FEM model attached. The input spectra for the coupled analysis are obtained from the launcher manual and the output is the new random spectra at the FDA interface which are then used for the full simulation.

3.6 Full simulation

The new spectra are applied to the FEM model and critical locations responses are evaluated. If the responses show insufficient design the whole process or parts of it may be repeated. Otherwise, the complete computation of the FEM model may be performed and if all calculations show positive margins of safety the Qualification and later Flight Model may be manufactured. The full simulation is described in Chapter 11.



4 Design description

The final design of the FDA was achieved based on requirements provided by the contractor as well as it was derived from previous designs which were usually unsuccessfully vibration tested or insufficient in some other way. The design process was very long and difficult, took many years and is not a topic of this thesis. The computations done in this thesis are considering the final design (with some minor changes during the testing), which is described in the following paragraphs. Design of electrical parts and circuits will not be covered since these have very small impact on the computations and are not a topic of this thesis.

4.1 Design requirements

Some of the most important requirements are described in Table 4.1. These are critical for understanding why is the FDA designed in the way it is and what are the functions of this subsystem.

Table 4.1 – Important requirements

Req. number	Requirement text
R-3102	The FDA should consist of: mounting flange, hinge system, lid, motor, position sensors, locking device, filters - High Density Diffuser (HDD) and Shadow Position Sensor (SPS)
R-4100	The FDA should have three stable positions: locked, open, closed
R-4102	At any time the FDA can be in the following states: locked, open, close, moving to open/close
R-4200	The FDA shall protect the coronagraph optics from light and dust during on-ground activities, launch, early orbit and during operation when the coronagraph is not in use
R-4202	The FDA shall be closable and re-openable in flight
R-4208	The FDA shall be equipped with filters (HDD, SPS) mounted on the lid to be used: -for in-flight photometric calibration -for instrument health checks on ground
R-4512	The FDA shall provide analog measurements of closed/open position status
R-5100	The FDA shall be mounted on the front flange of the Coronagraph Optical Box – onto the Tube
R-5102	The FDA external dimensions, in launch configuration, shall not exceed the defined envelope
R-5200	The FDA overall mass, in launch configuration, shall not exceed 1,5kg
R-6102	The FDA, in open position, shall be outside the field of view of the coronagraph
R-6202	The FDA shall be bolted to the Tube with 8 x M4 bolts

4.2 FDA design

The design of the FDA may be seen in Figure 4.1 with the main subassemblies and parts denoted. The subassemblies are: Flange, Lid assembly, Shaft assembly, Motor assembly, Connector assembly, and Locking device (Pin-puller). Those subassemblies will be described below. FDA has a total mass of 1.2kg with external dimensions of 231x176x47mm.

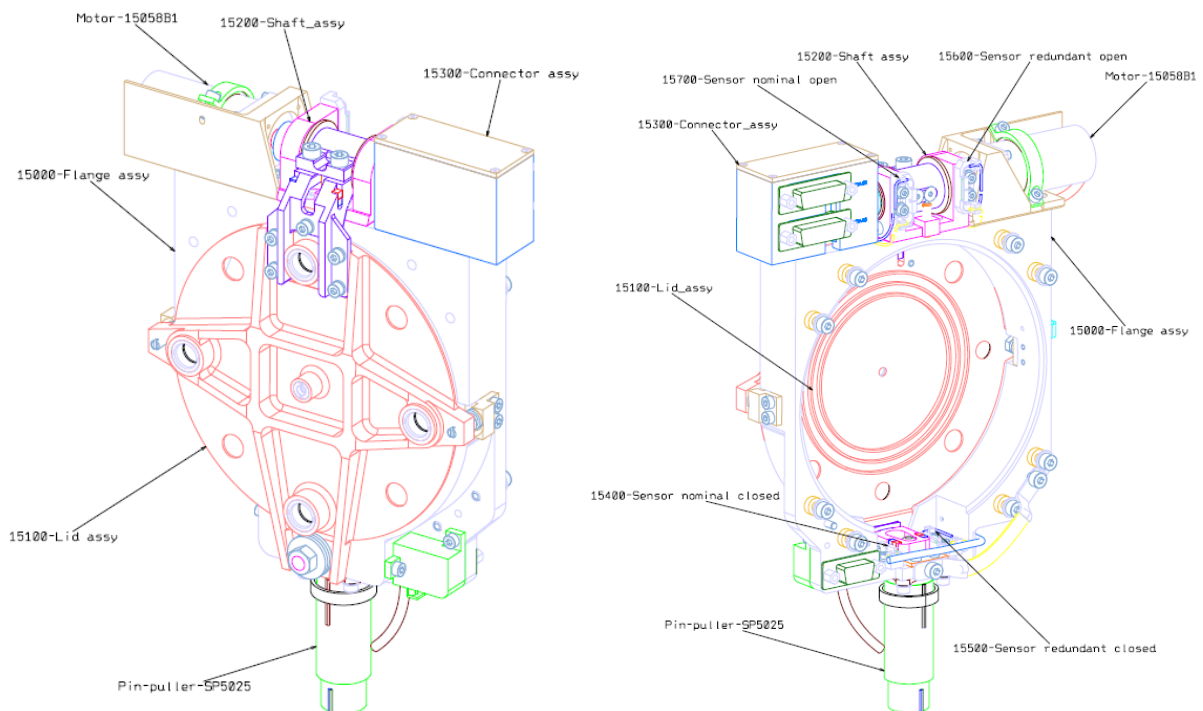


Figure 4.1 - FDA design

4.3 FDA configurations

The FDA may be found in three configurations shown in Figure 4.2 as described in requirement R-4100. The locked and the closed position protects the coronagraph optics during on-ground activities, launch and some in-flight operations as described in requirement R-4200. The unit is in the open position when the coronagraph is in operation.

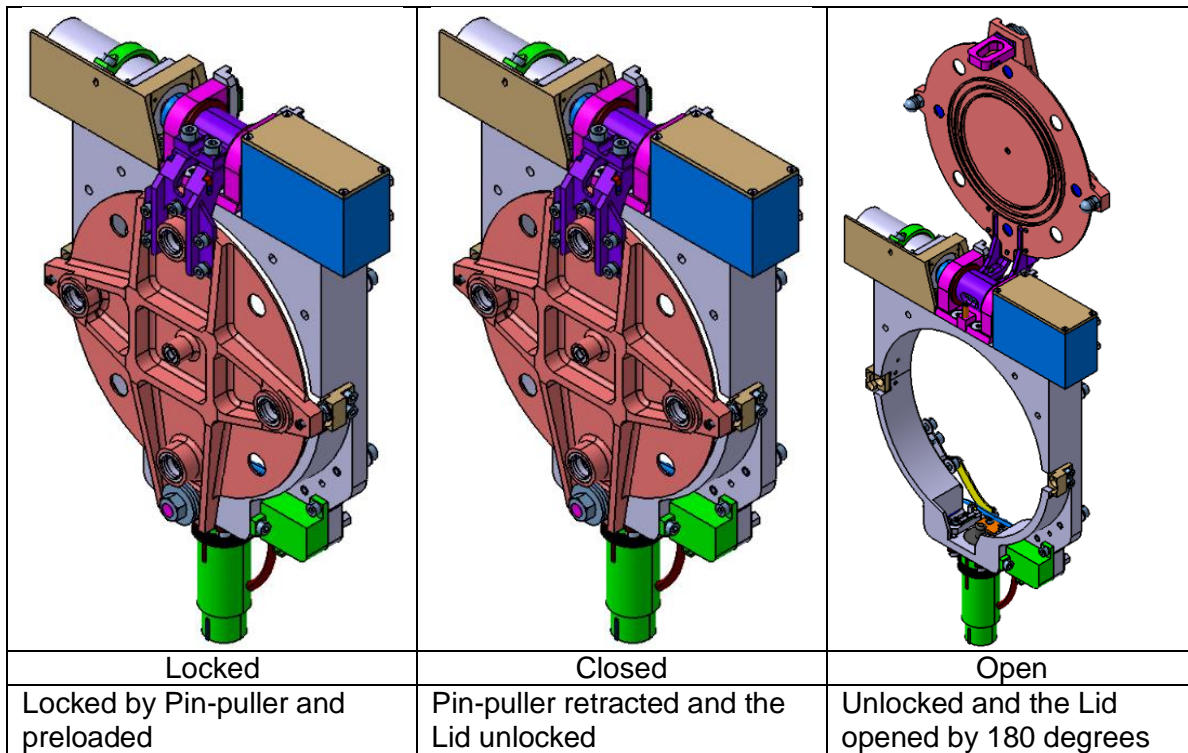


Figure 4.2 - FDA configurations

4.4 Materials

The following Table 4.2 shows all the materials used in the FDA and their material properties:

Table 4.2 - Material properties

			Aluminum EN AW 6082 T651	Steel AISI 316	A286 AISI 660	Titanium grade 5	PEEK	VESPEL SP3	Glass
Density	ρ	[kg/m ³]	2700	7850	7950	4430	1310	1600	2203
Young modulus	E	[MPa]	69 500	193000	200000	114000	4300	2413	70000
Poisson's ratio	ν	[-]	0.33	0.3	0.3	0.41	0.4	0.41	0.17
Yield Strength	σ_y	[MPa]	240	290	590	1100	115	N/A	N/A
Ultimate Strength	σ_{ult}	[MPa]	295	550	900	1170	115	58.5	50



4.5 Parts and subassemblies description

The following text describes the design and function of the most important parts and subassemblies which make the FDA.

4.5.1 Flange

It is the main structural part which holds all the other parts and subassemblies together while mounting the whole FDA to the Coronagraph Optical Box (COB) Tube by eight M4x16 bolts and special PEEK washers as defined in R-6202. The mechanical vibration loads are transmitted between FDA and the rest of the satellite through these bolts. There is also one pin used for correct positioning of the FDA before mounting, which is not considered in any computations. The connection of the Flange (and the whole FDA) to the COB may be seen in Figure 4.3.

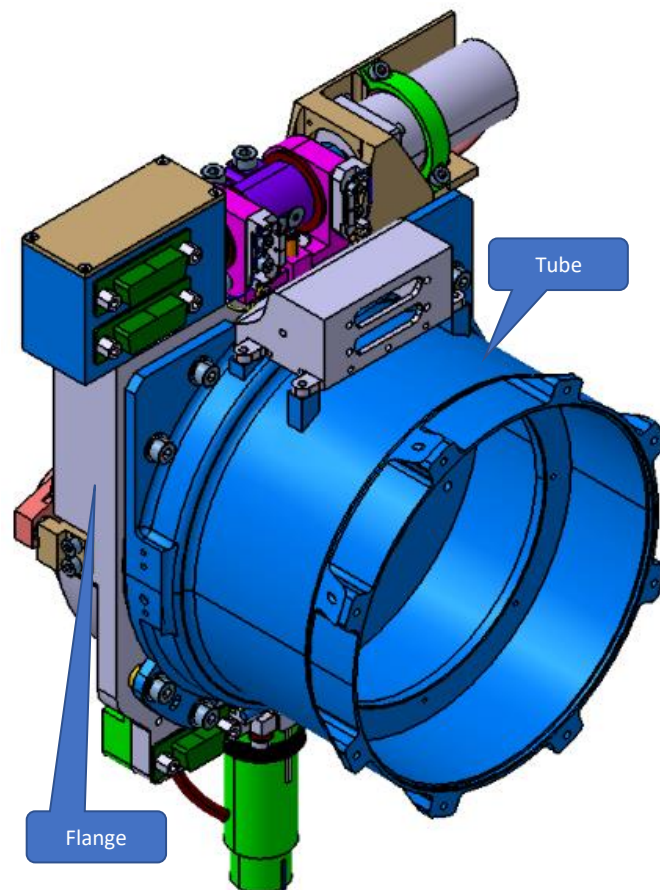


Figure 4.3 - FDA connected to the COB Tube

4.5.2 Lid assembly

It is the main moving part of the FDA. It covers and uncovers the coronagraph's optics. It consists of Lid, Lid arm, Lid nose, Touch screws and optical filters mounted in the Lid. These parts may be seen in Figure 4.4.

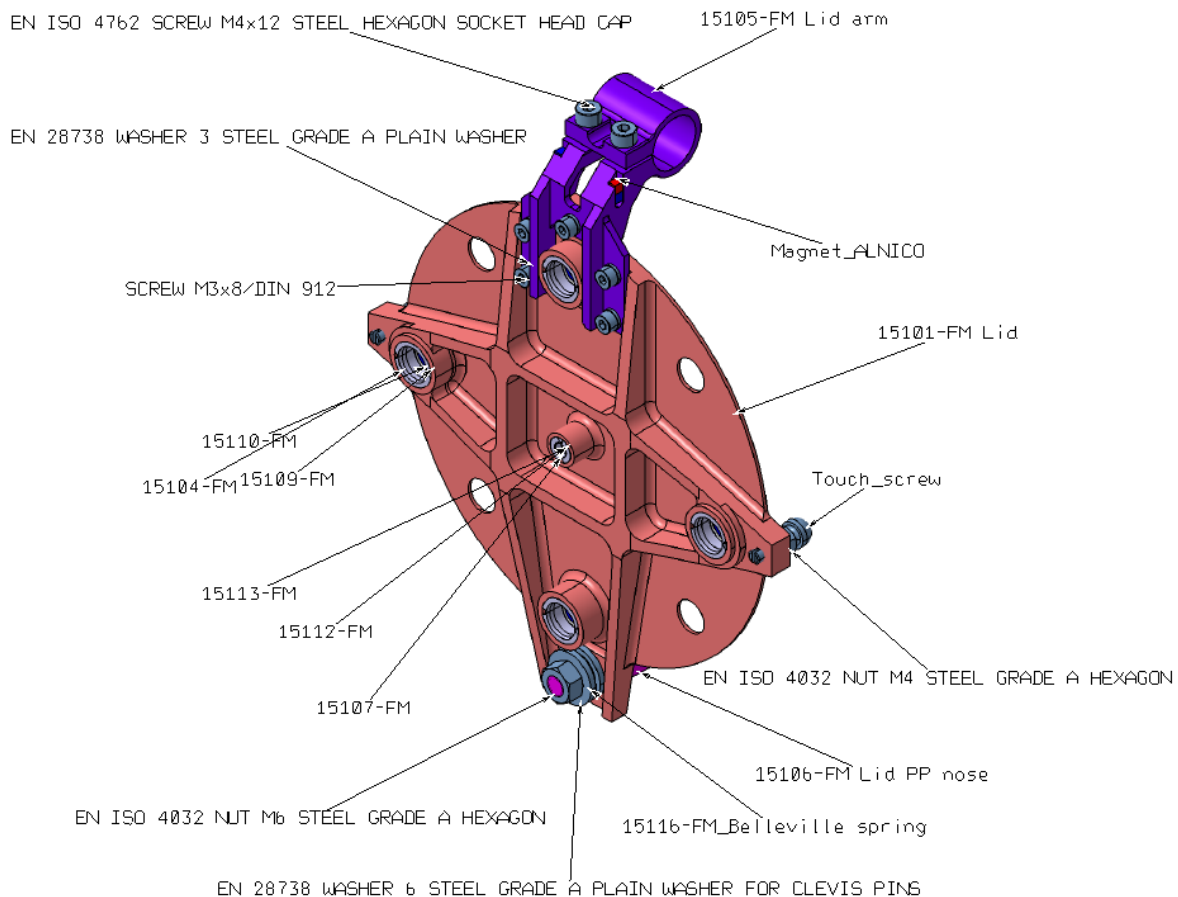


Figure 4.4 - Lid assembly

The Lid has five optical filters (HHD, SPS) mounted in five holes (req. R-4208). Special optics look at the Occulter through these filters to control the alignment and relative position of the two satellites. On the internal face of the Lid, there is a special labyrinth which fits (without any contact) to another labyrinth on the COB. These labyrinths prevent light and particles to pass through to the very sensitive optics inside the COB.

The Lid arm serves as connection between the Lid and a shaft which is connected to an electrical motor and will be described later. It also holds two magnets which are used to indicate the open position of the Lid (req. R-4512).



The Lid nose connects the Lid to a locking device which holds the Lid in a launch position and which will be briefly described later. There are two magnets glued on the Lid nose, which are used to indicate closed position of the Lid (req. R-4512).

The Touch screws are made of titanium and have a spherical head which fits into special cones mounted on the Flange called Touch-down. This fit holds the Lid in the correct position while locked in the launch position and also helps the Lid to find the right position while closing. The Touch screws are locked by a counter nut.

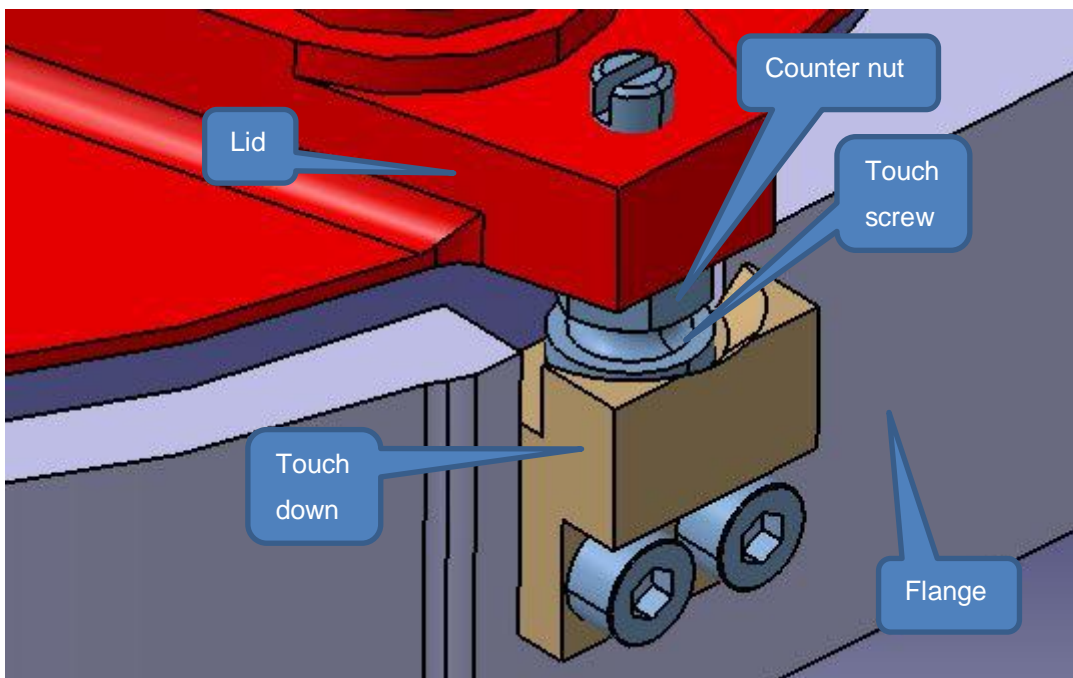


Figure 4.5 - Touch-down contact

The Lid needs to be preloaded in the locked position so that no gapping occurs during launch. This is done by a nut on the Lid nose, which can be tightened and presses the Lid against the Flange and preloads the Lid. The magnitude and a technique of the preload is discussed more in Chapter 7.

4.5.3 Hinge (shaft) assembly

This subassembly holds in place the Lid shaft, which transfers the torque between an electric motor and the Lid assembly. The Lid shaft is mounted in two friction journals which are press-fitted into the Hinge. There are two sensors (one nominal and one redundant) for open position mounted on the Hinge and these react to the magnets on the Lid arm getting close when the Lid is open (req. R-4512).

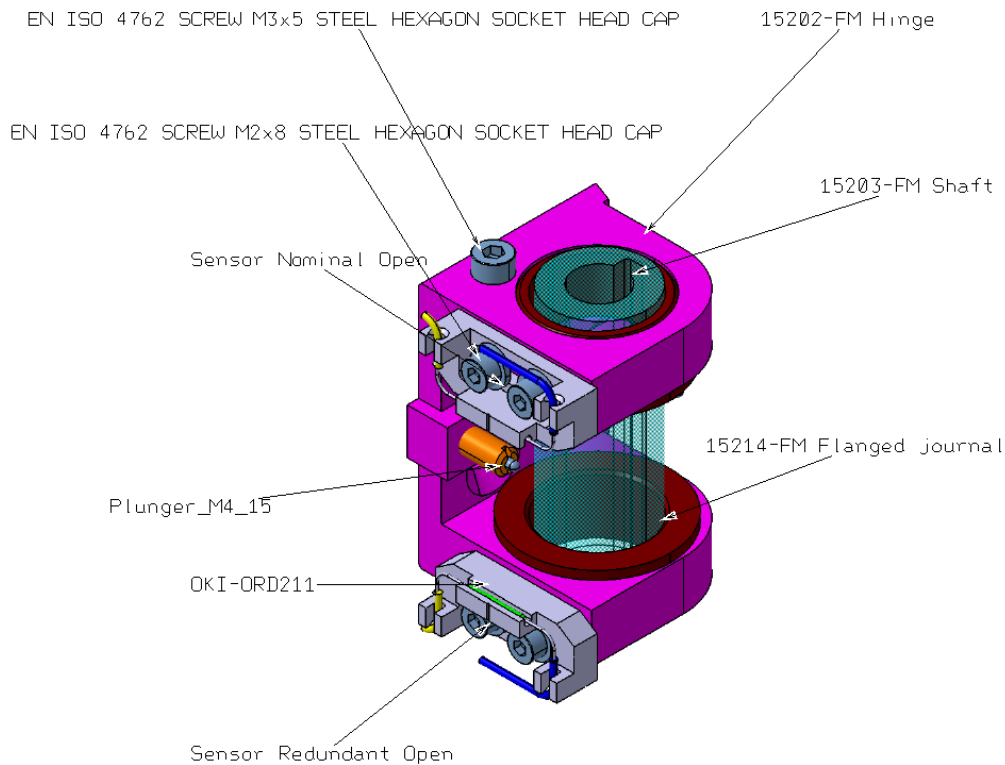


Figure 4.6 - Hinge assembly

This subassembly plays a very big role in the computations. The shaft is loosely inserted in the journals with a big clearance and the journals are made of VESPEL-SP3 which is relatively soft. During the launch locked position of the Lid, the shaft is pressed against the journals and there is a friction between those parts which determines the stiffness of this connection and the stiffness depends on the preload force. This stiffness has to be estimated for the computations and will vary with the preload as will the calculated responses.

4.5.4 Motor assembly

It is the most critical section of the FDA in terms of computations because of the high mass of the Motor. It is a stepper motor with a gearbox, torque of 1.2Nm and mass of 180,8 grams. It is mounted in the Motor bed by four M2x10 screws and a clamp which is bolted to the Motor bed by two M3x8 screws. The motor shaft is 7.98mm in diameter and is inserted into the Lid shaft while the torque is transferred by 3x3x14 key, which is clamped to the motor shaft to prevent it from falling out during the launch vibrations. The Motor bed which holds the Motor is bolted to the Flange by six M4x10 screws.

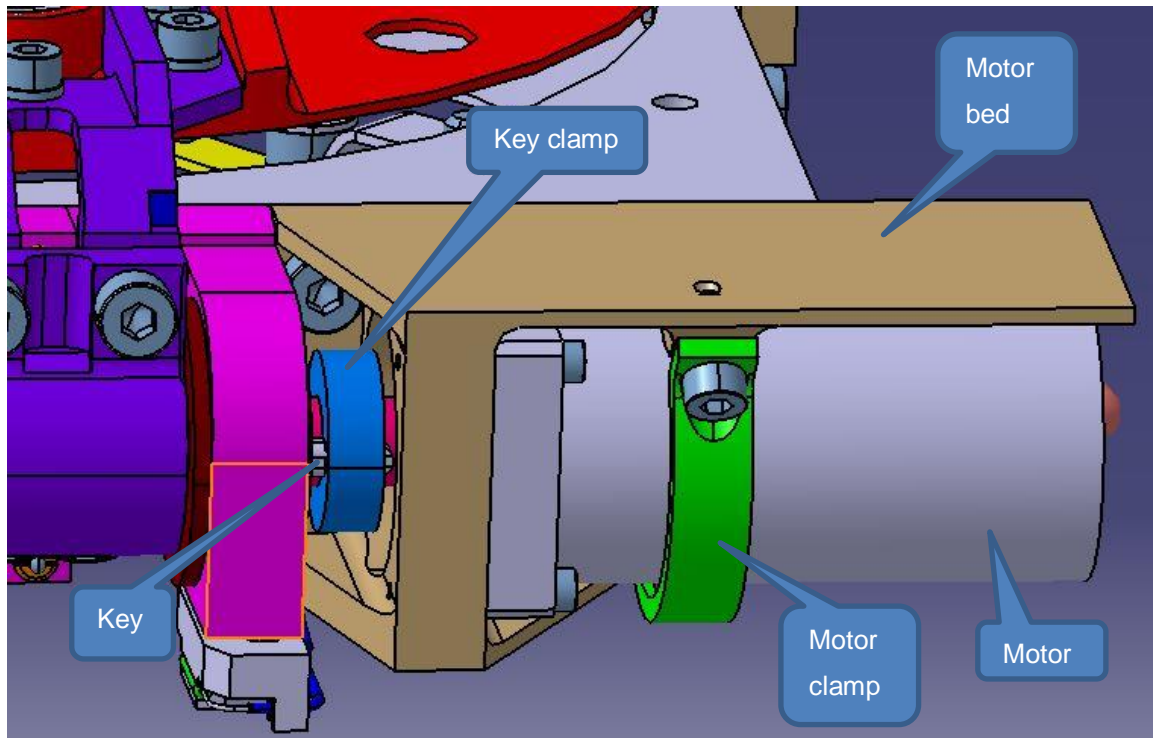


Figure 4.7 - Motor assembly

4.5.5 Locking device (Pin-puller)

The Lid is locked during launch using the Pin-puller (PP) which is a wax actuator working on a principle of thermal expansion of a special paraffin. The pin of the Pin-puller is inserted in the Lid nose when the Lid is locked and preloaded. When the Lid needs to be unlocked the Pin-puller will heat up the paraffin inside which will cause the pin to retract and enable the Lid to be opened. This will occur only once during the whole mission since the Lid will never need to be locked again.

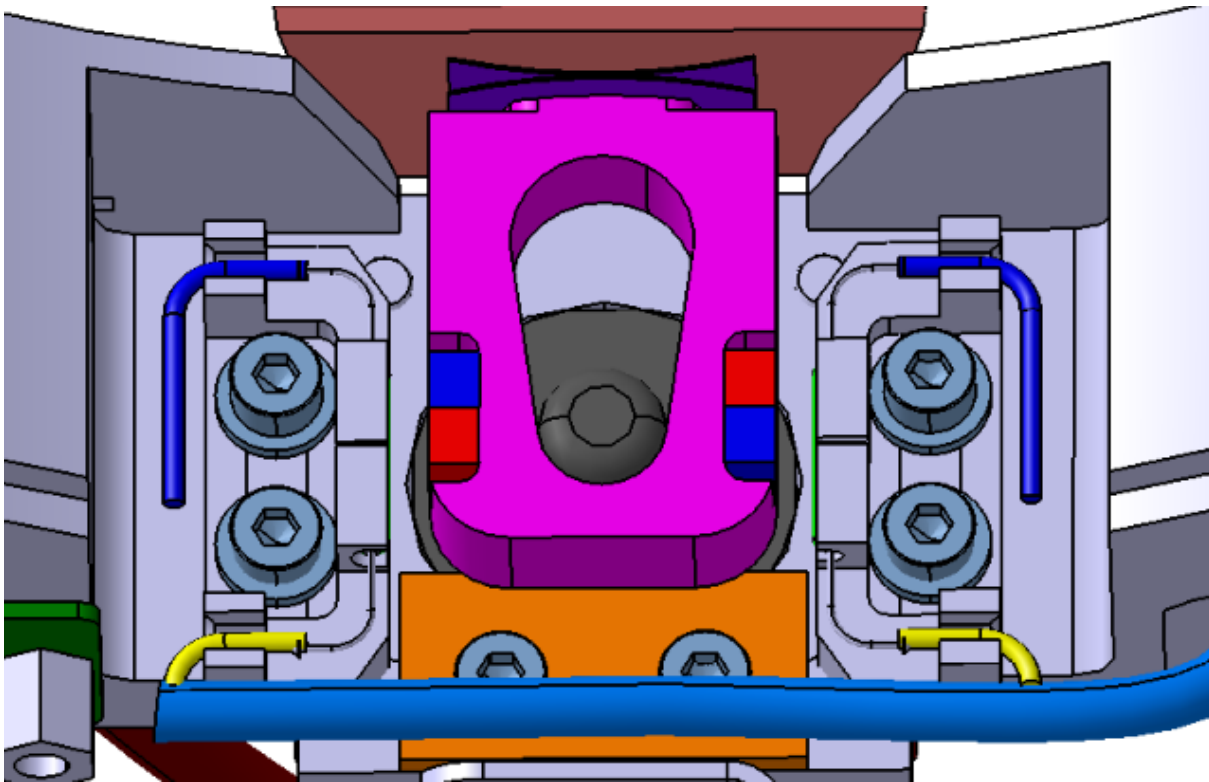


Figure 4.8 - Locking device

4.5.6 Connector box

Serves as a housing for connectors, which connect the FDA to a control unit. The harness is coming to the connectors from the Motor and the open/close sensors through a groove which is made in the Flange for that purpose. Therefore the two connectors located on the Connector box serve for control of the motor and monitoring of the position of the Lid. The Pin-puller is controlled through a different connector, which is located on the Flange close to the Pin-puller.

5 FEM description

The FEM model was created from a full CAD model created in Catia (V5R19) and provided by the FDA designer. Before any meshing was done the full CAD model was simplified so it would not contain unnecessary and structurally insignificant parts and components like harness, connectors, washers, and screws although the screws were modeled as described below. Small radii and holes were also removed from the model. The idealization of the model was done in Catia (V5R19) and the simplified model was then saved as STEP part and transferred to NX Nastran (v.10.0.0.24) in which all the meshing and computations were done.

5.1 Coordinate system

The coordinate system was set based on the requirement R-3200 which determines the origin of the coordinate system and the directions for the axis as shown in Figure 5.1.

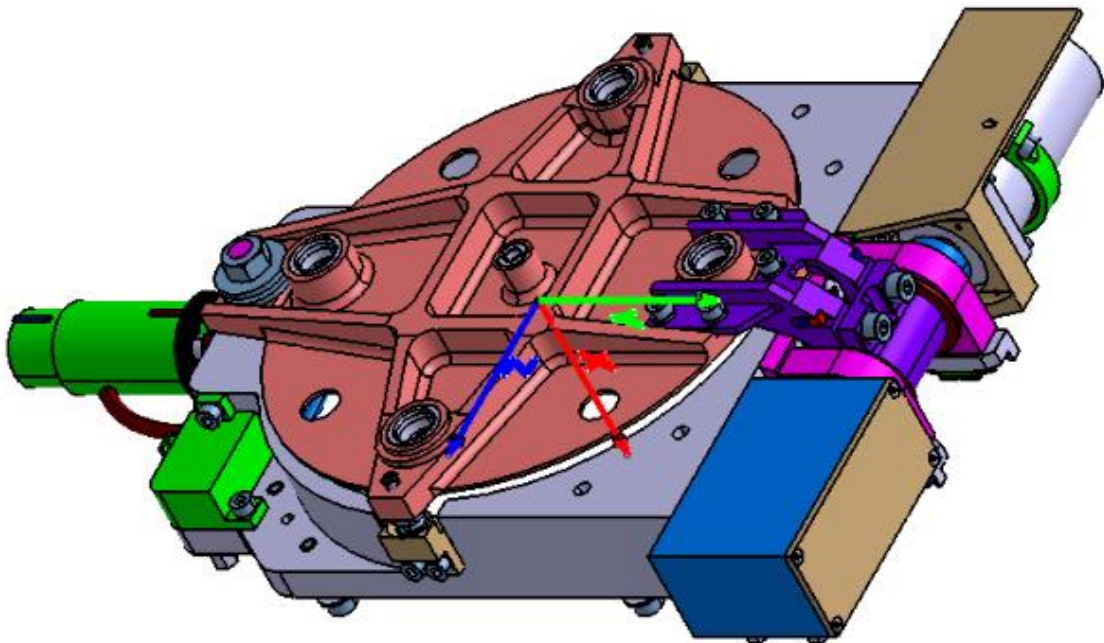


Figure 5.1 - FDA global CSYS

The origin of the coordinate system is in the center of the circle that creates the interface between the FDA and the COB Tube. The X-axis is directed to the coronagraph, the Y-axis in the direction of SPS (which is a unit that is not part of the



FDA and is not discussed in this thesis) and the Z-axis completes the right-handed set. This coordinate system is used for the design, the FEM model and all the testing and simulation.

5.2 Mesh

All the 3D deformable parts which were left in the simplified model were meshed using TETRA10 parabolic tetrahedral 3D elements. The request for a minimum of two elements through-thickness of any part was implemented, which is especially important for the Lid, the Motor bed and the Connector box which all have thin-walled structures.

The size of the elements was determined based on previous experience of the company taking into account the size of the specific part, the computation time, possible stress gradients and element checks. The elements type, element size, number of elements, number of nodes and the material property which specific properties may be seen in Table 5.1.

Table 5.1 - 3D mesh properties

Part	Element type	Material property	Element size (mm)	Number of elements	Number of nodes
Flange	TETRA10	Aluminum	3	74558	118877
Lid	TETRA10	Aluminum	2,5	148165	228034
Touchdowns	TETRA10	Steel	2	6526	10502
Nose	TETRA10	Steel	1	22742	37121
Lid arm	TETRA10	Aluminum	1,5	48788	78327
Motor bed	TETRA10	Aluminum	2	40095	63824
Hinge	TETRA10	Aluminum	2	19182	31683
Connector box	TETRA10	Aluminum	3	43646	67281
Lid shaft	TETRA10	Steel	2	18994	30993
Total 3D elements	TETRA10			422696	666642
Total 0D, 1D elements	RBE2, CBUSH,CONMASS			2917	10589
Total elements				425613	677231



5.3 Concentrated masses

The Motor, the Pin-puller, the electrical connectors and the filters in the Lid were not modeled as 3D meshes but as a 0D CONMASS concentrated mass elements connected to the model by RBE2 elements. The mass properties of the Motor and the Pin-puller were obtained from the supplier of these parts. The connectors and the filters were weighed by Serenum.

The Motor is a CONMASS element with a mass of 180,8 grams and is connected by four RBE2 elements to four screws modeled as CBUSH elements which connect the Motor to the Motor bed. In addition, there are two RBE2 elements and two CBUSH elements simulating the clamp of the Motor. This concentrated mass is creating the most critical modes.

The second biggest concentrated mass which is also quite significant in the modal analysis is the Pin-puller. It is modeled as a CONMASS element with a mass of 72 grams and is connected to the Flange by four RBE2 elements and four CBUSH elements.

The connectors and the filters are modeled as CONMASS elements with a mass of 3 grams which is quite insignificant relative to the mass of the whole assembly.

Table 5.2 - Concentrated masses

Part	Number of parts	Element type	Mass per part (g)	Total mass (g)
Motor	1	CONMASS	180,8	180,8
Pin-puller	1	CONMASS	72,0	72,0
Connector	11	CONMASS	3,0	33,0
Filter	6	CONMASS	3,0	18,0
Total mass				303,8

5.4 Material properties

Because of how the FEM model is simplified only three materials were used in the model and the properties of those material are listed in Table 5.3. The rest of the materials which are listed in Table 4.2 are not present in the model because the



corresponding parts were somehow replaced. In the final model, the Titanium was not used because the Touch screws are modeled by 1D elements and although some simulations were performed with titanium Motor bed it was decided that aluminum will be used in the final design.

Table 5.3 - FEM material properties

Material	Density (kg/m ³)	Young's Modulus (Mpa)	Poisson's Ratio (-)
Steel AISI 316	7850	193 000	0,3
Aluminum EN AW 6082 T651	2700	69 500	0,33
Titanium GRADE 5	4430	114 000	0,41

5.5 Modal and Random model

There is a different model used for the computation of modal properties (and tuning) and for random, quasi-static and sine loads computation. The model used for the modal properties and tuning is called the Modal model and the other one used for the rest of the computations is called the Random model. The difference between these models is in the mass budget. It is required for the Modal model to have the same mass properties as the real DM and for the Random model to have the mass budget increased by ten percent. The difference in the mass properties of materials and concentrated masses may be seen in Figure 5.4.

Table 5.4 - Modal and Random model mass budgeted

Material	Density in Modal model (kg/m ³)	Density in Random model (kg/m ³)	Increase (%)
Steel	7850	8635	10
Aluminum	2700	2970	10
Concentrated mass	Mass in Modal model (g)	Mass in Random model (g)	Increase (%)
Motor	180,8	198,9	10
Pin-puller	72,0	79,2	10
Connectors	3,0	3,3	10
Filters	3,0	3,3	10



5.6 Screws

All screws were modeled using 1D elements, specifically RBE2 elements and CBUSH elements. The absolutely rigid RBE2 elements were used to create a so-called “spider” which can be seen in Figure 5.2. Each bolted connection always has two spiders. One for each of the connected parts. The spider always connects a face to a point. The face is either an area in the threaded hole where the screw is actually screwed into the hole or the area of the countersunk hole where the screw is in contact with the part. The point is always at the interface of the two parts and in the center of the hole. An exception is the Touch screw which is modeled differently since it is not a typical bolted connection.

The two spiders are connected at the interface by a 1D zero-length CBUSH element. The coordinate system of the CBUSH element is defined so the X-axis is in the direction of the screws axis and stiffnesses for all six DOF’s may be set. These stiffnesses are the main parameters used for tuning the FEM, which is described in Chapter 10.

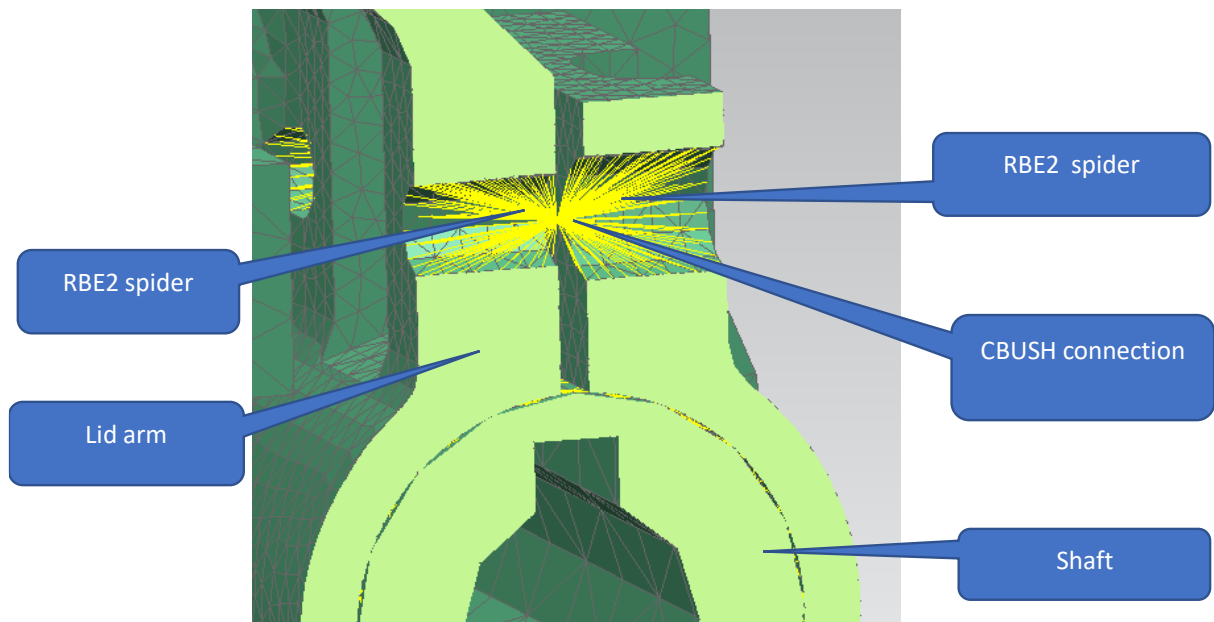


Figure 5.2 - Example of a screw modeling



5.7 Lid Shaft

The Lid shaft is connected to the Lid arm by a friction joint and that is modeled by mesh mating function which connects both meshes of the parts by rigid elements in the area where the two meshes are coincident with a certain tolerance. That results in a similar connection as if the two parts shared the same mesh which simulates the friction joint well.

The Lid shaft sits in the friction journals which are press-fitted in the Hinge. This connection is realized by a spider at each end of both the Lid shaft and the Hinge. Those spiders connect to the axis of the Lid shaft where they are connected by CBUSH elements similarly to bolted connections. Stiffnesses of these CBUSH elements are a very important and very complicated parameter of tuning of the FDA because it is much less stiff than a usual bolted connection and is dependent on the preload force. The Lid shaft is not connected to the Motor shaft in any way since those two are not in contact while the Motor is not running because of very big tolerances.

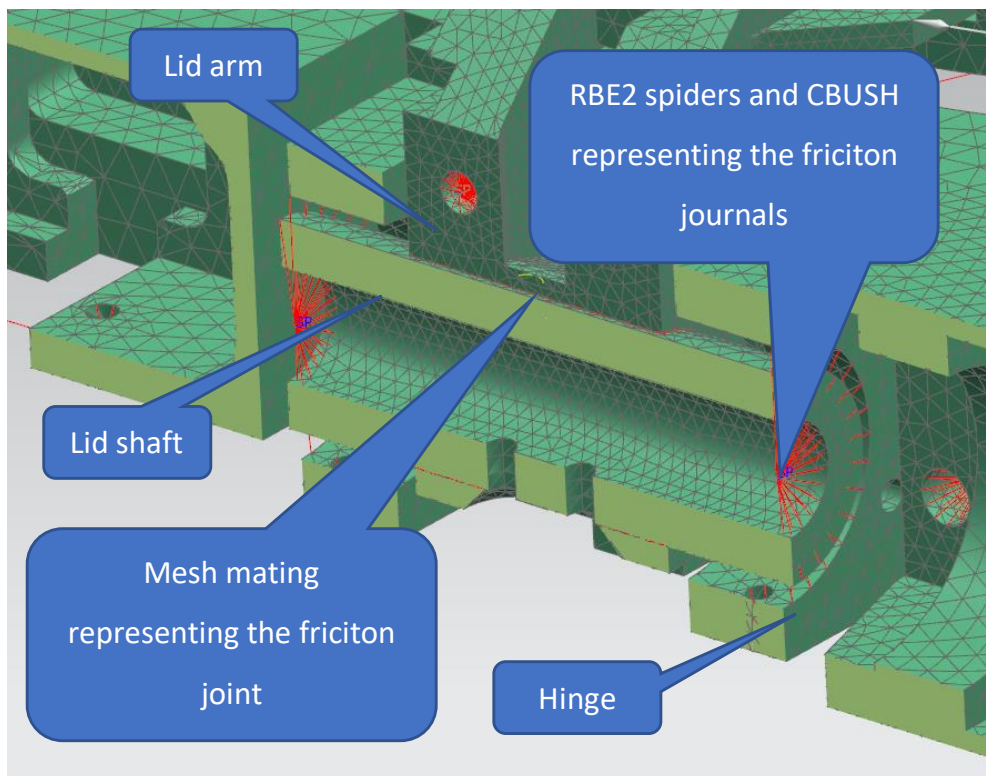


Figure 5.3 - Lid shaft connections

5.8 Pin-puller

The connection between the FDA Flange, the Pin-puller, and the Lid nose can be seen in the Figure 5.4. It uses two spiders, one RBE2 beam and a CBUSH element. The spiders are connecting the areas where the Flange and the Lid nose are in contact with the Pin-puller (which is not modeled in 3D) in the locked configuration with points on the axis of the Pin-puller. An RBE2 beam is connected to one spider and goes to the other one where it is connected by a CBUSH element simulating the stiffness of this connection.

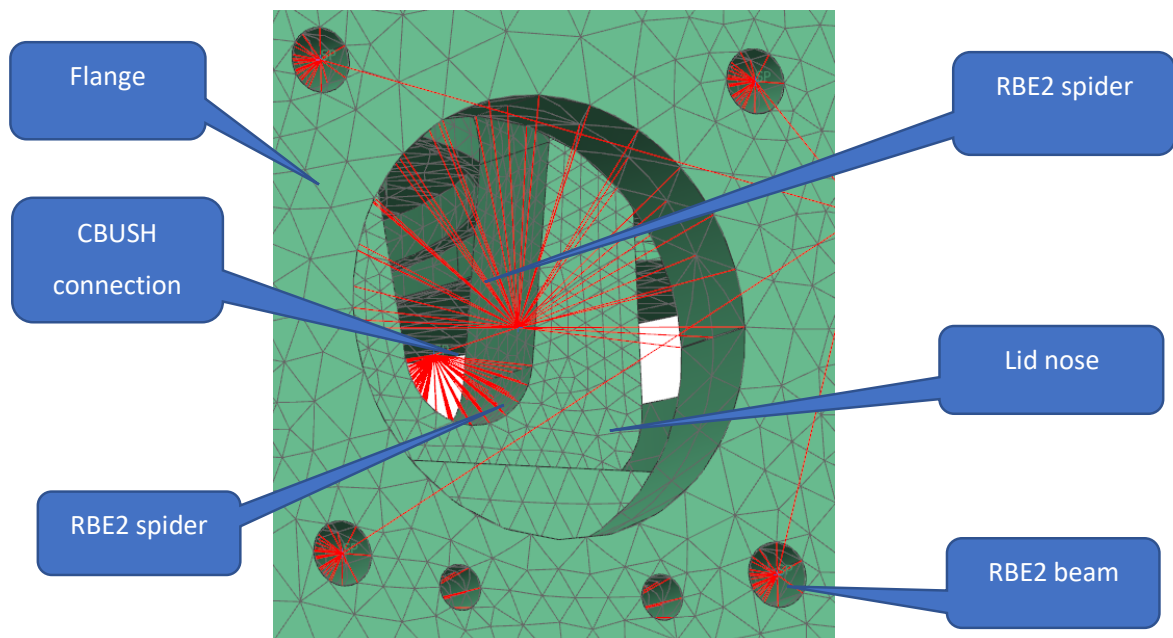


Figure 5.4 - Pin-puller connection

5.9 Touch screw

This connection is not a classical bolted connection but is modeled very similarly. It is realized by two RBE2 spiders and a CBUSH elements with a very low stiffness since it is just a contact. One spider is connecting the hole in the Lid where the Touch screw is screwed into the Lid to the CBUSH element in the center point of the Touch-down. The other spider is connecting the surface of the cone of the Touch-down where the spherical head of the Touch-screw is in contact with the Touch-down to the center point of the cone where both spiders are connected by a CBUSH element.

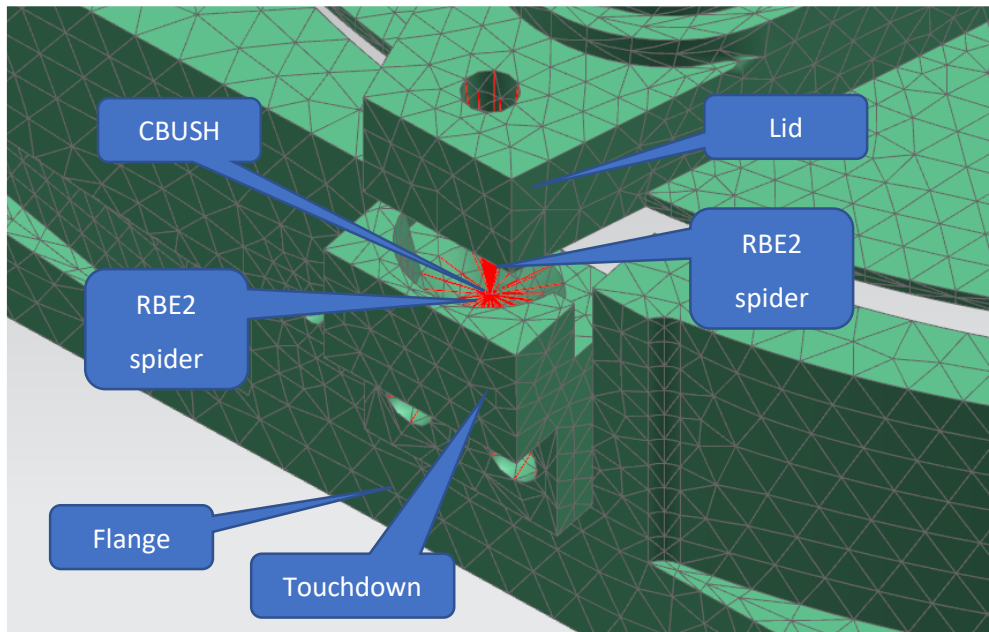


Figure 5.5 - Touch screw connection

5.10 Lid nose

The connection between the Lid and the Lid nose is done very specifically to ensure the possibility to apply the preload on the Lid. There is a washer modeled as 3D mesh connected to the Lid by mesh mating. In the real CAD model, there is a nut on the Lid nose which is used to apply the preload to the Lid and which is not modeled in the FEM. Instead, there are two RBE2 spiders and one BEAM element connecting those spiders. The BEAM element is on the axis of the Lid nose thread and a preload force can be set for this element.

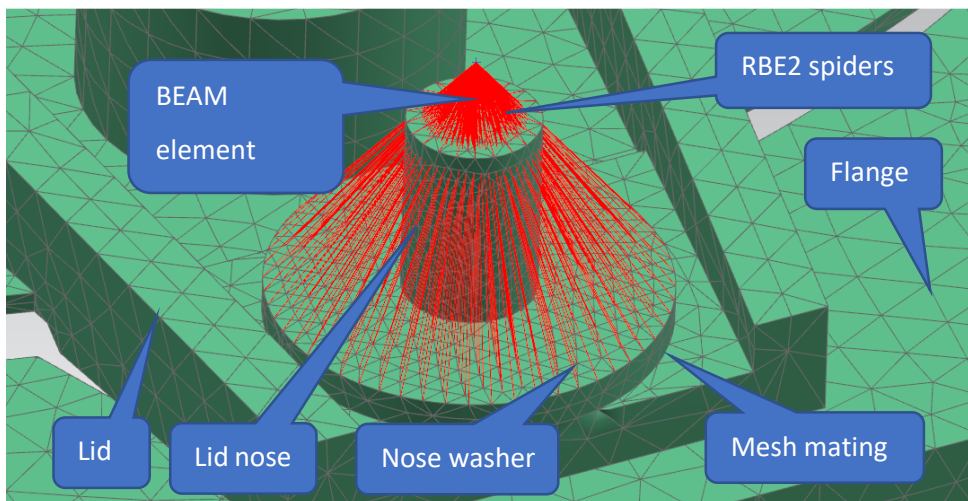


Figure 5.6 - Lid nose connection

5.11 Flange-Tube connection

The connection between the Flange (and thus the whole FDA) and the Tube (which is part of the coronagraph) might be the most important in the whole model. It creates the interface between the satellite and the FDA and all the vibration loads are transferred through this connection from the satellite to the FDA. There are eight screws in this connection which are modeled in the same way as other screws. A RBE2 element goes from each of those screws to the COG of the whole model where is an excitation point and all the vibration loads in all the simulations are forced at this point.

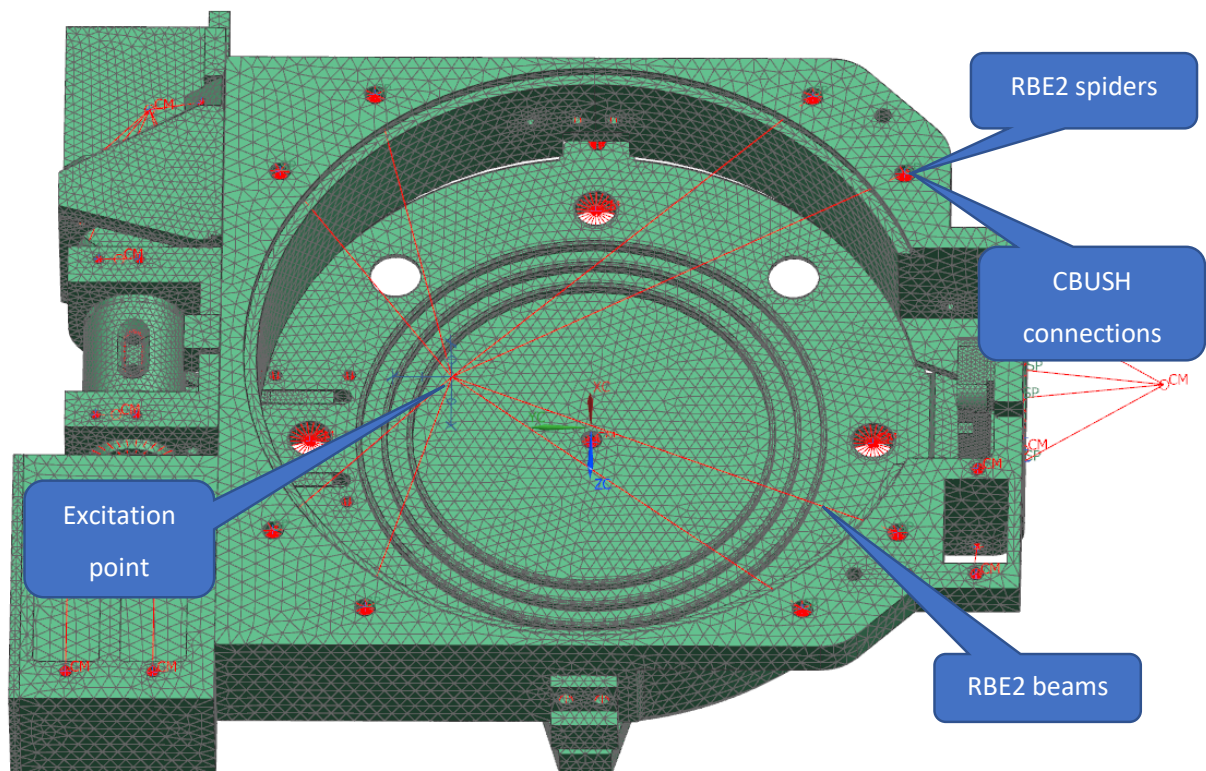


Figure 5.7 - Flange-Tube connection

5.12 FEM checks

The following model checks were performed before any simulation was run to verify that the model will act as a rigid body when unconstrained. Both checks were done with a free-free Modal model. That is a model without any loads or constraints



and without the RBE2 spider connecting the Flange to the excitation point (see Figure 5.7).

5.12.1 Strain energy check

The model passed the strain energy check with the maximum strain energy in all six directions summarized in Table 5.5. The pass limit was 10^{-2} J for translational DOFs (1,2,3) and 10^{-1} J for rotational (4,5,6) DOFs.

Table 5.5 - Strain energy check

DOF	Maximum strain energy (J)	PASS/FAIL
1	7.233076E-06	PASS
2	1.312619E-05	PASS
3	4.986362E-06	PASS
4	3.344242E-02	PASS
5	7.754335E-02	PASS
6	5.161255E-02	PASS

5.12.2 Modal check

The model passed the modal check with the first six modes showing a rigid body motion with frequencies below 10^{-2} Hz. The seventh mode is the first non-RBM mode of the free-free Modal model.

Table 5.6 - Modal check

Mode	Frequency (Hz)
1	3.833479E-03
2	2.691672E-03
3	7.281559E-04
4	1.724211E-03
5	2.769159E-03
6	5.217310E-03
7	5.373676E+02



6 Preliminary simulation

After the FEM model is done and before the DM can be assembled some preliminary simulations need to be done. At this point, the model was not correlated therefore the stiffnesses of the screws were set to an approximate value given by equation 3-1, which gives the stiffness values in order of 10^6 N/mm.

6.1 Tightening torques

In order to assemble the DM for the vibration testing the tightening torques for the screws needed to be delivered. To calculate those the forces in the screws have to be known and therefore a preliminary random vibration simulation was performed using the original spectra (see Appendix A). First, the forces in the connection between the Lid and the Pin-puller needed to be computed to determine the Lid preload force (see Chapter 7). The calculated forces may be seen in the following Table 6.1.

Table 6.1 - Preliminary random forces at PP-Lid

Excitation axis	Force component (N)		
	X	Y	Z
X	38	33	5
Y	16	19	2
Z	8	12	7

As expected, the biggest force is in the X direction with the excitation in X direction as that one is the most severe. The preload force necessary for preventing gapping (see Chapter 7) was then calculated using the Equation 7.1 and the biggest force which is 38N.

$$F_P = M \cdot k \cdot (3 \cdot F_{FEM}) = 2 \cdot 1,2 \cdot (3 \cdot 38) = 274 \text{ [N]} \quad (6-1)$$

This preload force was then applied to the FEM model and static simulation was run and gave a set of forces in the screws caused by the static preload. After that, a random vibration simulation for each axis with the original spectra was run and provided another three sets of forces in the screws. Appendix B contains a set of



forces for each axis excitation. The forces from random vibrations changes for each axis while the forces from the preload stay the same for each axis. The components of the forces are not consistent with the global CSYS but X is the axial force in the screw and Y, Z are the lateral forces. The sum of both sets is included and was used for the calculation of the tightening torques using the approach described in Chapter 12.

The tightening torques were then adjusted so all of the MoS are positive and are summed in Table 6.2.

Table 6.2 - Preliminary tightening torques

Part 1	Part 2	QTY.	SCREW	Tightening torque (N.mm)
Flange	Tube	8	M4x12	1100
Flange	Motor bed	6	M4x10 COUNTERSUNK	1100
Flange	Hinge	4	M4x8 COUNTERSUNK	1100
Flange	Conn. box	3	M4x10 COUNTERSUNK	1100
Flange	Touch down	2	M3x8	500
Flange	Pin puller	4	SCREW #6-32 3/8", C-606-N	640
Motor bed	Motor	4	M2x10	120
LID	Lid-arm	5	M3x8	500
LID	Touch-screw	2	M4	1100

Bolted connections which are not in this table were excluded from the calculation because of very small forces in the screws and the tightening forces were obtained from standards. The calculated torques were then used to assemble the DM which was then ready for the vibration testing.

7 Lid preload

During launch, the FDA is in a closed and locked position and a specific preload is applied on the Lid. The main function of the preload is to prevent gapping which may be caused by vibrations during launch. If the preload is too low gapping may occur between the Lid and the Flange where those two subassemblies connect. Specifically Touch screws, Lid nose, and the Hinge. If the preload is too high it causes unnecessarily high stress in the parts mainly in the Lid ribs. The preload is realized by tightening a nut on the Lid nose which causes the Lid to bend and preload.

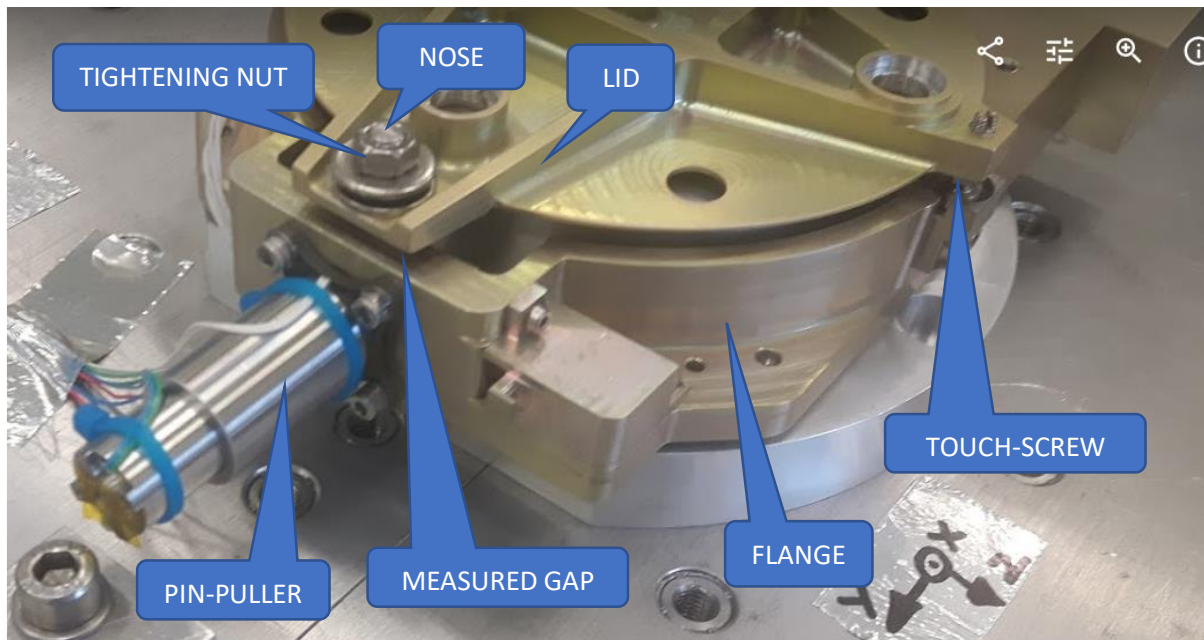


Figure 7.1 - Lid preload

7.1 Preload calculation

The correct preload force is obtained from the FEM computations. The FEM model is loaded with the random spectra in each direction and an axial force is measured in the BEAM element connecting the Lid and the Nose (see Figure 5.6). An axial force for each loading direction is obtained and the biggest one is considered for the preload force calculation given by:

$$F_P = M \cdot k \cdot (3 \cdot F_{FEM}) [N] \quad (7-1)$$

Where F_{FEM} is the axial force measured in the BEAM element and it is multiplied by three because the result from the simulation is considered with a standard deviation of 1σ . Coefficient k is a safety factor which in this case is 1,2 and M is a motorization factor which is another type of safety factor and is set to 2. This preload force may change many times during the design and computation process as the random spectra changes.

7.2 Preload application and measurement

On the physical design model, the Lid preload is controlled by measuring a gap between the Lid and the Flange. The gap may be seen in Figure 7.1 and the measuring of the gap is shown in Figure 7.3 (right). But in order to control the preload force, the relation between the gap size and the preload force has to be determined.

A special calibrated spring was used to determine the relationship between the gap and the preload force. First, the relationship between deformation and force was obtained for the spring by measuring changes of its length in relation to force applied by weights.

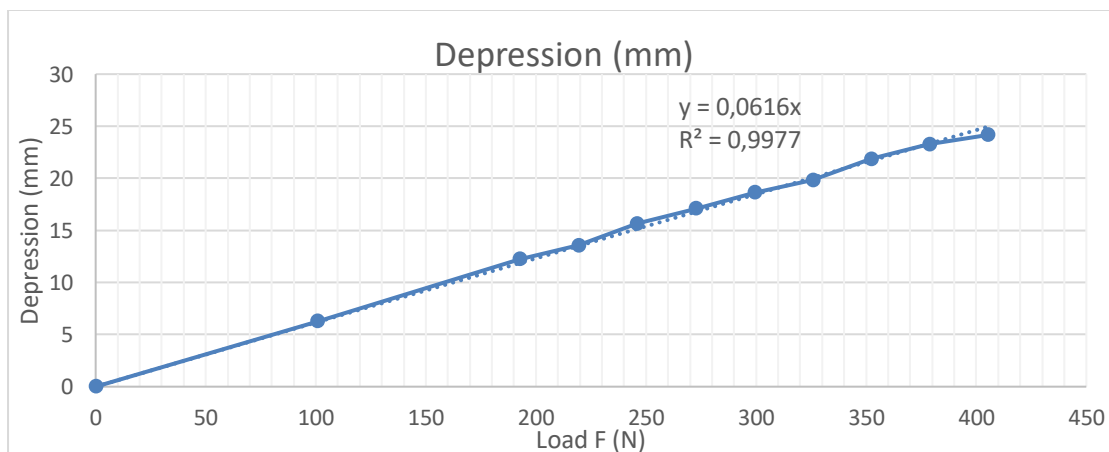


Figure 7.2 - Force-compression relation of the preload measuring spring

Then the special spring was mounted on the Nose and the preload of the Lid was applied by compression of this spring. It was decided to measure three preload forces which values (see Table 7.1) were based on preliminary simulations. Those preload forces were later used in the vibration testing and any other value may be interpolated. Measuring of the relationship may be seen in Figure 7.3.

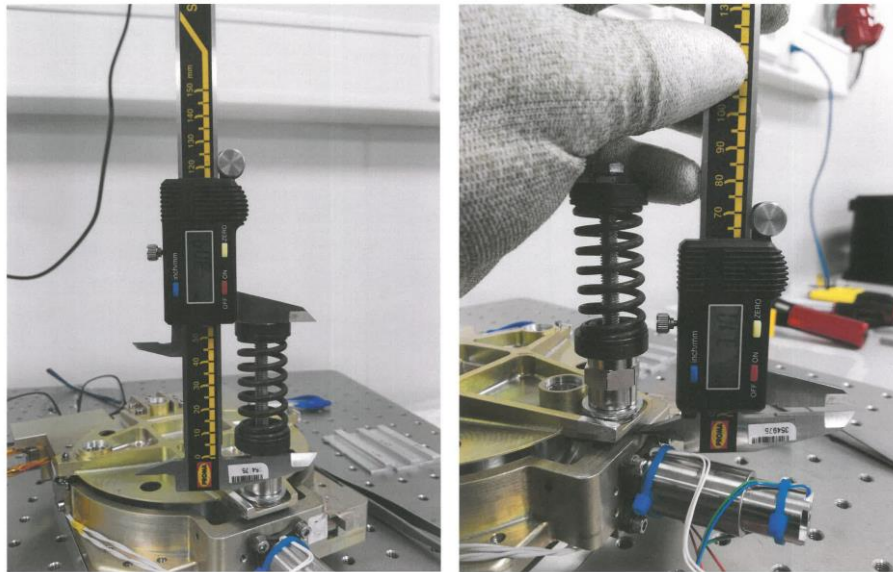


Figure 7.3 - Gap-preload relationship measurement

In the left, the compression of the spring is measured giving the preload force from the relation in Figure 7.2. In the right, the gap is measured to give the relation between the gap and the preload force. With this relation known the preload may now be set only by measuring the gap.

The three preloads picked for the relation measurement and for the vibration testing are in Table 7.1 with the according gaps measured.

Table 7.1 - Preloads selected for testing

Lid preload	Force (N)	Gap (mm)
Preload A	120-135	3,0
Preload B	190-200	2,6
Nominal	270-280	2,2

For easy control of the preload gauges were made from aluminum, each with the specific thickness. These gauges are put into the gap and the nut is tightened until the gauge is not loose but can be still easily removed. This method is not completely objective since it depends on the person performing the preload as he decides what is loose and what is easily removed. Therefore, the gap is also measured by a digital caliper.



8 Vibration testing

After certain preliminary computations are performed on the FEM model as described in Chapter 6, the physical DM may be manufactured and vibration testing may be performed. All the parts are sent for manufacturing and tightening torques for the assembly are calculated as described in Chapter 12 with forces obtained from the preliminary simulations mentioned above.

The manufactured parts of the DM are cleaned and assembled in the cleanroom according to the design and using original Motor and Pin-puller. The DM is only missing some harness, harness hooks, one small connector, and the surface finish. These deviations from the final model are negligible since those parts have a very small mass compared to the rest of the assembly.

The assembly is fastened onto a vibration adapter which is used to mount the FDA on a vibration table. The adapter has the same connection dimensions for the FDA as the Tube, which is the FDA's connecting part to the satellite. On the other side, the adapter has holes for connection to the vibration table. A very important parameter of the adapter is the first natural frequency. It is designed in a way that the first natural frequency is above the tested range of frequencies in this case above 2500Hz because it is unwanted for the adapter's natural frequencies to appear in the FDA resonance search or influence the random vibration responses.

8.1 Setup

The FDA DM was vibration tested in ESTEC (European Space Research and Technology Centre) in Noordwijk, Netherlands, which is the main research and engineering facility of the ESA. Some preliminary and additional vibration tests were also done in VZLU (Czech Aerospace Research Centre), Prague but the final results are from ESTEC.

The FDA DM was sent to ESTEC assembled, without the Lid preload and without accelerometers. Upon beginning of the testing, the FDA was mounted on the adapter by eight M4x16 screws with PEEK washers and tightened by 1,1 Nm torque calculated in Chapter 6. The adapter with the FDA DM was then mounted on the



vibration table by five M8x12 screws tightened by 33 Nm torque prescribed by the ESTEC test engineer.

The tested axis are in correspondence with the coordinate system in Figure 5.1.

8.2 Accelerometers

The three main locations for accelerometer placement were chosen based of the preliminary modal simulations which show the most significant mode shapes. These shapes are usually created by the high-mass components of the FDA which is the Motor and the Pin-puller. The main three locations are Motor inter-face (IF1), Pin-puller inter-face (IF2), and Lid center (T1). These main locations are marked in Figure 8.3 along with some other locations which were measured but the data were not used in the tuning of the FEM model. The drive accelerometer is placed differently for each axis but always on the vibration table and is denoted as C1.

Table 8.1 - Accelerometers list

Channel no.	Designation	Type	Part measured	Sensitivity (mV/g)	Measured axis		
					X excitation	Y excitation	Z excitation
1	C1	Triaxial	Vibr. table	62341	X	Y	Z
3,4,5	IF1	Triaxial	Motor IF	122691	X,Y,Z	X,Y,Z	X,Y,Z
6,7,8	IF2	Triaxial	Pin-puller IF	122689	X,Y,Z	X,Y,Z	X,Y,Z
9,10,11	T1	Triaxial	Lid center	93828	X,Y,Z	X,Y,Z	X,Y,Z
12,13,14	T2	Triaxial	Lid arm	94340	X,Y,Z	X,Y,Z	X,Y,Z
15,16,17	T3	Triaxial	Lid at Nose	171504	X,Y,Z	X,Y,Z	X,Y,Z
18,19,20	T4	Triaxial	Lid at Touch-s.	172986	X,Y,Z	X,Y,Z	X,Y,Z

8.3 Test plan

The vibration testing has three main objectives:

- 1) Perform a resonance searches to obtain transfer functions which are needed for the FEM model correlation (tuning)
- 2) Explore the effect of the Lid preload on the responses
- 3) Learn about possible settling of the DM and its influence on the responses



In order to complete these objectives, the DM needs to be tested in each axis, with at least two different Lid preloads and for both low-level sine sweep and random vibrations. The testing plan for each axis is:

- 1) Mount the DM onto the table and mount all the accelerometers
- 2) Set a specified preload and measure the gap
- 3) Run LL sine to acquire the transfer functions and check for possibly dangerous amplifications
- 4) Run -12dB random vibration to gain responses and possibly force the settling
- 5) Run LL sine to learn about possible settling during the random vibrations
- 6) Measure the gap a check the responses for possible changes due to settling
- 7) Set a different preload
- 8) Repeat 2) to 6)

This process requires six runs for each axis which makes the testing eighteen runs total considering everything goes as planned.

The LL sine spectra for all axes can be seen in Table 8.2.

Table 8.2 - Low-level sine spectra

Frequency (Hz)	Levels (g)	Sweep Rate (oct/min)
5-2000	1	2 (up)

The random vibration loading spectra which were used are the original spectra (see Appendix A) but were run at -12dB to avoid any risk of damaging the components especially the Motor or the PP. Previous testing in VZLU showed very high amplification at the Motor IF which could lead to damaging loads of the Motor if exposed to the full spectra. On the other hand, this decrease of the spectra probably results in lower effect of the random vibrations on the settling and possibility of bigger impact with full load should be taken into account.

8.4 Settling

It is very common for mechanisms to settle while being exposed to vibration loads. Every mechanism has moving parts, which are not rigidly connected to the rest of the unit. Before launch, the mechanism needs to be locked to avoid excessive



vibrations and moving of the parts. When the mechanism is locked the parts take some relative position and create some contacts. Even though this prevents excessive movement the parts will move relative to each other at least a little bit after being exposed to the vibration loads. This is usually caused by the vibration forces overcoming the friction forces between the parts and moving the parts to some more stable position. This shift in position may lead to changes of resonance frequencies and amplitudes during launch and it should be taken into account.

In our case, the Touch screws settles in the Touch-downs, the Lid shaft settles in the bearings and the Nose settles on the Pin-Puller pin. Those are the locations where the moving part (Lid assembly) is in contact with the rest of the FDA.

This settling may be measured by change of the gap between the Lid and the Flange. The same gap that is used to control the preload (see Chapter 7).

8.5 The testing

Below is described the step by step procedure of the vibration testing as it was performed with description of what was done and what results it brought.

8.5.1 Z-axis

The FDA DM was mounted on the vibration table as described above, all the accelerometers were mounted on their respective positions and the testing started with the Z-axis.

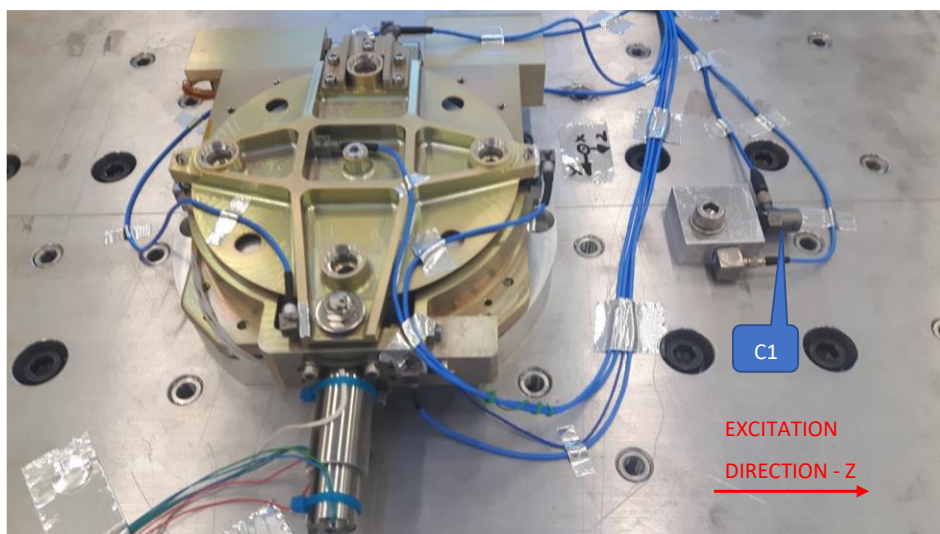


Figure 8.1 - Z-axis testing

8.5.1.1 Preload B

The first applied preload was the Preload B (see Chapter 7). Measuring the gap with the caliper is quite uneasy so the gap was measured to be between 2,75 and 2,80. Then the LL sine, -12dB random and second LL sine tests were performed and the gap was measured again with results between 2,79 and 2,82 which shows some settling but the difference in the gap is so little, that it can not be completely relied on and since the changes in the gap are very small and the measuring technique is not very precise it was decided that the settling will be mainly judged based of the responses and may also be confirmed by checking the gap if desired.

The resonance search before and after the random were compared and an example of the comparison may be seen in Figure 8.2. It is the Lid center in the Z direction and it shows increase of the amplitude of the first two peaks and almost a disappearance of the peaks around 900 and 1000Hz. It is important to realize that these changes are only caused by exposing the FDA to -12dB random vibration loads and therefore settling of the assembly is present. It was decided that the responses after the random vibration should be used for the FEM model correlation as the unit may be vibration loaded after final assembly to ensure the settled responses will occur during launch.

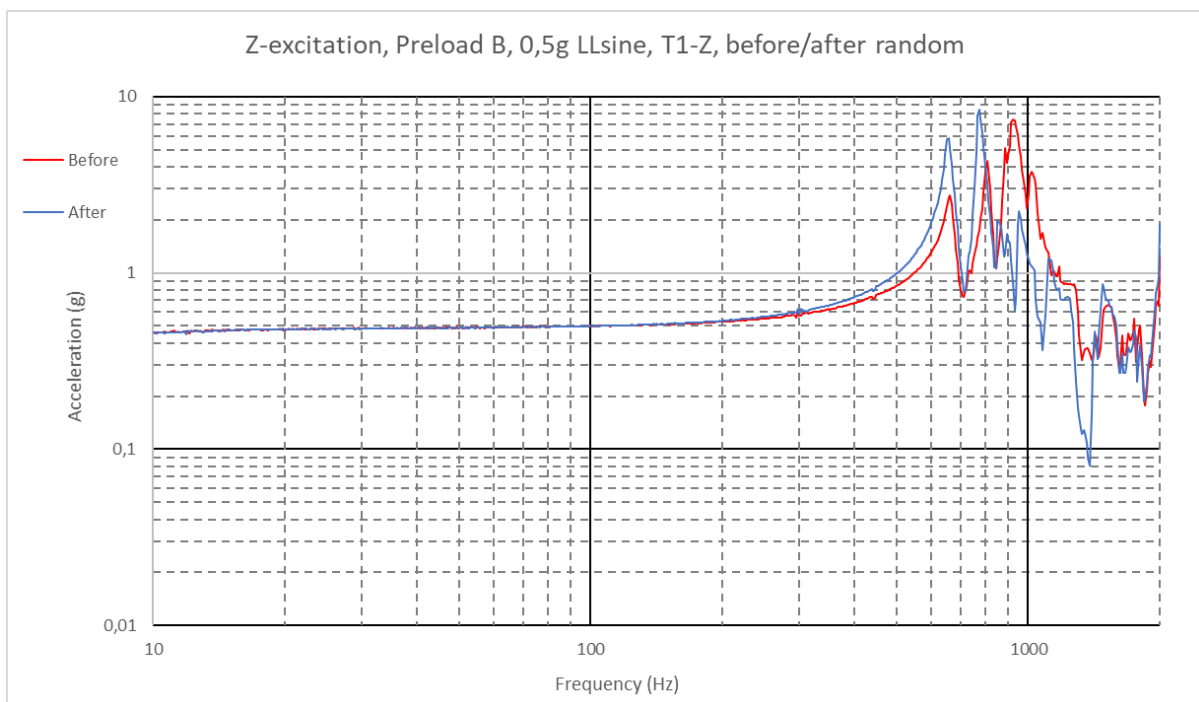


Figure 8.2 - Example of settling

8.5.1.2 Nominal preload

The Lid was tightened to the Nominal preload and the three test were run again. The responses were checked for settling and it was discovered that none settling occurred which was also confirmed by measuring the gap. This absence of settling may have two reasons: the Lid was already settled after the previous vibrations or the Nominal preload is high enough to prevent the settling.

8.5.2 Y-axis

The testing continued with Y-axis. Figure 8.3 shows the Y-axis setup and the position of all accelerometers, which is the same for each axis testing (except the control accelerometer C1).

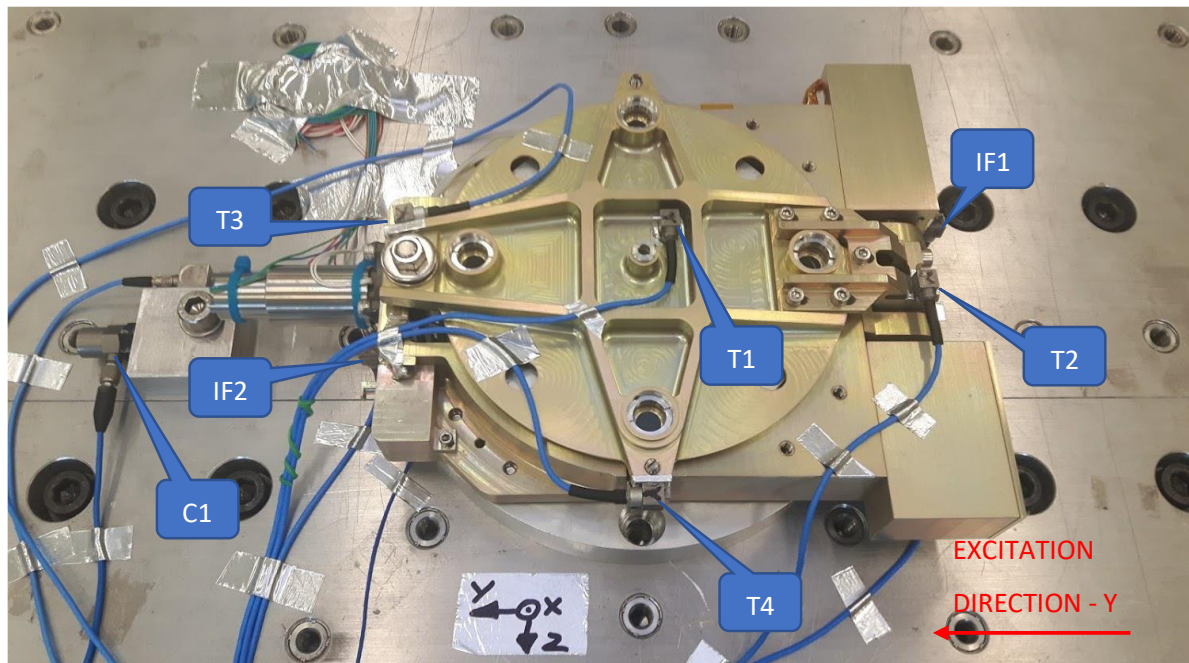


Figure 8.3 - Y-axis testing

8.5.2.1 Nominal preload

The Nominal preload was applied first this time to learn more about the settling. The three runs were performed and responses were checked for settling. This time the settling was very small, which again may have couple reasons:

The nominal preload is actually not high enough to prevent settling. It could have been high enough in the previous case, that is Z-axis with Nominal preload and still can be not sufficient in this case because the spectra and excitation axis changed.

Or some settling is always present after the Lid is opened and closed again, which is necessary for changing the excitation axis since the adapter needs to be removed from the table and the screws are unreachable while the Lid is closed. This option is very possible since after the Lid is closed it is only roughly settled in place and even though it is preloaded it can still find a different position when exposed to vibrations.

8.5.2.2 Preload B

The Lid was loosened to the Preload B and the three runs were performed. The responses were checked for settling and some shifts in frequencies were observed. Since these test were not run after the opening and closing of the Lid and previous testing was done with higher preload it seems that the Preload B is not sufficient for this excitation.

8.5.3 X-axis

The last tested axis was X, which was not tested on the slip table but directly on the vibration table.

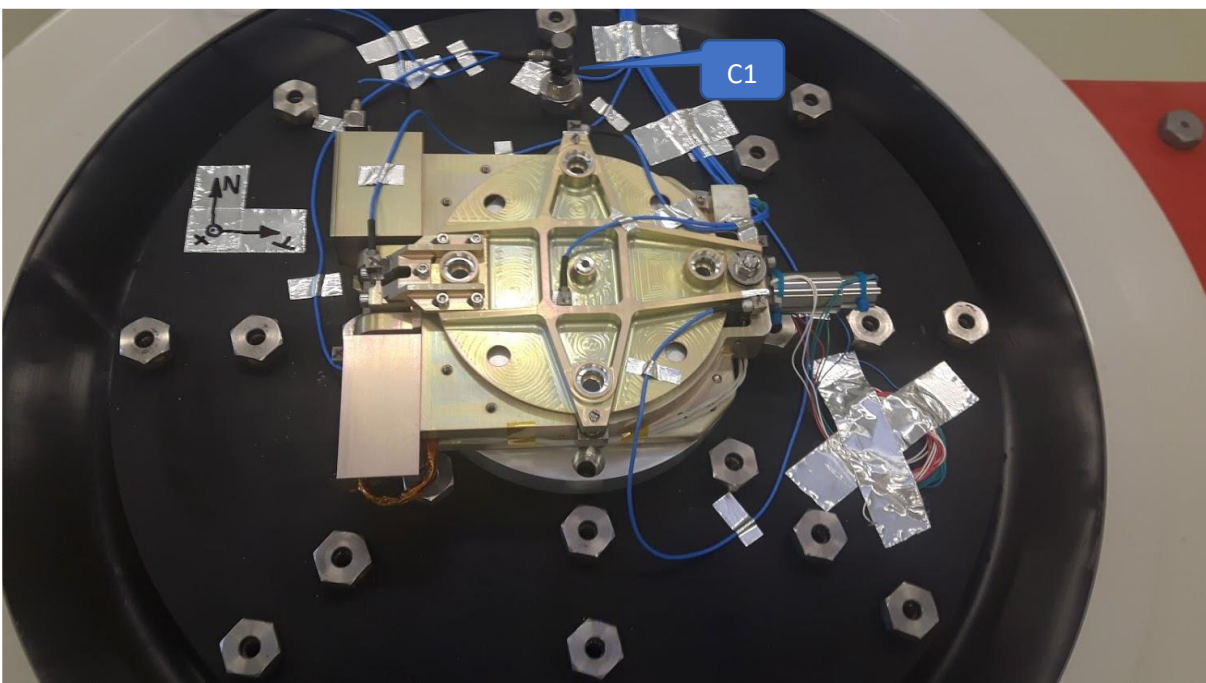


Figure 8.4 - X-axis testing

As previous testing showed, excitation in this axis is the most severe for the FDA. It causes especially big amplifications on the Motor and the test should proceed with caution to prevent some unnecessary overtesting of the components.

8.5.3.1 Nominal preload

First, the Nominal preload is set and the LL sine is run. Responses from the LL sine shows a very big amplification on the Motor IF accelerometer (IF1) in the X direction, specifically a peak at about 870Hz (Figure 8.5) with acceleration of 40g which is an amplification of 80. After checking the loading random spectra it was calculated that this peak could mean a response of $450\text{g}^2/\text{Hz}$ which is unacceptable and could lead to overtesting or damaging the Motor. This has two consequences:

The loading spectra need to be notched before further testing and the design is probably not sufficient to withstand these loads.

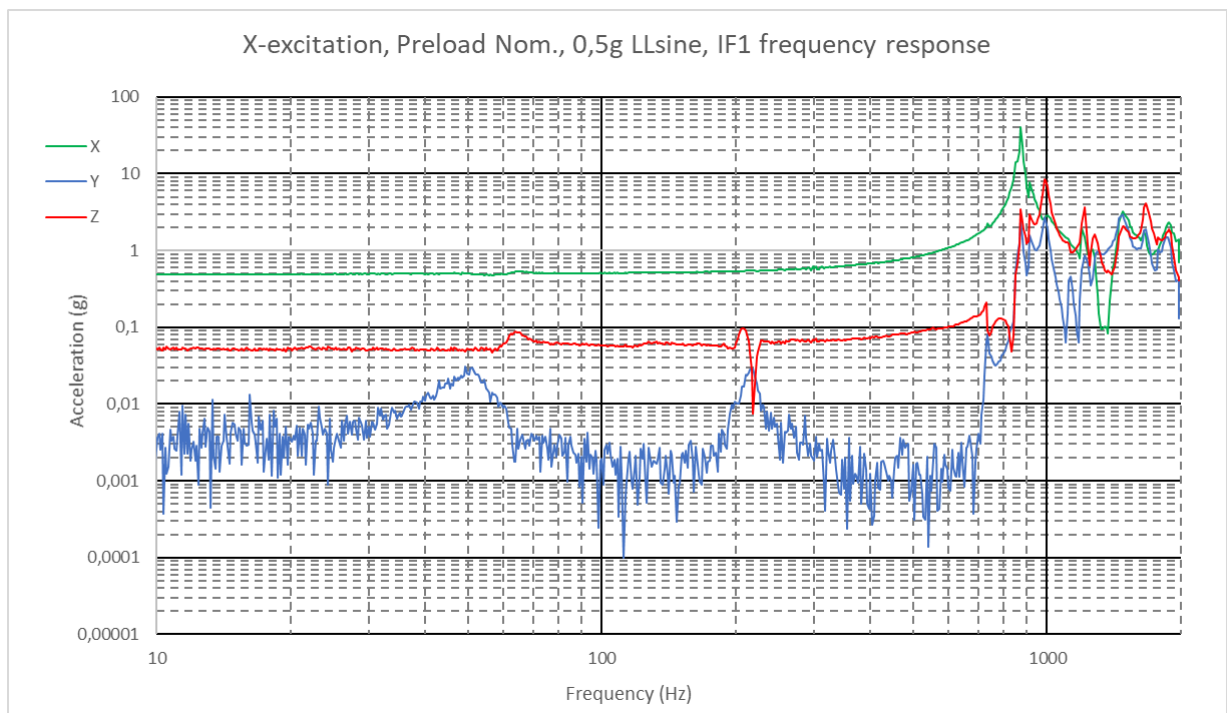


Figure 8.5 - Severe resonances in X-axis testing

8.5.3.2 Notching

Before the -12dB test could be performed the loading spectra needed to be notched to prevent possible overtesting. That means that on some chosen interval of frequencies the load is lowered by some specific amount, while the rest of the spectra remains the same. Other option is to further increase the damping of the whole spectra but since the test is already on -12dB it can not be lowered anymore. The notching allows the test to proceed and obtain the responses while avoiding any damage of the tested subject.

The notch needs to cover the very high peak at 870Hz (Figure 8.5), which couples with the peak around 900Hz in the original loading spectra (Figure 8.6), therefore, the load was set hundred times lower to $10^{-3}g^2/Hz$ on 780 to 1000Hz to cover the big resonance on the IF1. The original and the notched spectra may be seen in the Figure 8.6 below.

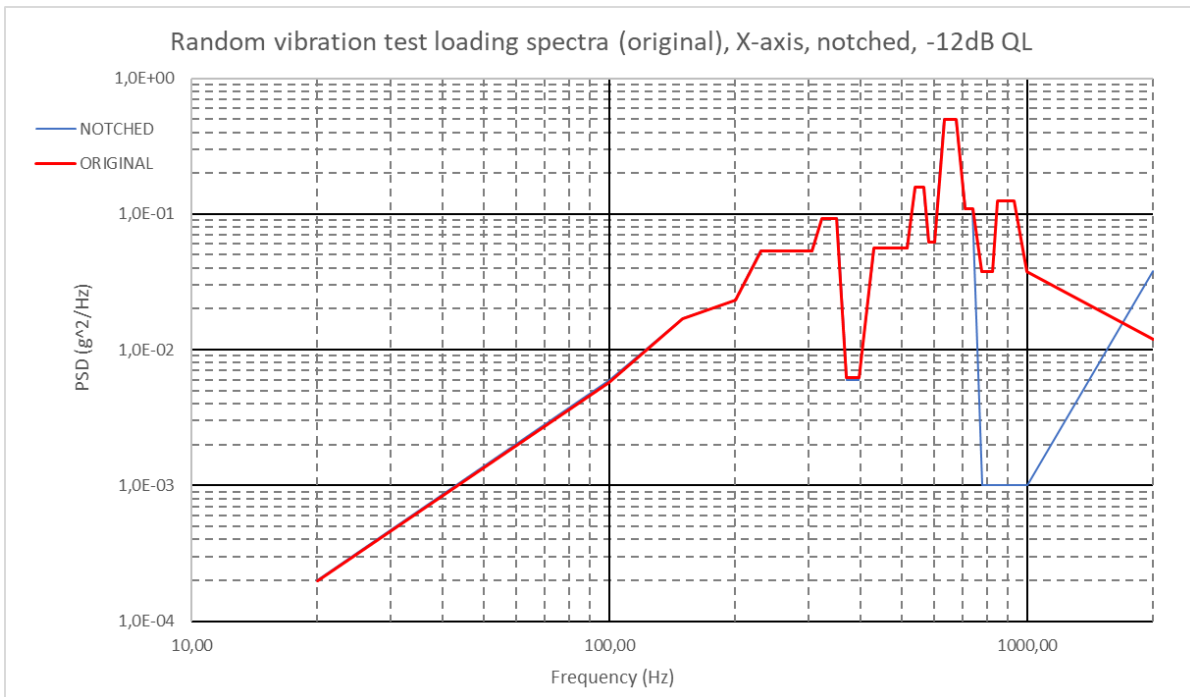


Figure 8.6 - Original/notched spectra

After the random and the second LL sine is performed the responses show almost no settling. This again may have a couple reasons:

The Nominal preload is high enough to prevent settling in this direction or notching of the spectra lowered the overall load so much that it is so low it can not cause the settling.

8.5.3.3 Preload B

After the preload is loosened to the Preload B the LL sine was run and responses were checked before further testing. The change in the preload the above mentioned big peak to a lower frequency and therefore the notching needed to be adjusted a little bit to safely cover this big peak. After the notching was done the random and second LL sine teste were run and again almost none settling was recognized.



8.6 Key failure

After the last test was performed the Lid was unlocked and opened it was found that the key that is supposed to be on the Motor shaft and should be transferring the torque from the Motor to the Lid shaft is not in place. The key fell out of the groove in which it was pressed. The big clearances between the two shafts enabled it to fall out completely. This must have occurred during some of the last couple runs since the FDA was checked and opened regularly during the testing.

Because of this failure, which could be absolutely crucial for the mission, the FDA had to stay in ESTEC for further investigation. The designer of the FDA had to come back to ESTEC one week after the testing and the FDA had to be disassembled and carefully inspected to precisely determine the reason behind the failure.

The press-fit which was used to secure the key in the shaft was not strong enough and the vibration loads shook out the key. Since there are very big clearances around the key it could fall out completely and thus could not serve its purpose anymore which would lead to complete failure of the FDA and the whole coronagraph. It was agreed that it was good that this possible threat was discovered and precautions were made to eliminate this threat.

Multiple solutions were proposed. Stronger press-fit or gluing of the key was denied as possibly not sufficient enough and still leaving a chance for failure. Securing the key by a screw was denied because it would require drilling of the Motor shaft which could possibly damage the Motor. Change of the clearances could have negative effect on the right function of the Lid. It was agreed that some kind of clamp needs to be used to secure the key. The Motor bed needed to be moved away from the Hinge to make space for the clamp which is securing the key and may be seen in Figure 4.7.

8.7 Results

The most important results of this testing are the responses used for the tuning of the FEM model. For each direction of excitation, the responses measured for the Nominal preload and after the random vibrations were chosen for the correlation and may be found in Appendix A. Figure 8.7 serves as an example.

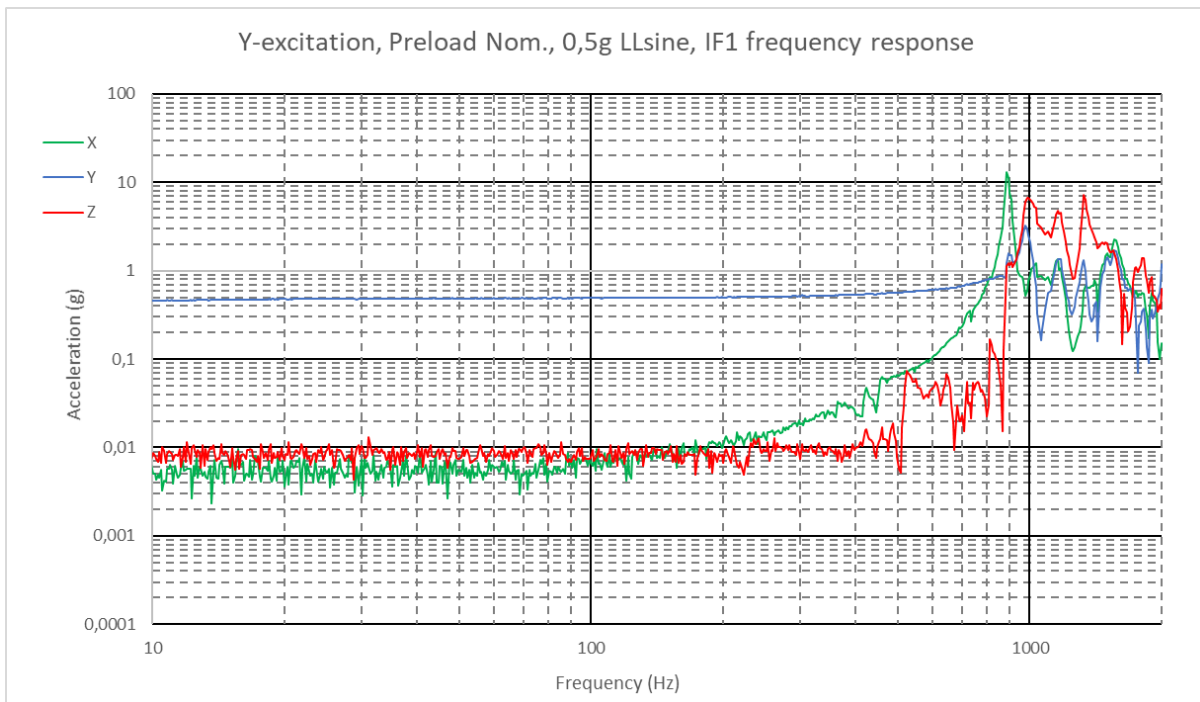


Figure 8.7 - Example of vibration testing results

8.8 Conclusion

The main goal of the testing, which is the measurement of the responses was achieved and tuning of the FEM model could begin. The dangerous resonances of the Motor were discovered and that lead to design changes described above. More was learned about the settling and effect of the Lid preload on the responses and the settling but it needs to be said, that the random loads were at -12dB and the specimen will most likely behave differently when subjected to the full spectra. On the other hand, it is expected that the spectra will change dramatically after the FEM model is tuned and send for coupled analysis.



9 Experimental modal analysis

In order to make tuning of the FEM model easier and more precise an experimental modal analysis was performed to obtain natural frequencies of certain FDA subassemblies. The second goal of the experiment is to learn more about the effect of the Lid preload on those natural frequencies. The analyzed subassemblies were the PP, the Motor and the Lid which are also measured in the vibration analysis and which are also the main tuning locations. In addition, Connector bed was measured to obtain some additional information about the FDA's resonances.

9.1 Test setup

The FDA was assembled and fastened onto the vibration adapter so the results may be comparable to the results from the vibration analysis. For each measured subassembly, locations for accelerometers placement were picked. Two three-axial accelerometers were used for each subassembly. One of those was put on the same location as for the vibration testing and the other one was placed on some other location to show more about resonances of the part of interest that is the PP, the Motor and the Lid. The Connector bed was an exception since it was not measured in the vibration testing. The locations of the accelerometers may be seen in the figures of each measurement setup.

The impulses for the resonance excitation were applied by special self-made device build by an electrical engineer in Serenum. Its hammer may be seen in the figures below as a small aluminum sphere with rubber coating. It uses a coil to induce a short magnetic force which strikes the hammer with the same force every time. It is very good for this experiment since the impulse is repeatable and gives nice responses.

The time-domain responses obtained from the accelerometers were run through a Scilab script which performer a FFT and plotted the frequency-domain responses with the highest peak marked and the frequency at which it occurred noted.



9.2 Measurements

It was decided to measure the PP in X and Z direction, the Motor in X and Y direction, the Lid in X direction and the Connector bed in each direction. That makes eight total measurement series. In order to learn about the effect of the Lid preload on the responses the preload was set to Nominal (see Chapter 7) before each measurement series and the nut was loosened by sixth of a revolution before each measurement until no preload was present anymore which occurred in a dramatic change of the responses. That makes nineteen measurements for each series.

Example of setup and response for one measurement for the three main locations may be seen below. The accelerometers are noted so the number one is in the same location that is used for vibration testing. The pictures with responses are exported from the Scilab and show an acceleration (g) on the frequency range up to 2000Hz for the biggest preload (Nominal). There are six lines, one for each axis of both accelerometers. The coordination system is according to FDA global CSYS (see Chapter 5.2). One of the accelerometers uses darker and one uses lighter colors and the axis are X(res), Y(green), Z(blue). It is not that important to distinguish the lines but only to find the first natural frequency of the measured subassembly (which is not always the biggest one) which is noted in the responses.

9.2.1 Motor X-axis

The setup is with the accelerometers placed at the Motor-Motor bed interface and at the end of the Motor. The hammer is exciting the Motor from the bottom in the X-axis of the FDA. The response shows the first natural frequency just below 800Hz.

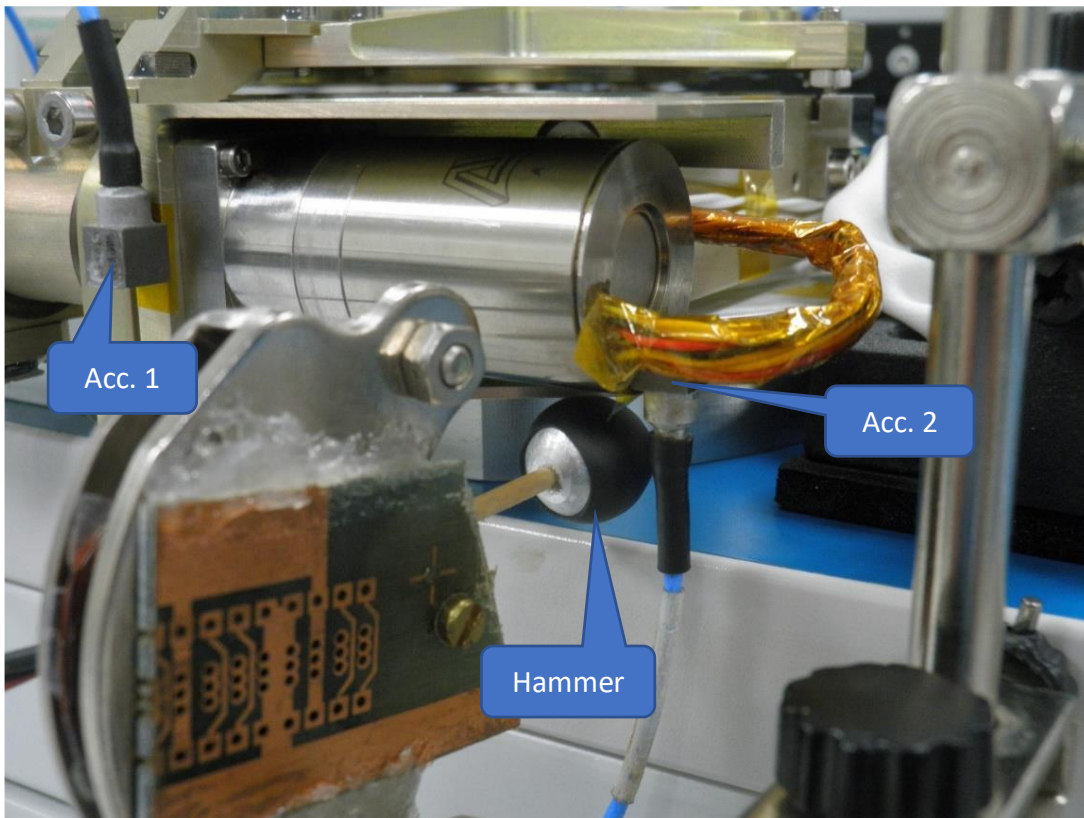


Figure 9.1 - Motor - X-axis excitation setup

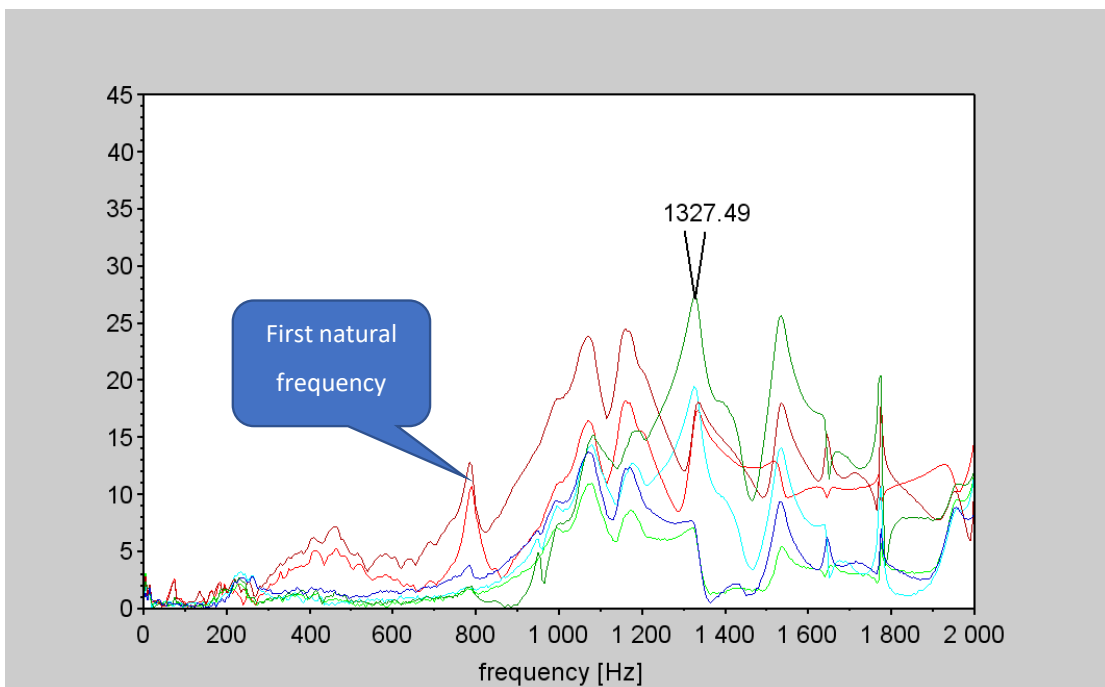


Figure 9.2 - Motor - X-axis excitation response

9.2.2 Pin-puller Z-axis

One of the accelerometers is placed close to the interface of the Pin-Puller (PP) and the Flange and the other one is placed on the end of the PP. The hammer strikes the PP from the side in the Z direction and the response shows the first natural frequency of the PP at 907Hz.

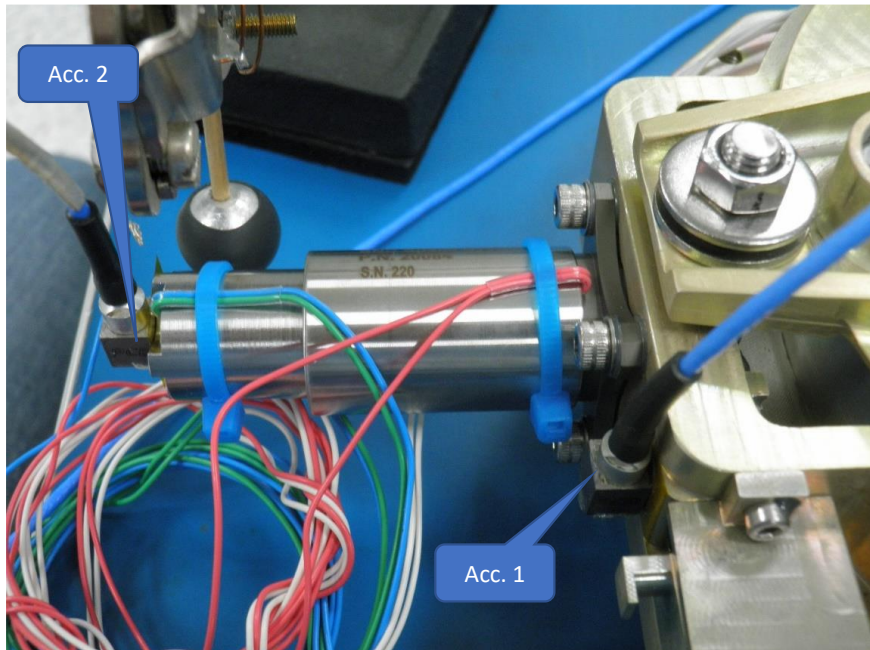


Figure 9.3 - Pin-puller - Z-axis excitation setup

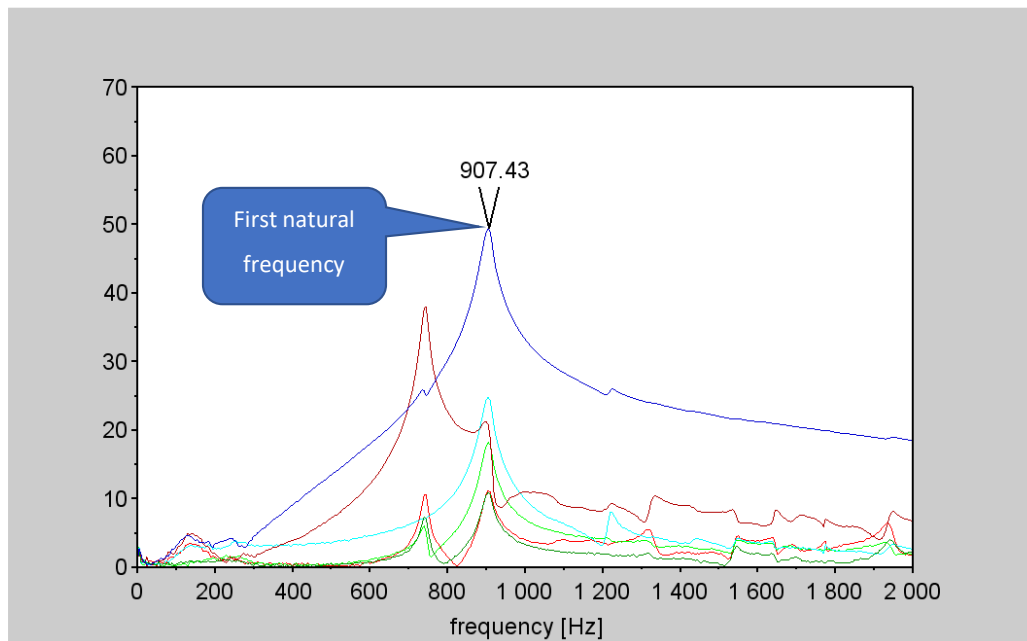


Figure 9.4 - Pin-puller - Z-axis excitation response

9.2.3 Lid X-axis

The first accelerometer is placed in the center of the Lid and the second one is on the very thin part of the Lid close to the edge. The hammer strikes the Lid from above in the X direction and the response shows the first natural frequency just below 1000Hz. The response also shows how much more complex and complicated is the Lid from the vibration response perspective. The PP is the simplest one as it is almost a perfect cantilever, the Motor is a little more complicated with the Motor bed and the Lid is the most complex.

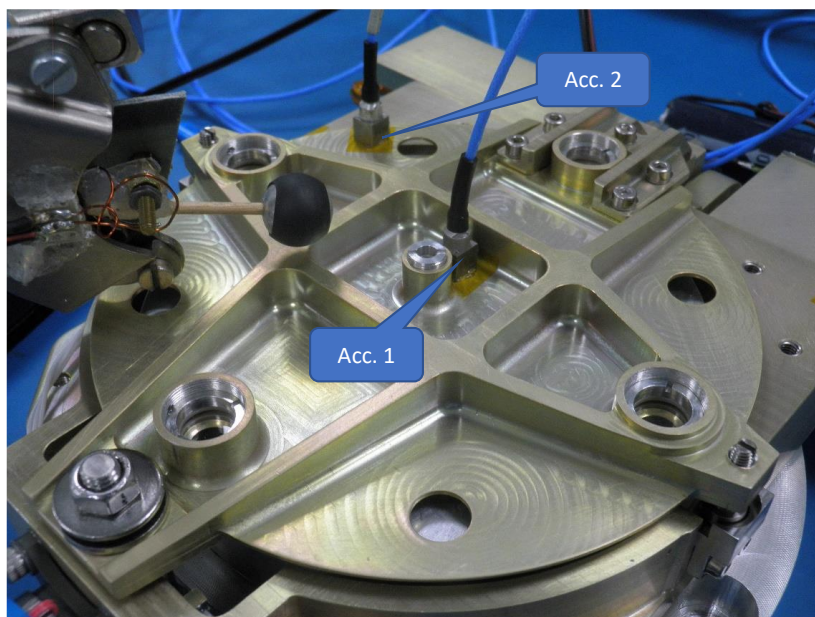


Figure 9.5 - Lid - X-axis excitation setup

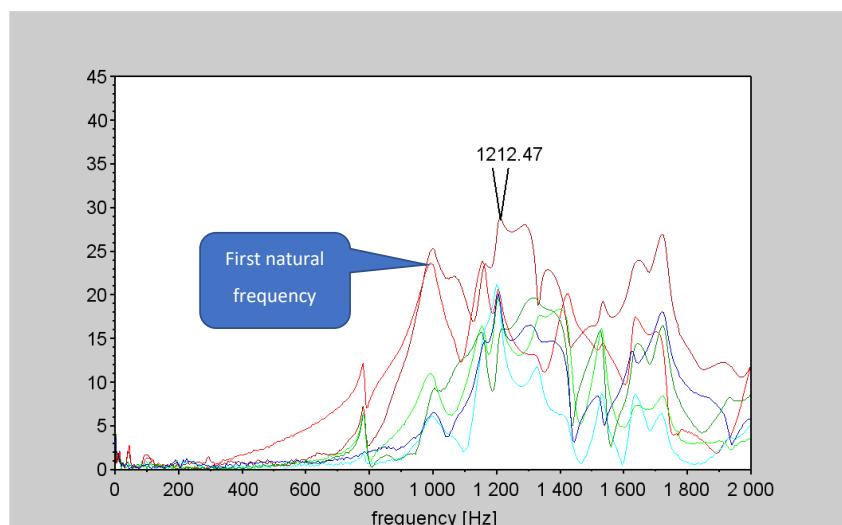


Figure 9.6 - Lid - X-axis excitation response



10 FEM model tuning

After the FEM model is created it can not provide results that would correspond to reality since lot of simplifications were applied in the creation of the model as described in Chapter 5. Some features and parts were taken out of the model, no contacts were modeled, some parts were replaced by a point mass and the screws were modeled by rigid elements and springs. With all of these simplifications, the results from a computation would be far from correct and the model could not provide any information about the mechanical behavior of the FDA.

For this reason, the model needs to be tuned (correlated) so its results correspond to reality. In order to do that, the results from real vibration test are required so the results from the FEM analysis may be compared to something. Those results are obtained from vibration testing of the FDA DM which is described in Chapter 8. After the vibration testing is done it provides responses to 0,5g LL sine in certain points of the DM (IF1, IF2, T1) These responses may be found in Appendix A and are used to create transfer functions which describe the relationship between the excitation acceleration and the response acceleration at certain point in terms of amplification. Then the a 1g LL sine load may be applied to the FEM model at the excitation point and acceleration responses in the same locations may be obtained from FEM analysis. These responses are also transfer functions and show amplification since the input is 1g. The transfer functions from the vibration testing may be then compared to the transfer functions from the FEM analysis and the goal of the correlation is to tune certain parameters of the model to make the transfer functions match as much as possible. This process is often said to be the most difficult part of the FEM model creation and the whole mechanical analysis.

10.1 Locations

Before the vibration testing and the tuning begins the locations at which the responses will be compared need to be chosen. Those locations are then mounted with accelerometers during the vibration testing and also are measured in the FEM computations.



In case of FDA, three locations were chosen based on preliminary vibration simulations and recommendation from ESA.

The first and probably the most important location is the interface of Motor and Motor bed (IF1). The Motor makes almost fifth of the total mass of the FDA and the biggest responses are expected here.

The second location is the PP-Flange interface (IF2). The PP is also a high-mass component of the FDA and is similar to the Motor as kind of a cantilever beam so high and low-frequency responses may be expected. The Motor and PP interfaces are also measured to learn about possible dangerous loads of the expensive equipment which the Motor and PP are.

The third location is the center of the Lid (T1). The Lid is the moving part of the FDA a even though it is locked and preloaded when the vibrations are applied it may still move and vibrate a extensively since it is not rigidly connected and may cause some important eigenmodes.

The locations of the accelerometers may be seen in Figure 8.3 as IF1, IF2, and T1. Some additional locations were measured during the vibration testing but those were only for further information about behavior of the unit and are not used for the tuning. The locations measured in the FEM analysis may be seen in the following Figure 10.1.

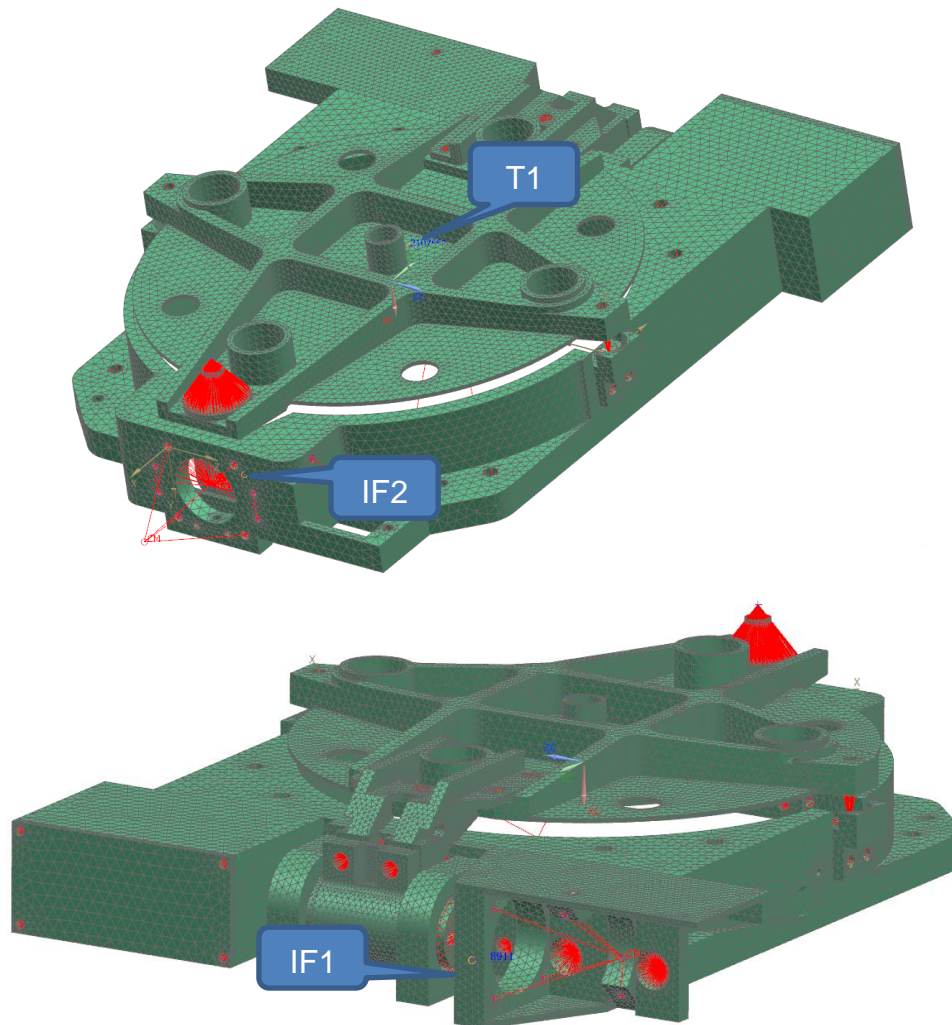


Figure 10.1 - FEM model tuned locations

10.2 Parameters

There are many parameters of the FEM model that can be tuned to correlate the model. These parameters may be material properties of used materials, masses of concentrated mass-points and most importantly stiffnesses of the screws which are the most suitable parameters for tuning. The screws are modeled as described in Chapter 5.6 and the stiffness of the CBUSH element may be set as desired. Each CBUSH element has a stiffness in each axis and rotational stiffness about each axis. That is six parameters for each CBUSH element. There is thirteen groups of screws and other connections with varying number of screws in the groups which makes it about fifty CBUSH elements that may be tuned. That is total of three hundred



parameters which is a very large number and thus some simplifications and time-saving choices needed to be made to make the correlation possible.

10.3 Method

Multiple methods of automatization of the tuning process are known and used but none of those were used for the following reasons.

Even though the number of parameters is very high and it would be suitable to use some automatization, the computation time of one iteration was about ten minutes and that is too much for the methods that tries a very high number of iterations in order to find the optimal parameters.

As found later in the tuning process the system sometimes behaves very unpredictably as various parameters and resonances influence each other differently at different frequencies and so on. This could be very difficult for the tuning algorithm since it could not really predict the behavior and know if it is or if it is not getting closer to the optimal result.

The final reason is that the company at that time simply have not had the capacity to create such optimization algorithm and could not afford hiring an external company especially when the possible results were uncertain.

For those reasons the tuning of the FEM model was done manually. The process may be summarized as follows:

- 1) Set the tuned parameters or change them based on previous results
- 2) Run the simulation (about 10 minutes)
- 3) Export the responses to a spreadsheet where they are compared to previous results and with the responses from vibration testing
- 4) Analyze the results and determine the effects of the changed parameters
- 5) Determine changes in parameters for next iteration
- 6) Repeat the process

This process was unfortunately very time consuming and each iteration took from thirty minutes to hours or days depending on how long the step 4) was. Over a hundred iterations were done and the whole tuning took months to finish and still the results are far from perfect.



10.4 The procedure and simplifications

During the first weeks of the tuning, it was decided which parameters will be tuned. All of the tuned parameters are stiffnesses of selected screws and the list of the parameters may be found in Appendix C. At the beginning the model was only tuned in the X-axis. The three translational stiffness always had the same value and the rotational ones had half the value. This was fine-tuned later.

During the process as the understanding of the model behavior grew bigger it was observed which connections has the biggest impact on the measured locations. That may be summarized in the following table:

Table 10.1 - Connections impactful for the tuning

Location	Impactful connection
IF1 – Motor IF	Flange – Tube
	Flange – Motor bed
	Motor bed – Motor
IF2 – PP IF	Flange – Tube
	Flange – Pin-Puller
	Flange – Nose
T1 – Lid center	Flange – Tube
	Touch-screw – Touch down
	Flange – Nose
	Hinge - Shaft

After this observation most of the other connections were set as relatively rigid which was decided to be 200×10^6 N/mm. Then all the connections listed in Table 10.1 were tuned for weeks, except the Flange-Motor bed connection which was also decided to be rigid.

Table 10.1 shows that the Flange-Tube connection has a big impact on all the locations. That is very much expected since this connection is the interface between the whole model and the rest of the satellite or in this case the excitation point.



10.5 Results

After months of tuning the results were found sufficient and may be found in Appendix C. The table of the tuned parameters shows the final values of the parameters. Some values are very low (around 10^3 N/mm) which is usually true for the contact connections but also for the Flange-PP connection where the low stiffness is caused by the use of plastic washers. The most difficult location to tune was definitely the Lid center since the Lid has quite complex shape and the Lid is tuned by three contact connections which stiffnesses are very hard to define.

The figures comparing the test and FEM transfer functions may also be found in Appendix C and those figures represent the final quality of the tuning which is far from perfect. The transfer functions differ especially in the higher frequencies where the behavior of the model starts to be quite unpredictable and in the Y and Z directions since it was very difficult to tune the model for each direction with the same parameters.

Despite these imperfections in the correlation the results were accepted and found sufficient enough after months of tuning. Further improvement would not be certain and could possibly severely delay the whole project.



11 Mechanical analysis

After the FEM model is created and tuned a series of simulations need to be performed according to general and specific requirements and discussion with ESA. The static analysis is performed to check if the FDA parts and screws can withstand the Lid preload. The modal analysis is performed to obtain the information about the general modal behavior of the unit. The quasi-static analysis is performed to check the structure against the quasi-static accelerations during the launch and the random analysis checks the FDA against the random vibrations loads that also occur during launch. The sine and shock analyses were excluded from the thesis even though these were performed in the project. The reason for exclusion from the thesis is very low loads which causes insignificant responses which are unnecessary to be discussed in the thesis.

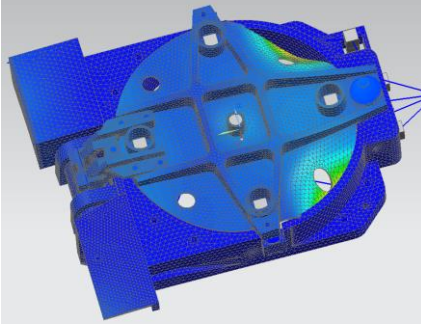
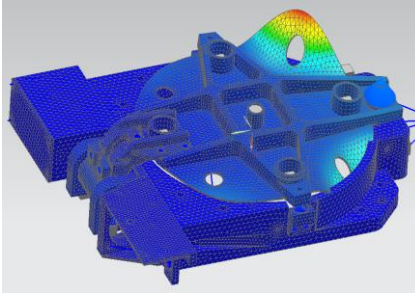
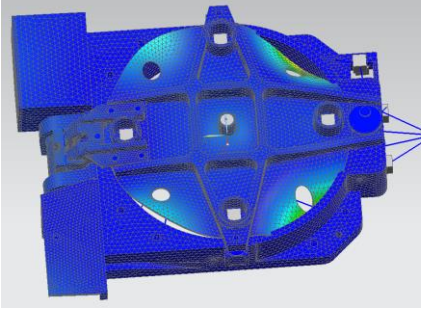
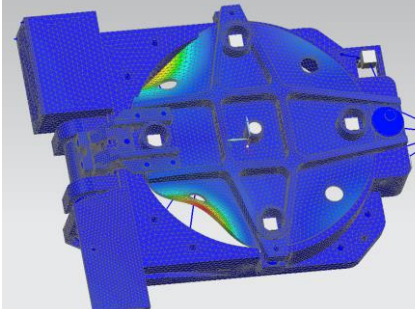
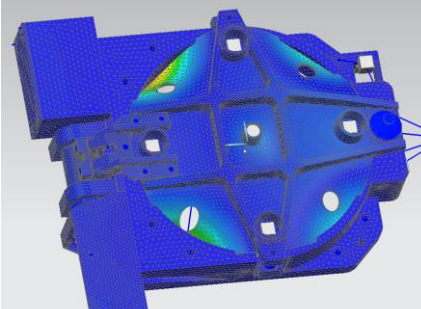
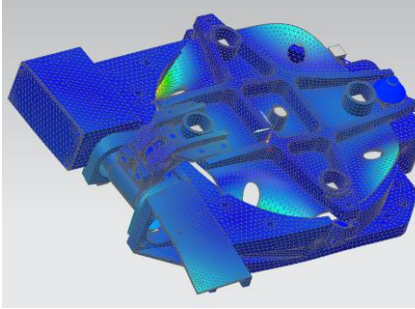
11.1 Modal analysis

It was required to perform the modal analysis to up to 10 000Hz and summarize the eigenmodes and modal effective masses. The modal FEM model (see Chapter 5) was used without the Lid preload or any constrains. The NX NASTRAN's solution SOL103 Response Simulation was used. This solution performs the same modal analysis as for this purpose usually used SOL103 Real Eigenvalues solution but can be then used for response simulation such as random vibration loads. The eigenmodes frequencies and shapes up to 2000Hz are summarized in the following Table 11.1.



Table 11.1 - Modes up to 2000Hz summary

Modes		Eigenmodes Shape	Modes		Eigenmodes Shape
No	Freq		No	Freq	
1	921		2	968	
3	1015		4	1208	
5	1269		6	1311	
7	1336		8	1358	

Modes		Eigenmodes Shape	Modes		Eigenmodes Shape
No	Freq		No	Freq	
9	1426		10	1480	
11	1523		12	1614	
13	1687		14	1821	

The modal effective mass fractions of modes up to 2000Hz are summarized in Table 11.2. The bigger fractions are highlighted. The most significant modes may be observed in this table. It is especially the first mode created by the high-mass Pin-puller, the second mode with main participation of the Lid shaft oscillation in the friction journals and the fourth mode as the main Motor mode. These modes are causing the biggest responses in the random analysis.



Table 11.2 - Modal effective mass fractions up to 2000Hz summary

Mode (-)	Eigenfrequency (Hz)	Effective mass fraction					
		X(%)	Y(%)	Z(%)	RX(%)	RY(%)	RZ(%)
1	921	9.9	0.0	0.0	0.0	0.0	20.1
2	968	0.1	0.0	19.2	5.8	1.0	0.1
3	1015	12.2	2.1	0.0	0.0	0.1	0.3
4	1208	23.0	5.8	0.7	0.1	9.1	35.9
5	1269	0.1	0.3	1.8	0.4	16.5	0.0
6	1311	0.5	0.0	0.0	0.1	3.4	0.4
7	1336	0.0	0.0	5.1	10.4	0.3	0.0
8	1358	4.2	4.1	0.2	0.9	0.1	11.7
9	1426	1.5	7.9	0.0	0.1	0.2	0.2
10	1480	0.0	0.0	2.6	3.9	1.7	0.0
11	1523	0.0	0.6	0.0	0.0	0.1	0.5
12	1614	0.0	0.0	0.0	0.8	1.3	0.0
13	1687	0.2	0.0	0.0	0.1	0.0	0.0
14	1821	0.1	0.0	4.9	11.7	0.3	0.0
Effective mass fraction sum		85.1	93.1	91.9	94.6	80.6	91.5

11.2 Random simulation

Despite the fact that the random vibration loading levels were significantly lowered after the coupled analysis with the tuned model the random vibrations are still the most significant loads of the unit. The random vibration analysis was performed to determine the required Lid preload force and to check the stresses in parts and forces in screws.

11.2.1 Boundary conditions

The model was constrained in the excitation point which may be seen in Figure 5.7. A Fixed Rotation constraint about each axis was applied with an Enforced Motion constraint applied in the direction of each axis. This constraint in default fixes the translation in the given direction while at the same time enables application of an excitation in the response simulation.



Table 11.3 - Random simulation boundary conditions

DOF	X	Y	Z	RX	RY	RZ
Constraint	Enforced motion	Enforced motion	Enforced motion	Fixed rotation	Fixed rotation	Fixed rotation

The loads are applied separately for each axis and the computation is also done separately for each axis. The random vibration loads are applied to the excitation location on the enforced motion constraints. The new random vibration loading spectra may be found in Appendix D where they are also compared to the original spectra so the reduction in the loads is apparent.

11.2.2 The simulation

A Response Simulation add-on of NX 10 was used to compute the responses. It takes results from the SOL103 Response Simulation modal analysis. Two very important parameters need to be specified before the random simulation and that is the additional spectral lines and the damping. These parameters influence what the transfer functions calculated from the modal analysis look like. The modal analysis only computes the eigenfrequencies and the eigenshapes and therefore it does not provide the results between the individual eigenfrequencies. To obtain the full transfer functions the damping and additional spectral lines parameters were specified. The additional spectral lines parameter basically defines how fine is the approximation of the transfer function between the eigenfrequencies and was set to 100 spectral lines between each eigenfrequency. The damping parameter influence how high the peaks at the eigenfrequencies are and what does the transfer function looks like between the peaks and was set to 1% viscous damping.

The response simulation is, in fact, a very simple computation. After the excitations are applied a request for response in a certain node is applied and the transfer function is calculated. This transfer function gives a relation between the acceleration at the excitation point and at the node of interest. Then the input excitation spectra is simply multiplied by the transfer function and the result is the response (PSD) at that node. Therefore, the random response computation may be very fast if only a couple of nodes is computed but for the whole model, it took

around one day. Figure 11.1 shows the input spectra multiplied (amplified) by the transfer function and giving the output response at the Motor bed IF node.

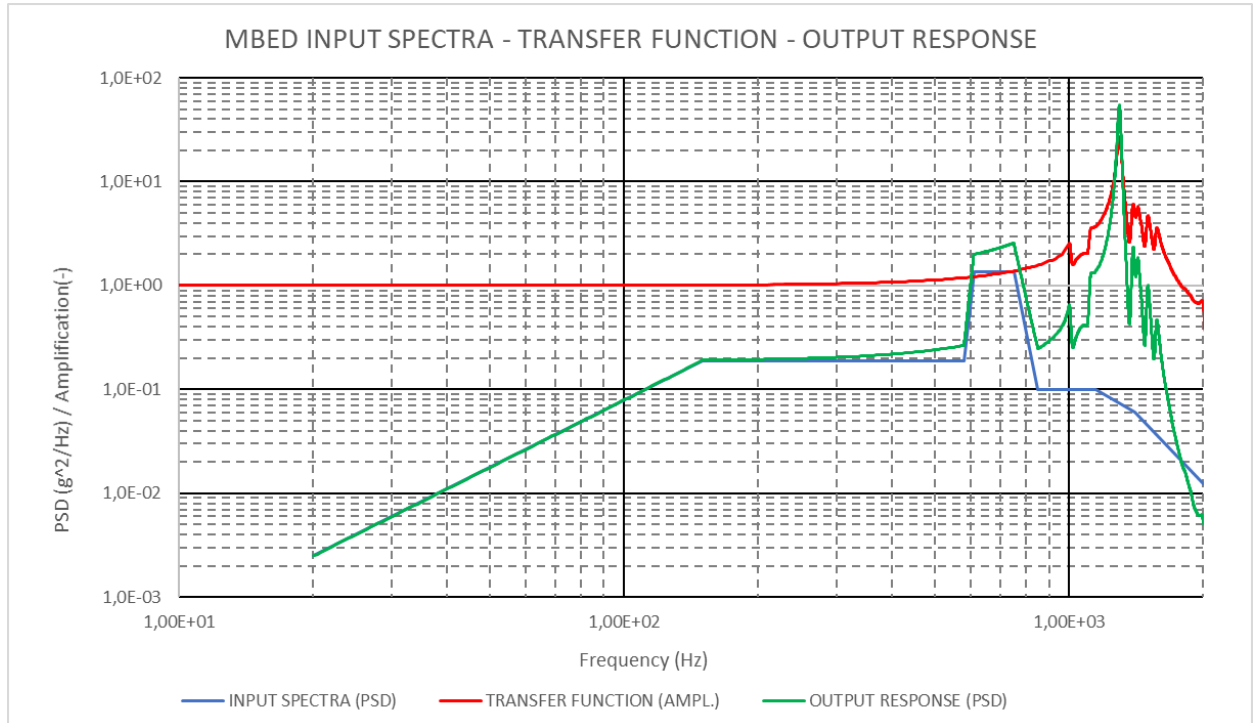


Figure 11.1 - PSD calculation example

Using much more complicated equations than just a simple multiplication the software can also compute stresses in given 3D elements and forces in the CBUSH screw elements. The results are discussed later.

The Lid preload force (see Chapter 7) was calculated in the same way as in the preliminary simulation (see Chapter 6). The random loading spectra were applied in each direction and the force in the element connecting the Lid and the Pin-puller was calculated in each direction. The biggest value, which is 26N, was then used to calculate the preload force using equation 7-1.

Table 11.4 – Random forces at PP-Lid

Excitation axis	Force component (N)		
	X	Y	Z
X	26	11	2
Y	11	4	1
Z	2	1	8



$$F_p = M \cdot k \cdot (3 \cdot F_{FEM}) = 2 \cdot 1,2 \cdot (3 \cdot 26) = 187 [N] \quad (11-1)$$

This force will be used in the static preload analysis and in the actual preload of the Lid on the Qualification and Flight model.

11.3 Quasi-static simulation

The preload calculated in the random simulation was applied on the Lid along with the quasi-static acceleration loads summarized in Table 11.5. The QS simulation was done separately for each axis and also separately for positive and negative direction of each axis because the output loads could be different. After the six simulation were performed it was found that the results in positive and negative direction are nearly the same so only results from the positive direction were used later in the stress and force calculations.

The model was constrained at the excitation point with a fixed constraint for all six DOFs and the acceleration was applied to all elements in the model.

Table 11.5 - Quasi-static analysis boundary conditions

DOF	X	Y	Z	RX	RY	RZ
Constraint	Fixed translation	Fixed translation	Fixed translation	Fixed rotation	Fixed rotation	Fixed rotation

Table 11.6 - Quasi-static loads summary

Excitation axis	Quasi-static loads (g)
X	81
Y	121
Z	83

The biggest force between the Lid and the Pin-puller was 63N which is lower than the 3σ value of 78N from the random simulation and therefore the preload will be set according to the random simulation.

11.4 Static simulation

The preload force of 187N calculated from the random simulation was applied in the X direction at the BEAM element connecting the Lid and the Lid nose (see Figure 5.6). The model was constrained the same way as in the QS simulation. Figure 11.2 shows the maximum elemental Von-Mises stress of 53,8MPa at the Lid rib.

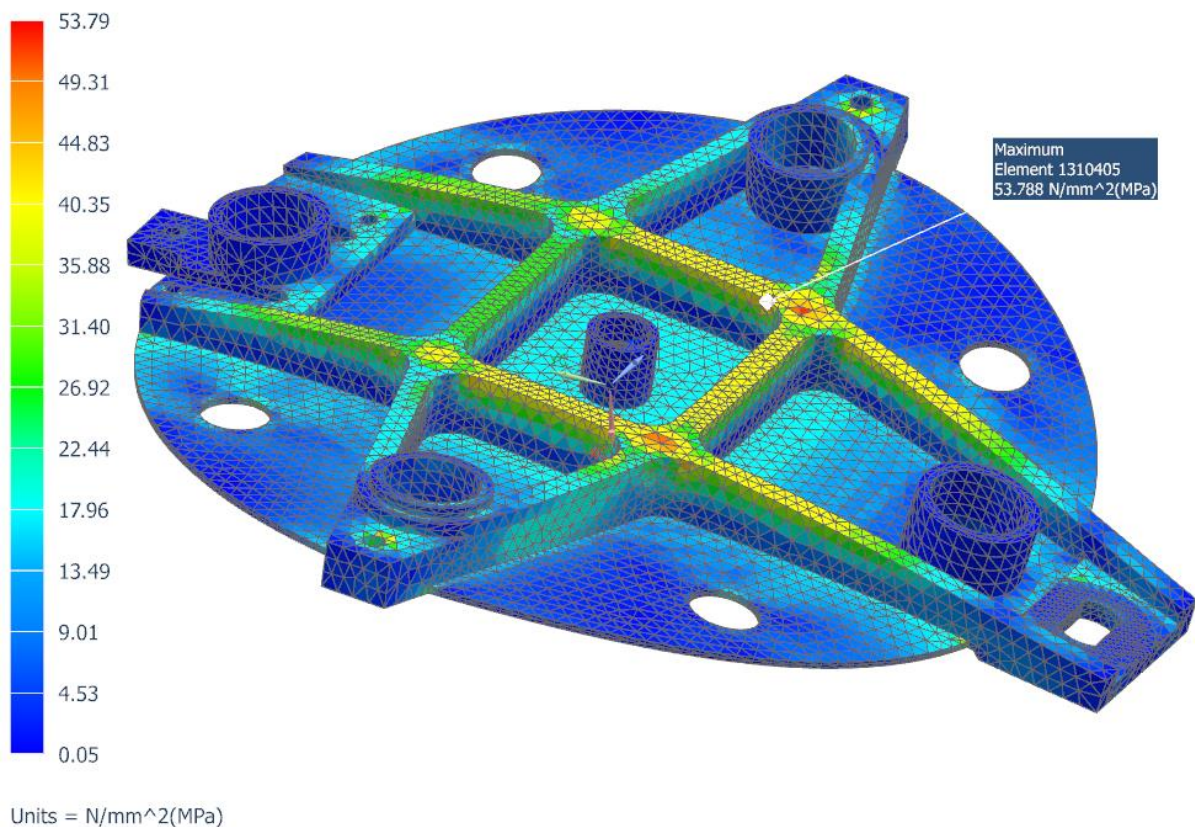


Figure 11.2 - Lid Static simulation Von-Mises stress contour

11.5 Stress evaluation

The stress in parts was evaluated for two loading cases. The first one was random loads combined with the Lid preload and the second one was the quasi-static loads combined with the Lid preload. Both cases were calculated for each loading direction and the Margins of Safety (MoS) were evaluated against both yield and ultimate strength. The Factors of Safety (FoS) were set according to the requirements to 1,65 against yield failure and 2,25 against ultimate failure.



11.5.1 Random

The model was loaded with the random loading spectra (Appendix D) in each direction separately and the maximum average elemental VonMises stress was evaluated in the chosen parts. Some parts with very low mass were excluded from the evaluation. The stresses in elements directly adjected to the screw holes were not taken into account despite the fact that those elements showed the biggest stresses the loading of these elements is not representative due to the RBE2 connections causing high stress concentrations. Therefore, for every evaluated part the element with the highest stress and at the same time not adjected to a hole was chosen for the calculation.

Because the random vibration simulation can not be run with the Lid preload applied the static preload simulation was run separately and the results from both analyses were combined using post-processing tool before the stress evaluations. The results for each loading axis including the highest stresses and positive MoS may be found in Appendix E.

11.5.2 Quasi-static

The model was loaded with the quasi-static accelerations in each direction separately with the static Lid preload always present. In this case, the simulation can be run with both the QS acceleration and the preload acting together. Then the maximum average elemental VonMises stress was obtained for each evaluated part and the results from this analysis with all the positive MoS for each axis may also be found in Appendix E.

11.6 Screw forces evaluation

In both Random and Quasi-static simulations described above the forces in screws need to be evaluated. It was done for selected groups of fasteners (see Table 12.1) and the biggest and second-biggest axial and two lateral force components were evaluated in the CBUSH elements. The results may be found in Appendix E and are used in the following chapter.



12 Threaded fasteners

All threaded fasteners have to show positive Margins of Safety (MoS) against tightening failure, tensile failure, gapping, slipping and thread pullout. In addition, a worst-case scenario where one of the screws in a group fails and the rest of the screws in that group have to carry the load has to be evaluated. The MoS were calculated using a handbook provided by ESA [5] which shows a recommended procedure of the MoS calculations.

12.1 Loads

The first and often also the biggest load which the screws are subjected to is the tightening torque. It results in a tensile and shear load and the screw has to withstand the combination of those two. The tightening torque leaves the screw preloaded which is very important for the right function of the joint especially for the resistance against gapping and slipping but also for resistance against fatigue although fatigue is not calculated for the FDA threaded fasteners. The theory behind preloaded joints can be also found in the handbook [5].

As mentioned above all the screws are preloaded and therefore constantly subjected to tensile load. The Lid is then preloaded (see Chapter 7) which leads to more tensile and also shear loads of the screws. During the launch, the whole FDA is subjected to shock, random and sine loads which leads to additional tensile and shear loads. The loads from the shock, random and sine loads are obtained from the FEM simulation and with many other parameters then serve as an input to a spreadsheet which calculates MoS of the threaded fasteners based of the handbook. The procedure used in the spreadsheet will be detailed later.

The calculations were done for fasteners groups shown in Table 12.1. The remaining groups were excluded from the calculations based on previous calculations which showed insignificant loads in those groups.



Table 12.1 - Calculated groups of fasteners

Part 1	Part 2	QTY.	SCREW	VENTED	MATERIAL
Flange	Tube	8	M4x12	N	AISI304(A2)
Flange	Motor bed	6	M4x10 COUNTERSUNK	Y	AISI304(A2)
Flange	Hinge	4	M4x8 COUNTERSUNK	N	AISI304(A2)
Flange	Conn. box	3	M4x10 COUNTERSUNK	Y	AISI304(A2)
Flange	Touch down	2	M3x8	N	AISI304(A2)
Flange	Pin puller	4	SCREW #6-32 3/8", C-606-N	N	AISI304(A2)
Motor bed	Motor	4	M2x10	N	AISI304(A2)
Lid	Lid-arm	5	M3x8	N	AISI304(A2)
Lid	Touch-screw	2	M4	N	Titanium
Motor bed	Motor clamp	2	M3x8	N	AISI304(A2)

12.2 Calculation

The procedure of calculation of the MoS will be detailed in this chapter. The calculation process is quite complicated and uses a lot of formulas, terms, and symbols and not all of those are explained every time they appear in the text but all may be found in the list of symbols at the end of the thesis. The theory behind the following formulas will not be detailed since it can be found in the handbook [5] and many other sources and since it is not a topic of this chapter to teach this theory but only to detail how the MoS were evaluated.

The first input into the calculation spreadsheet for each group of screws is the type of the used screw, what kind of thread does it have, how many screws is in the group, if the screw is vented and if a helicoil insert is used. Based on these inputs the geometrical parameters of the thread are acquired from standards.

Vented screws have a hole going through the whole screw on the axis of the thread and are used in case the threaded hole in the second clamped part does not go all the way through the part and therefore a cavity is created after the screw is mounted as shown in Figure 12.1. If the screw is not vented the air trapped in the cavity will expand dramatically during launch because of the fast decrease of the ambient pressure in the fairing of the launcher and that could lead to damaging of the bolted joint.

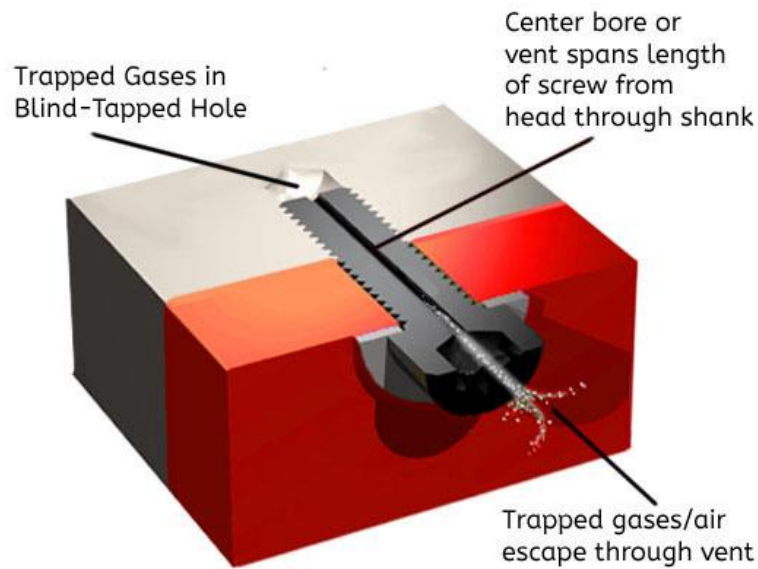


Figure 12.1 - Illustration of a vented screw

The use of helicoil inserts is requested in the Requirements document (R-6224) for all screws. The helicoil inserts give the thread a longer effective length of the thread so the load is distributed over larger area and the thread is much more resistant against thread pullout failure.

The next input of the spreadsheet are the materials properties of the screw and of all the clamped parts which in this case is always just two. The material properties are obtained from standards and may be seen in Table 12.3. Also, the geometry of the whole joint needs to be specified in order to calculate the force ratio and other important parameters of the joint. The geometry parameters of the joint is tensile loaded length of the screw, thickness of both clamped parts and diameter of the hole in the clamped parts.

Table 12.2 - Material properties of clamped parts

Material	Young's modulus E (MPa)	Yield strength σ_y (MPa)	Ultimate strength σ_{ult} (MPa)
AISI304(A2)	193000	505	215
Titanium grade 5	114000	1100	1170

Based on these input parameters the compliance of the screw is calculated simply as a compliance of a cylinder with given geometry and material:



$$\delta_b = \frac{L}{E_b A_0} \left[\frac{mm}{N} \right] \quad (12-1)$$

The compliance of the clamped parts is calculated similarly. The area around the screw contributing to the compliance of the parts is simplified to a “sleeve” with inner diameter D_h and outer diameter D_{uh} .

$$\delta_c = \frac{L_1}{E_{c1} \frac{\pi}{D_{(uh,brg)}^2 - D_h^2}} + \frac{L_2}{E_{c2} \frac{\pi}{D_{(uh,brg)}^2 - D_h^2}} \left[\frac{mm}{N} \right] \quad (12-2)$$

Since no bolted connection on the FDA clamps two parts using a nut all the calculated connections have a thread in one of the parts which is referred to as the second part. That means that there is actually only one clamped part in each bolted connection which contributes to the compliance of the clamped parts and therefore the value L_2 is always zero and the compliance is simplified to the first term of the equation 12-2.

The compliance of the bolt and the compliance of the clamped part is then used to calculate the force ratio:

$$\Phi_n = n \left(\frac{\delta_c}{\delta_c + \delta_b} \right) [-] \quad (12-3)$$

Where n is the loading pane factor which according to the handbook can be set to 0.5 for simple joint geometries.

The last parameters of the joint are the friction coefficients. Namely, the coefficients of under-head friction, thread friction and friction between the clamped parts. All of these friction coefficients are considered to be 0.2 as recommended in the requirement R-6230.

12.2.1 Pretension

In order to calculate the pretension force, the applied tightening torque has to be defined in the spreadsheet. The original value is based upon recommended values for different threads and can be later adjusted in case some of the MoS are negative. Adjusting the tightening torque is much easier than adjusting any other parameters of the joint and can usually lead to all positive MoS.

First, the thread helix angle needs to be calculated:



$$\varphi = \tan^{-1} \left(\frac{p}{\pi d_{uh}} \right) [-] \quad (12-4)$$

And then the maximum pretension force can be obtained:

$$F_{V,max} = \frac{M_{app,max}}{\frac{1}{2} d_2 \left(\tan \varphi + \frac{\mu_{th,nom}}{\cos \frac{\theta}{2}} \right) + \frac{1}{2} d_{uh} \mu_{uh,nom}} [N] \quad (12-5)$$

12.2.2 Tightening

Application of the tightening torque results in stress in the shank of the screw. The stress is composed of tension caused by the pretension force and a shear stress caused by the torque. The screw has to sustain the combination of these stresses during the tightening.

The applied tightening torque is reacted by under-head friction forces moment and in-thread friction forces moment. The biggest shear stress occurs at the shank just under the head of the screw, therefore, the maximum shear stress is:

$$\tau_{max} = \frac{M_{app,max} - M_{uh,min}}{W_p} [MPa] \quad (12-6)$$

Where W_p is the polar section modulus:

$$W_p = \frac{\pi d_0^3}{16} [mm^3] \quad (12-7)$$

$M_{app,max}$ is the maximum applied tightening torque and $M_{uh,min}$ is the minimum under-head frictional torque given by:

$$M_{uh,min} = \frac{d_{uh}}{2} F_{V,max} \mu_{uh,min} [Nm] \quad (12-8)$$

The maximum pretension stress is given by:

$$\sigma_{V,max} = \frac{F_{V,max}}{A_0} [MPa] \quad (12-9)$$

The torque shear stress and the pretension tensile stress are combined by Von-Mises:

$$\sigma_{v.m.} = \sqrt{\sigma_{V,max}^2 + \tau_{max}^2} [MPa] \quad (12-10)$$



Then the tightening MoS are calculated for yield:

$$MoS_{ti,y} = \frac{\sigma_y}{\sigma_{v.m.}} - 1 [-] \quad (12-11)$$

And for ultimate:

$$MoS_{ti,ult} = \frac{\sigma_{ult}}{\sigma_{v.m.}} - 1 [-] \quad (12-12)$$

Where σ_y is the yield strength and σ_{ult} is the ultimate strength of the screw material. The handbook does not recommend using any safety factor for these failures.

12.2.3 Loads and safety factors

To calculate the rest of the MoS the loads and the safety factors have to be determined. The safety factors are given in the requirement R-6230 and are summarized in Table 12.4.

Table 12.3 - Threaded fasteners safety factors

Type of failure	Denomination	Safety factor
Yield	sf_y	1,65
Ultimate	sf_{ult}	2,25
Gapping (separation)	sf_{sep}	1,25
Slipping	sf_{slip}	1,25
Worst case	sf_{wc}	1

The loads are obtained from the FEM analysis as an axial and two lateral forces for each screw in each group which is being evaluated. The forces are calculated in the CBUSH elements connecting the RBE2 spiders of the bolted connection (see Chapter 5). In each group, the biggest and the second biggest force in each direction over all the screws in the group is inputted in the spreadsheet. The second biggest forces are used in the worst-case calculation as described later. The forces are evaluated for two different loading cases (see Chapter 11.6) and are summarized in Appendix E.

The forces for the worst-case calculations are evaluated from a case where the second-most loaded screw fails and the forces which were acting on it are equally



distributed to the other screws in the group, which means that the most loaded screw in the group will have even bigger forces acting on it.

The worst-case axial force is calculated as follows:

$$F_{a,wc} = F_a + \frac{F_{a,2}}{m-1} [N] \quad (12-13)$$

Where $F_{a,wc}$ is the worst-case force, the F_a is the biggest axial force in a given group of screws, $F_{a,2}$ is the second biggest axial force in that group and m is the number of screws in that group.

12.2.4 Tension failure

This type of failure may occur when the fastener yields or cracks under the total stress combined from tightening preload force and force caused by external loading.

The MoS are calculated as follows for yield:

$$MoS_{tot,y} = \frac{A_S \sigma_y}{F_{V,max} + \Phi_n F_a s f_y} - 1 [-] \quad (12-14)$$

And for ultimate:

$$MoS_{tot,u} = \frac{A_S \sigma_{ult}}{F_{V,max} + \Phi_n F_a s f_{ult}} - 1 [-] \quad (12-15)$$

For the worst-case, the calculation is similar but the safety factor is different and the external force F_a is replaced by the worst-case external force $F_{a,wc}$:

$$MoS_{tot,y} = \frac{A_S \sigma_y}{F_{V,max} + \Phi_n F_{a,wc} s f_{wc}} - 1 [-] \quad (12-16)$$

And

$$MoS_{tot,y} = \frac{A_S \sigma_{ult}}{F_{V,max} + \Phi_n F_{a,wc} s f_{wc}} - 1 [-] \quad (12-17)$$

12.2.5 Gapping

Also called joint separation is a type of failure in which the force between the two clamped parts goes to zero and the parts are no longer in contact, which is not allowed.



The MoS is given by:

$$MoS_{sep} = \frac{F_{V,max} - F_{K,req}}{(1 - \Phi) F_a s f_{sep}} [-] \quad (12-18)$$

And for the worst case:

$$MoS_{sep,wc} = \frac{F_{V,max} - F_{K,req}}{(1 - \Phi) F_{a,wc} s f_{wc}} [-] \quad (12-19)$$

Where the term $F_{k,req}$ is the required force between the clamped parts and can be set to any desired value. In this case, it is set to zero which corresponds to no separation of the parts.

12.2.6 Slipping

Slipping may occur in so-called friction grip joints where the parts clamped together do not slip relative to each other because of high friction forces caused by the tightened screw. If there is some geometry preventing this movement like for example some flange it is called a bearing joint and this type of failure can not occur.

Absence of slipping is also very important because it ensures that the screw is not shear loaded by the external lateral forces since the parts can not slip and shear the screw.

The MoS for slipping is given by:

$$MoS_{slip} = \frac{(F_{V,max} - (1 - \Phi_n) F_a) \mu_s}{F_q s f_{ult}} [-] \quad (12-20)$$

And for the worst case:

$$MoS_{slip,wc} = \frac{(F_{V,max} - (1 - \Phi_n) F_{a,wc}) \mu_s}{F_{q,wc} s f_{wc}} [-] \quad (12-21)$$

12.2.7 Thread pull-out

With high enough axial force acting on the joint the threat on either the fastener or the threaded part may be pulled-out (stripped). This is a failure caused by a shear stress in the thread. Usually, the fastener is made of much stronger material than the joined parts and therefore the pull-out is checked only for the female thread. In this



case, the fasteners are made of steel and the parts are made of aluminum so pull-out will be evaluated only for the female threads.

One more parameter has to be inputted into the spreadsheet in order to make this check and that is the engaged length L_{eng} of the female thread, that is how far is the fastener screwed into the female thread. Then the effective length of engaged thread is calculated:

$$L_{eng,eff} = L_{eng} - 0.8 p \text{ [mm]} \quad (12-22)$$

Which accounts for the beginning portion of the engaged thread, which does not transmit any significant load. In order to determine the shear strength ration of the female and male threads R_s , which will be needed later, the failure surface area has to be calculated for the female thread:

$$A_{th,n} = \pi d_h \left(\frac{L_{eng,eff}}{p} \right) \left[\frac{p}{2} + (d_h - d_{2,h}) \tan \left(\frac{\theta}{2} \right) \right] \text{ [mm}^2\text{]} \quad (12-23)$$

And for the male thread:

$$A_{th,b} = \pi d_{1,h} \left(\frac{L_{eng,eff}}{p} \right) \left[\frac{p}{2} + (d_{2,h} - d_{1,h}) \tan \left(\frac{\theta}{2} \right) \right] \text{ [mm}^2\text{]} \quad (12-24)$$

This is where the positive effect of the helicoil inserts can be seen. The dimensions of the thread d_h , $d_{1,h}$, $d_{2,h}$ are the dimensions of the insert and are bigger than if there are no inserts. Therefore the failure surface areas of the threads are bigger which makes the threads more resistant against the pull-out.

Now the shear strength ration of the threads R_s can be calculated:

$$R_s = \frac{\tau_{ult,n} A_{th,n}}{\tau_{ult,b} A_{th,b}} [-] \quad (12-25)$$

Where $\tau_{ult,n}$ is the ultimate shear strength of the threaded part's material and $\tau_{ult,b}$ is the ultimate shear strength of the screw's material.

With the ratio R_s evaluated the empirical coefficients C_1 and C_2 can be calculated. These coefficients are the last values needed to determine the critical fastener load.

The coefficient C_1 may be calculated for a threaded nut or set as 1.0 for a threaded hole, which is the case for all the evaluated joints, therefore $C_1=1.0$.



The calculation of the coefficient C_2 depends on the value of R_s :

$$\text{For } R_s \geq 1.0 \quad c_2 = 0.897 [-] \quad (12-26)$$

$$\text{And for } 0.4 < R_s < 1.0 \quad c_2 = 0.728 + 1.769R_s - 2.896R_s^2 + 1.296R_s^3 [-] \quad (12-27)$$

Now the critical fastener load for failure of the female thread can be given by:

$$F_{ult,th,n} = \tau_{ult,n} A_{th,n} c_1 c_2 [-] \quad (12-28)$$

And the MoS for the total load is:

$$MoS_{th,tot} = \frac{F_{ult,th,n}}{F_{V,max} + \Phi F_a s f_{ult}} - 1 [-] \quad (12-29)$$

And for the worst-case:

$$MoS_{th,tot,wc} = \frac{F_{ult,th,n}}{F_{V,max} + \Phi F_{a,wc} s f_{wc}} - 1 [-] \quad (12-30)$$

When all the MoS are evaluated some input parameters may be changed if all the MoS are not positive. The design of the bolted joints may be changed but the easiest parameter to change is the tightening torque, which can be usually adjusted until all the MoS are positive. The adjusted tightening torques are then applied when the DM is assembled.

12.3 Results

After the mechanical analysis was performed and the forces needed for the calculation were obtained the MoS may be calculated. Total of six calculations were done. Three (one for each loading axis) for the combination of preload and random loads and three for the combination of preload and quasi-static loads. The forces obtained from the simulations, which served as an input to the calculations may be found in Appendix E. The tightening torques were adjusted to make all the MoS positive and may be found in Table 12.5.



Table 12.4 - Final tightening torques

Part 1	Part 2	QTY.	SCREW	TIGHTENING TORQUE (mNm)
Flange	Tube	8	M4x12	1100
Flange	Motor bed	6	M4x10 COUNTERSUNK	750
Flange	Hinge	4	M4x8 COUNTERSUNK	1100
Flange	Conn. box	3	M4x10 COUNTERSUNK	750
Flange	Touch down	2	M3x8	500
Flange	Pin puller	4	SCREW #6-32 3/8", C-606-N	640
Motor bed	Motor	4	M2x10	120
Lid	Lid-arm	5	M3x8	500
Lid	Touch-screw	2	M4	1100
Motor bed	Motor clamp	2	M3x8	450

The calculations results show all the MoS positive and may be found in Appendix F.



13 Conclusion

Upon submission of this thesis, the mechanical analysis of the FDA is completed and in the process of being reviewed by the ESA. All the necessary parts of the analysis were successfully completed, and the results show that the assembly should be able to withstand the loads, which occur during the launch.

The whole FDA mechanical analysis process described in this thesis took about eighteen months from which the most of the time took the tuning of the FEM model. It needs to be said that as the thesis is written the whole analysis process is somewhat idealized. The process is described as if almost no problems occurred and no mistakes were made. In fact, the process is much more complicated and iterative and lot of the calculations and simulations described in the thesis had to be done multiple times as minor design changes, mistakes, and input changes occurred.

The biggest problem of the whole analysis was definitely the tuning. The methods used for the correlation of the FEM model were quite inefficient and time-consuming. For future projects requiring the tuning some more sophisticated and at least partly automatized processes need to be learned and implemented.

After the mechanical analysis was finished the manufacturing of the qualification model had begun and when it is completed and assembled the qualification test campaign may begin. That will include functional tests, thermal vacuum tests, life cycle tests as well as multiple vibration test, which results may be then used to learn more about the quality of the mechanical analysis.

After the test campaign the flight model will be manufactured, assembled, tested and send to ESTEC for integration. The PROBA-3 mission should be launched from Kourou launch site by Vega launcher in late 2020.



Literature

- [1] PROBA-3 (Project for On-Board Autonomy-3) [online]. [2019-02-09] At: <https://directory.eoportal.org/web/eoportal/satellite-missions/p/proba-3>
- [2] FORTESCUE, Peter W., John STARK a Graham SWINERD. *Spacecraft systems engineering*. 4th ed. Hoboken, N.J.: Wiley, c2011. ISBN 9780470750124
- [3] WIJKER, Jaap J. *Spacecraft structures*. Berlin: Springer, c2008. ISBN 978-3-540-75552-4
- [4] WIJKER, Jaap J. *Random vibrations in spacecraft structures design: theory and applications*. New York: Springer, c2009. ISBN 978-90-481-2727-6.
- [5] ECSS-E-HB-32-23A: *Threaded fasteners handbook*. ESA Requirements and Standard Division, 2010
- [6] ECSS-E-ST-33-01C: *Mechanisms*. ESA Requirements and Standard Division, 2019
- [7] ECSS-E-ST-32C: *Structural general requirements*. ESA Requirements and Standard Division, 2008
- [8] ECSS-E-ST-32-03C: *Structural finite element models*. ESA Requirements and Standard Division, 2008
- [9] ECSS-E-HB-32-26A: *Spacecraft mechanical loads analysis handbook*. ESA Requirements and Standard Division, 2013



Symbols

A	[mm ²]	minimal cross-section of a screw
A_0	[mm ²]	Minimum cross-sectional area of a fastener shank
A_s	[mm ²]	Effective cross-sectional area of a fastener for stress analysis
A_{th}	[mm ²]	Area of the (cylindrical) surface assumed to fail during thread pull-out
$D_{uh,brg}$	[mm]	Outer diameter of the under-head or under-nut bearing surface
d_0	[mm]	Minimum diameter of a fastener shank
d_{1h}	[mm]	Diameter of helicoil's thread root
d_2	[mm]	Pitch diameter of a fastener thread
d_{2h}	[mm]	Pitch diameter of helicoil
D_h	[mm]	Nominal diameter of a hole
d_h	[mm]	Nominal diameter of helicoil
d_{uh}	[mm]	Effective diameter at which under-head or under-nut frictional forces act
E	[MPa]	Young's modulus
E_b	[MPa]	Young's modulus of a bolt/screw
E_c	[MPa]	Young's modulus of a clamped part
F_a	[N]	Axial force transmitted by joint
$F_{k,req}$	[N]	Clamping force acting at the interstice between two flanges
F_q	[N]	Shear force transmitted by joint
$F_{ult,th,n}$	[N]	Critical thread pull-out force
F_v	[N]	Pretension force
k	[N/mm]	tensile stiffness of a screw
l	[mm]	effective length of a screw
L	[mm]	tensile/compression loaded length of a joint
L_{eng}	[mm]	Length of engaged thread
$L_{eng,eff}$	[mm]	Effective length of engaged thread



M_{app}	[Nmm]	Torque applied to the fastener or nut during tightening
M_{uh}	[Nmm]	Torsional moment transmitted by frictional forces at the under-head
ν	[-]	Poisson's ratio
n	[-]	Loading plane factor
p	[mm]	Pitch of a thread
ρ	[kg/m ³]	Density
R_s	[-]	Shear strength ratio
sf	[-]	Safety factor
W_p	[mm ³]	Polar section modulus
δ_b	[N/mm]	Compliance of a fastener
δ_c	[N/mm]	Compliance of clamped parts
θ	[-]	Half angle of thread grooves
μ_{th}	[-]	Nominal friction coefficient at the thread interface
μ_{uh}	[-]	Nominal friction coefficient at the under-head or under-nut interface
μ_{uh}	[-]	Friction coefficient at the slipping interface
σ_{ult}	[MPa]	Ultimate strength
σ_{ult}	[MPa]	Ultimate stress
σ_v	[MPa]	Axial stress in fastener due to nominal preload
$\sigma_{v.m.}$	[MPa]	Von-Mises stress
σ_y	[MPa]	Yield strength
σ_y	[MPa]	Yield stress
τ	[MPa]	Shear stress
ϕ	[-]	Thread helix angle
φ_n	[-]	Force ratio



Abbreviations

ASPIICS	Association of Spacecraft for Polarimetric and Imaging Investigation of the Corona of the Sun
CoG	Center of Gravity
CAD	Computer Aided Design
CSYS	Coordinate System
COB	Coronagraph Optical Box
CSC	Coronagraph Spacecraft
DOF	Degree of Freedom
DM	Design Model
ESA	European Space Agency
ESTEC	European Space Research and Technology Centre
FoS	Factor of Safety
FEM	Finite Element Method (Model)
FM	Flight Model
FDA	Front Door Assembly
GPS	Global Positioning System
HDD	High Density Diffuser
MoS	Margin of Safety
OSC	Occulter Spacecraft
PP	Pin-Puller
PROBA-3	Project for On-Board Autonomy-3
QS	Quasi-static
SPS	Shadow Position Sensor
VZLU	Czech Aerospace Research Centre



Figures

Figure 2.1 – External (left) and internal (right) view of Occulter Spacecraft [1].....	7
Figure 2.2 - External (left) and internal (right) view of Coronagraph Spacecraft [1].....	8
Figure 2.3 - Illustration of the PROBA-3 mission [1].....	8
Figure 2.4 - Formation requirements (left) and nominal orbit (right) [1]	10
Figure 3.1 - FDA mechanical analysis flowchart.....	11
Figure 4.1 - FDA design	15
Figure 4.2 - FDA configurations	16
Figure 4.3 - FDA connected to the COB Tube.....	17
Figure 4.4 - Lid assembly	18
Figure 4.5 - Touch-down contact	19
Figure 4.6 - Hinge assembly.....	20
Figure 4.7 - Motor assembly.....	21
Figure 4.8 - Locking device	22
Figure 5.1 - FDA global CSYS.....	23
Figure 5.2 - Example of a screw modeling	27
Figure 5.3 - Lid shaft connections	28
Figure 5.4 - Pin-puller connection	29
Figure 5.5 - Touch screw connection	30
Figure 5.6 - Lid nose connection.....	30
Figure 5.7 - Flange-Tube connection	31
Figure 7.1 - Lid preload	35
Figure 7.2 - Force-compression relation of the preload measuring spring.....	36
Figure 7.3 - Gap-preload relationship measurement.....	37
Figure 8.1 - Z-axis testing.....	41
Figure 8.2 - Example of settling	42
Figure 8.3 - Y-axis testing.....	43
Figure 8.4 - X-axis testing.....	44
Figure 8.5 - Severe resonances in X-axis testing.....	45
Figure 8.6 - Original/notched spectra.....	46
Figure 8.7 - Example of vibration testing results	48
Figure 9.1 - Motor - X-axis excitation setup.....	51
Figure 9.2 - Motor - X-axis excitation response	51
Figure 9.3 - Pin-puller - Z-axis excitation setup.....	52
Figure 9.4 - Pin-puller - Z-axis excitation response	52
Figure 9.5 - Lid - X-axis excitation setup	53
Figure 9.6 - Lid - X-axis excitation response.....	53
Figure 10.1 - FEM model tuned locations.....	56
Figure 11.1 - PSD calculation example	65
Figure 11.2 - Lid Static simulation Von-Mises stress contour	67
Figure 12.1 - Illustration of a vented screw.....	71



Appendixes

Appendix A – Vibration testing spectra and results

Appendix B – Preliminary threaded fasteners forces

Appendix C – FEM model correlation results

Appendix D – Random vibration loading spectra after coupled analysis

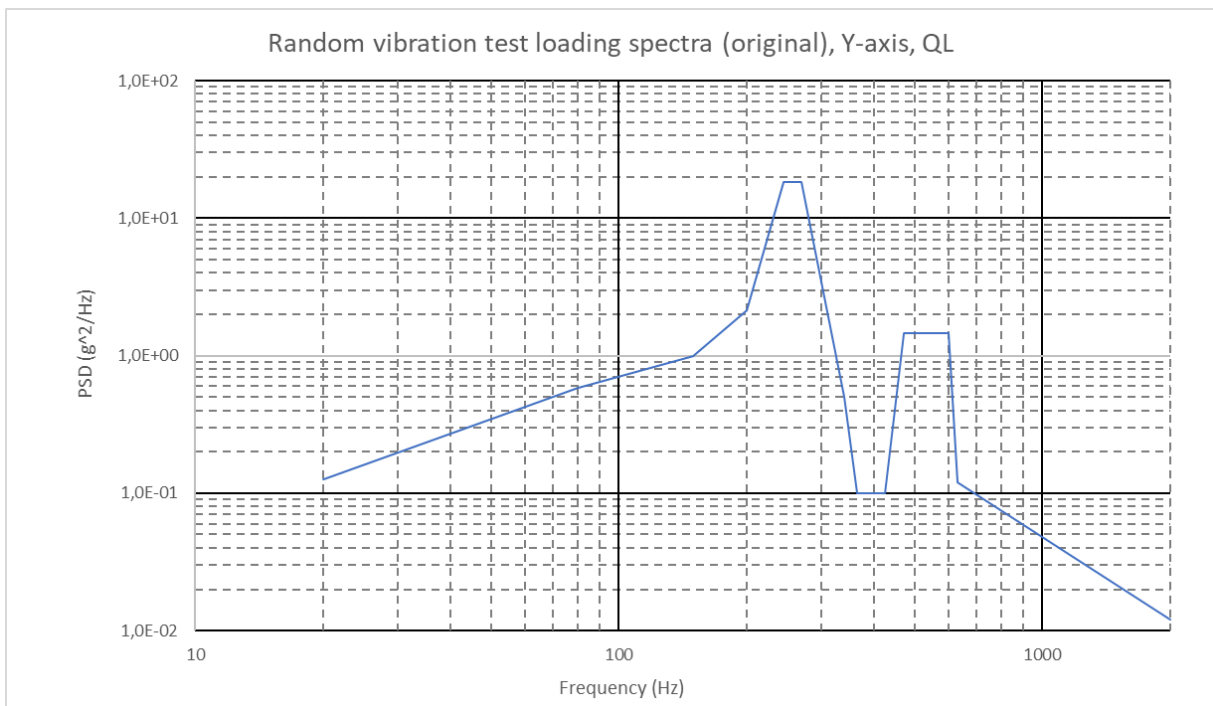
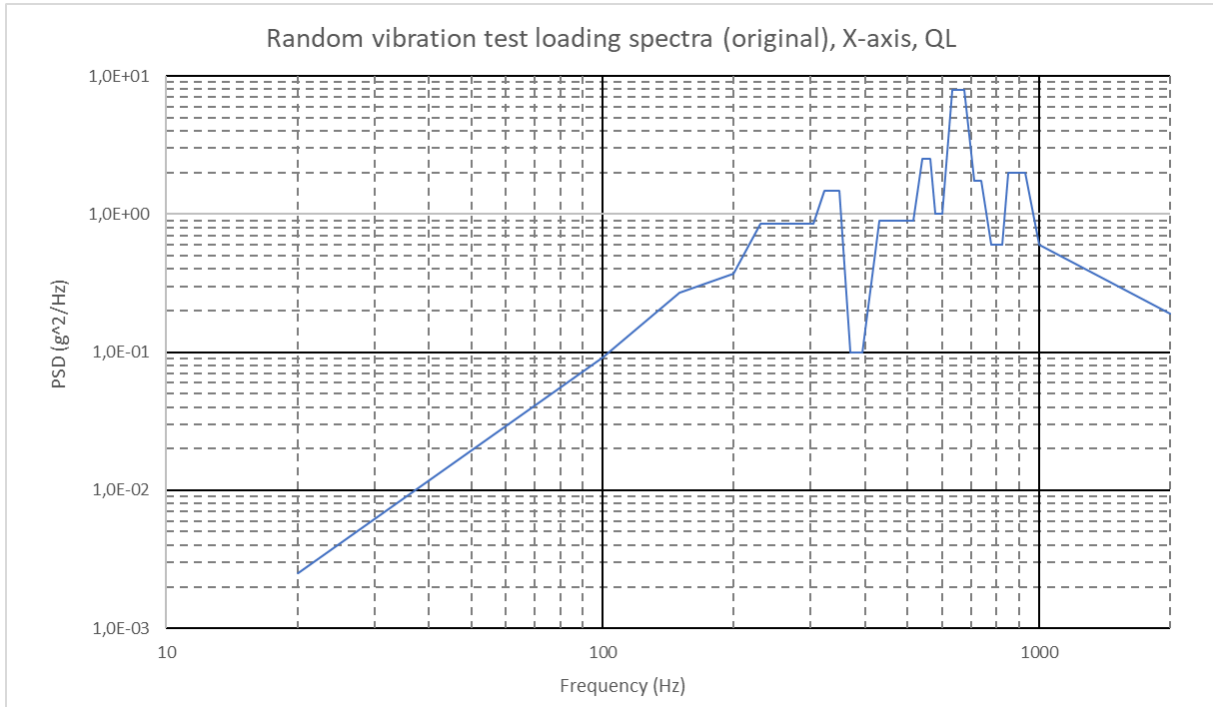
Appendix E – Mechanical analysis stress and threaded fasteners forces results

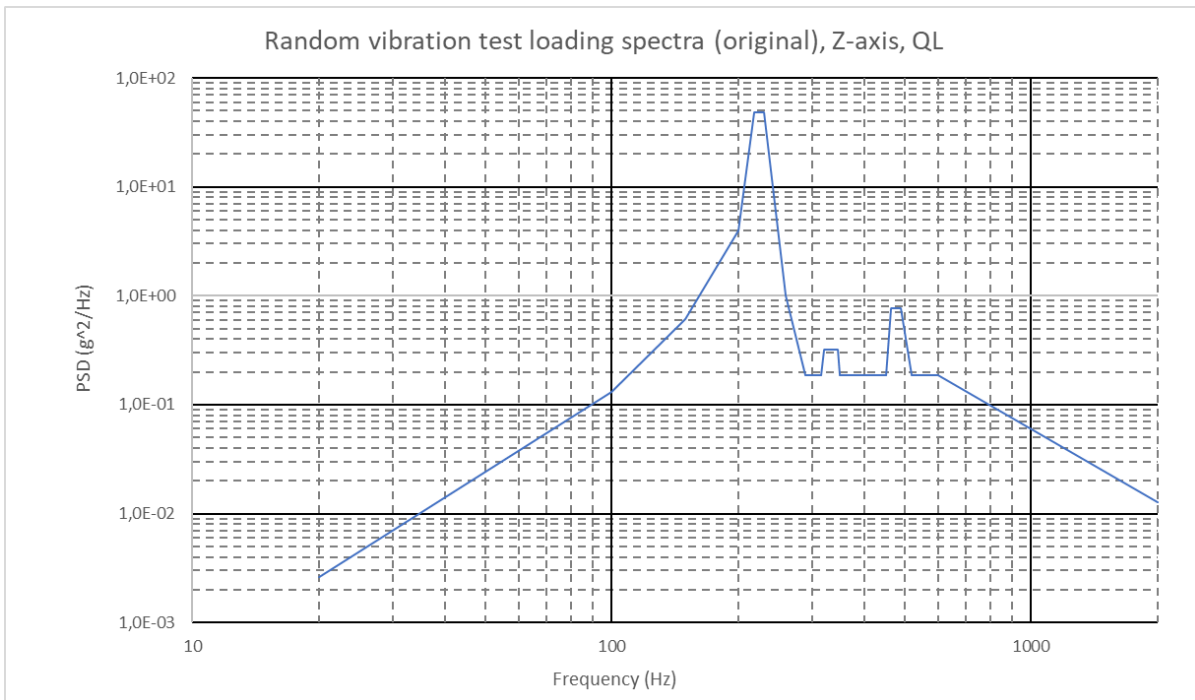
Appendix F – Threaded fasteners MoS



Appendix A – Vibration testing spectra and results

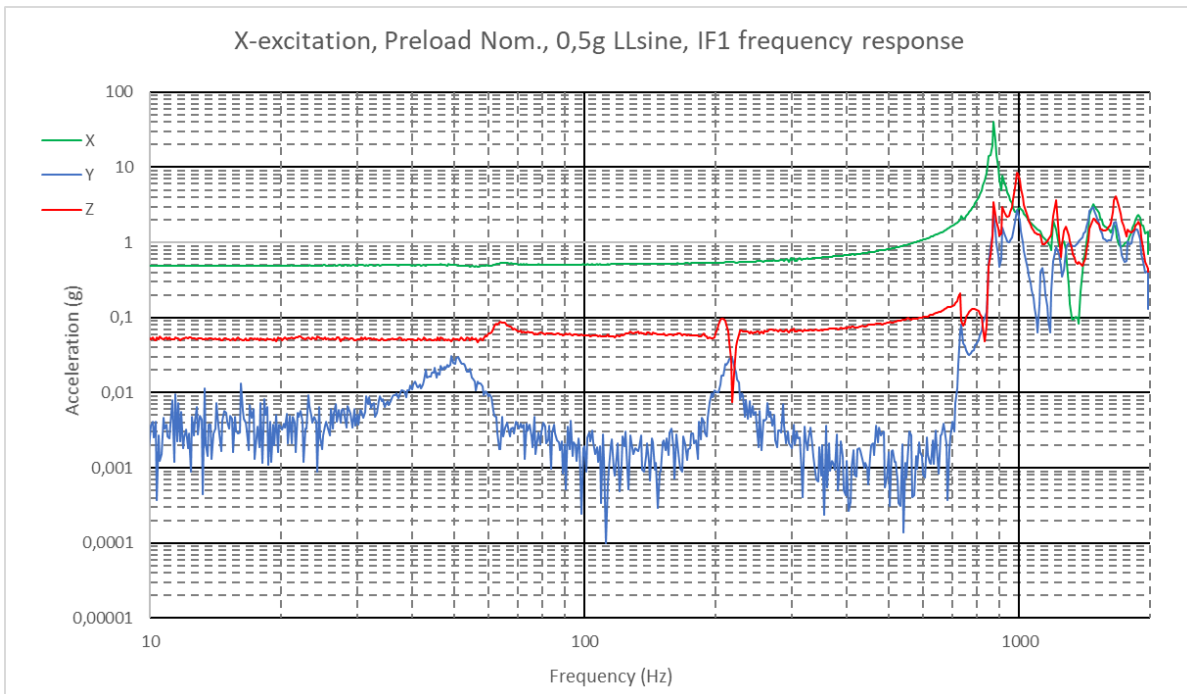
Original random vibration test loading spectra - Qualification levels

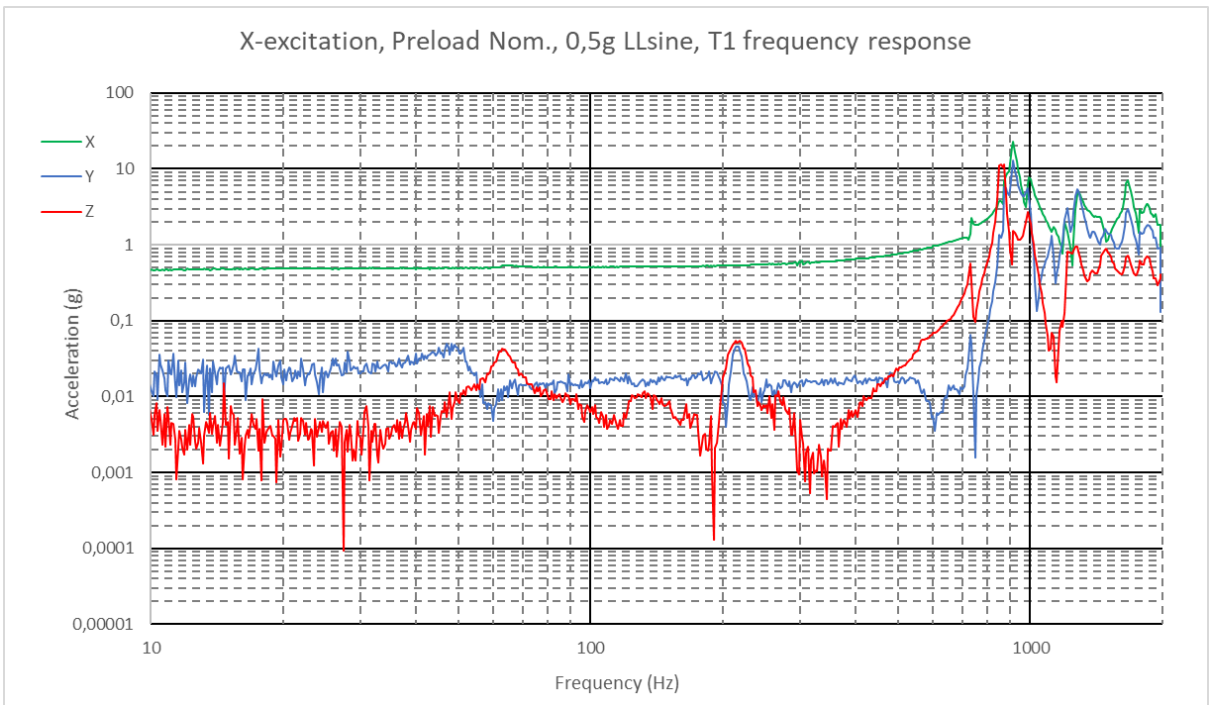
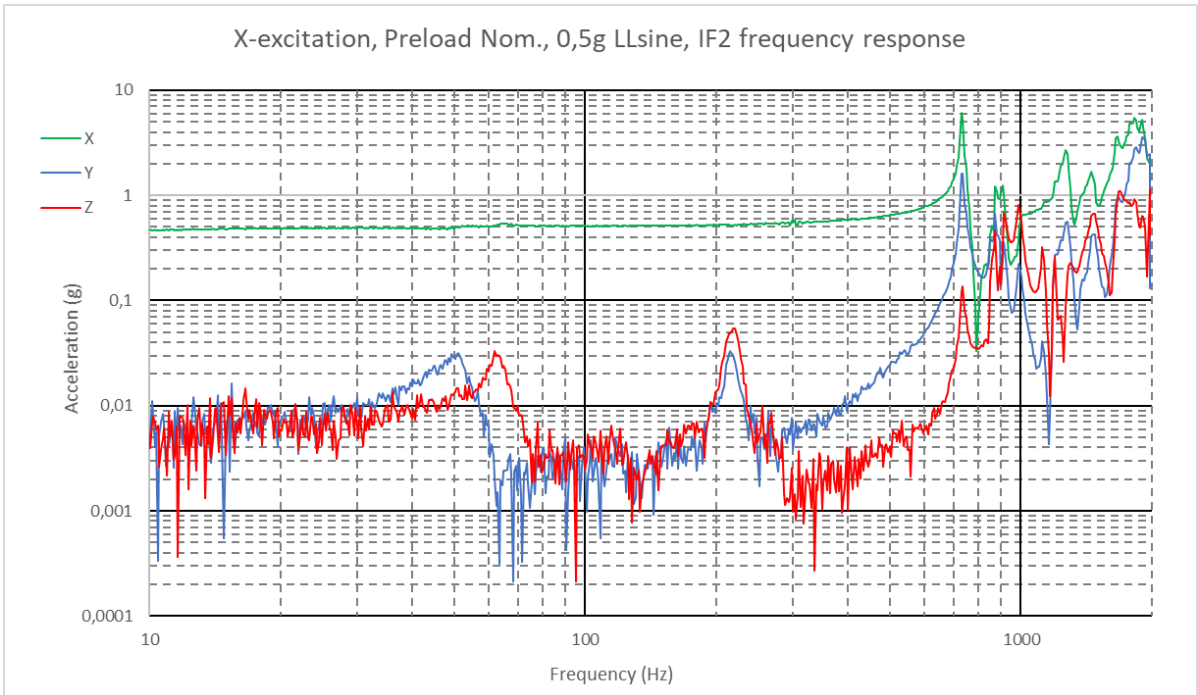




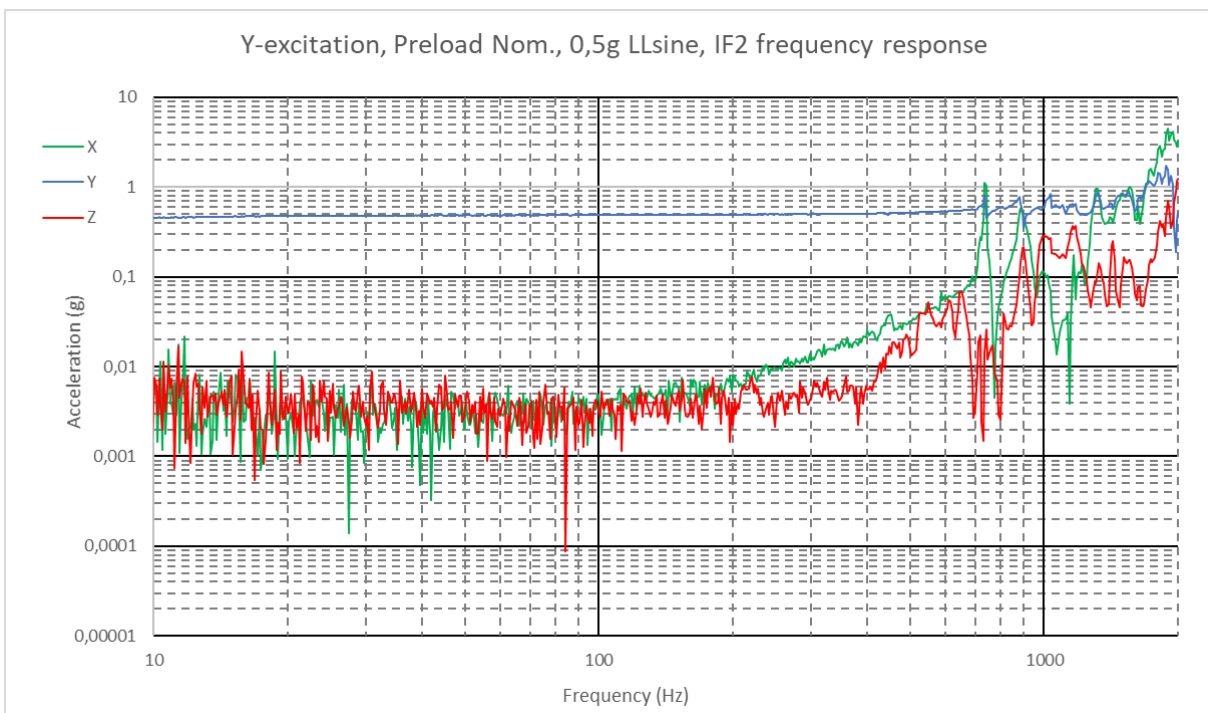
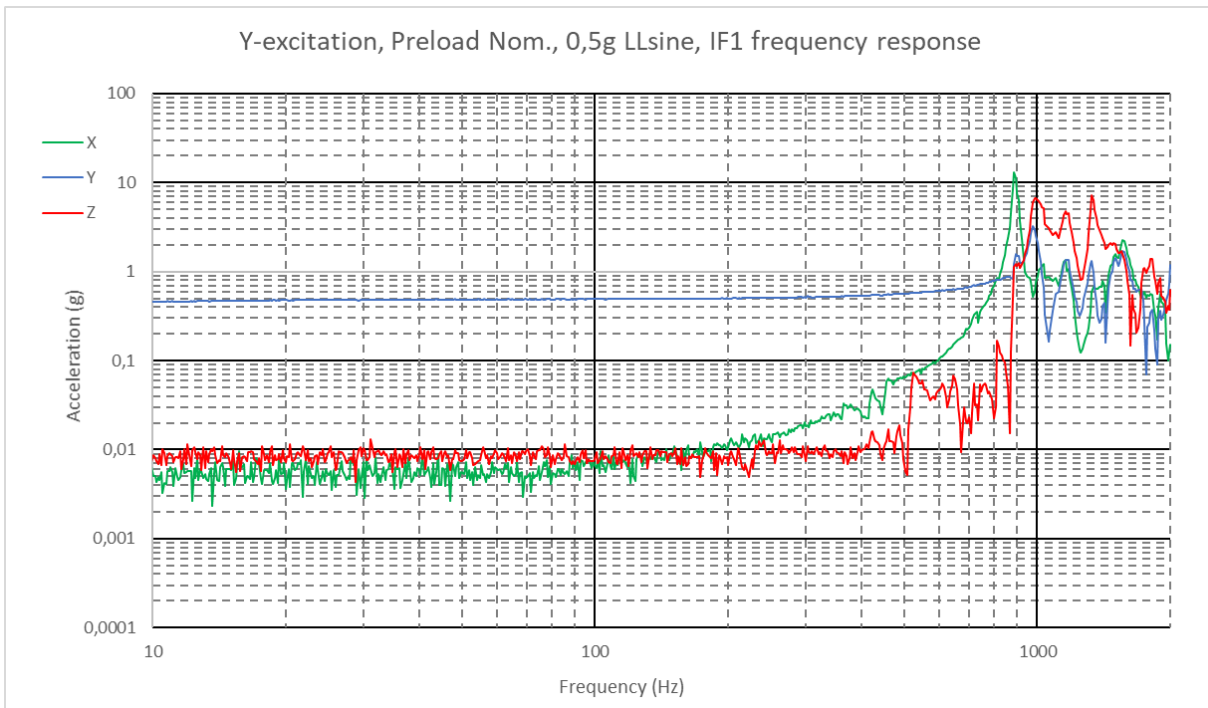
Low-level sine responses used for FEM model correlation

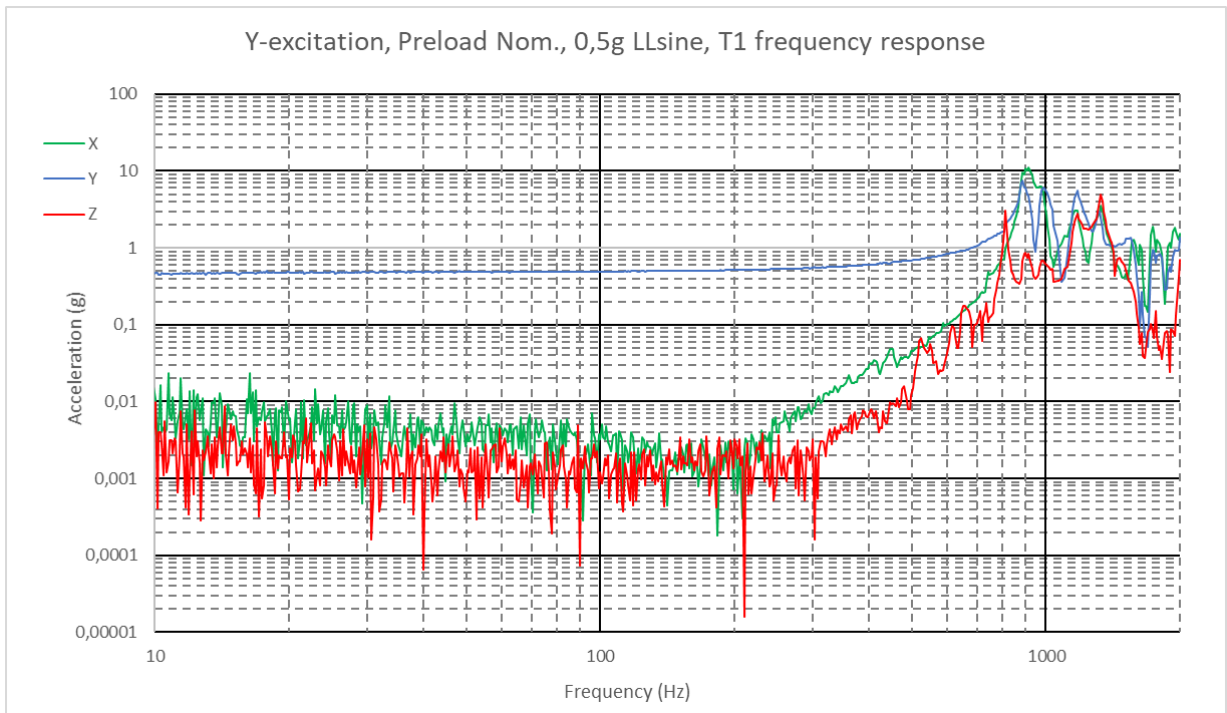
X-excitation



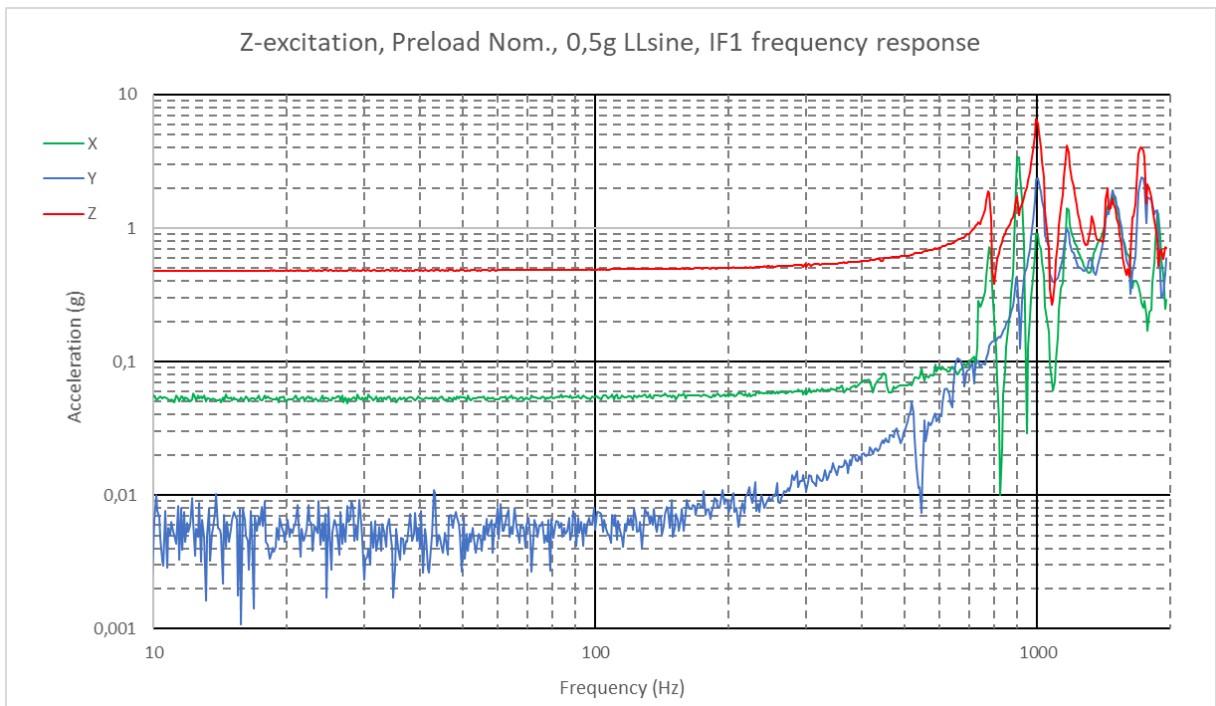


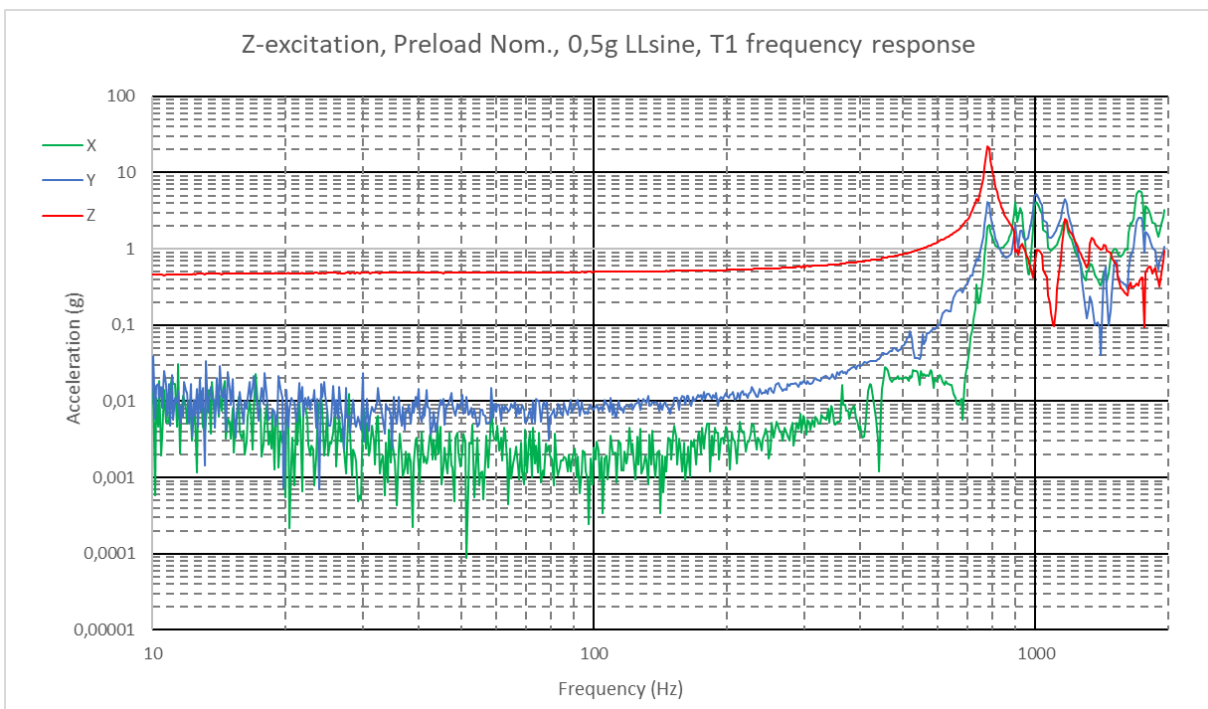
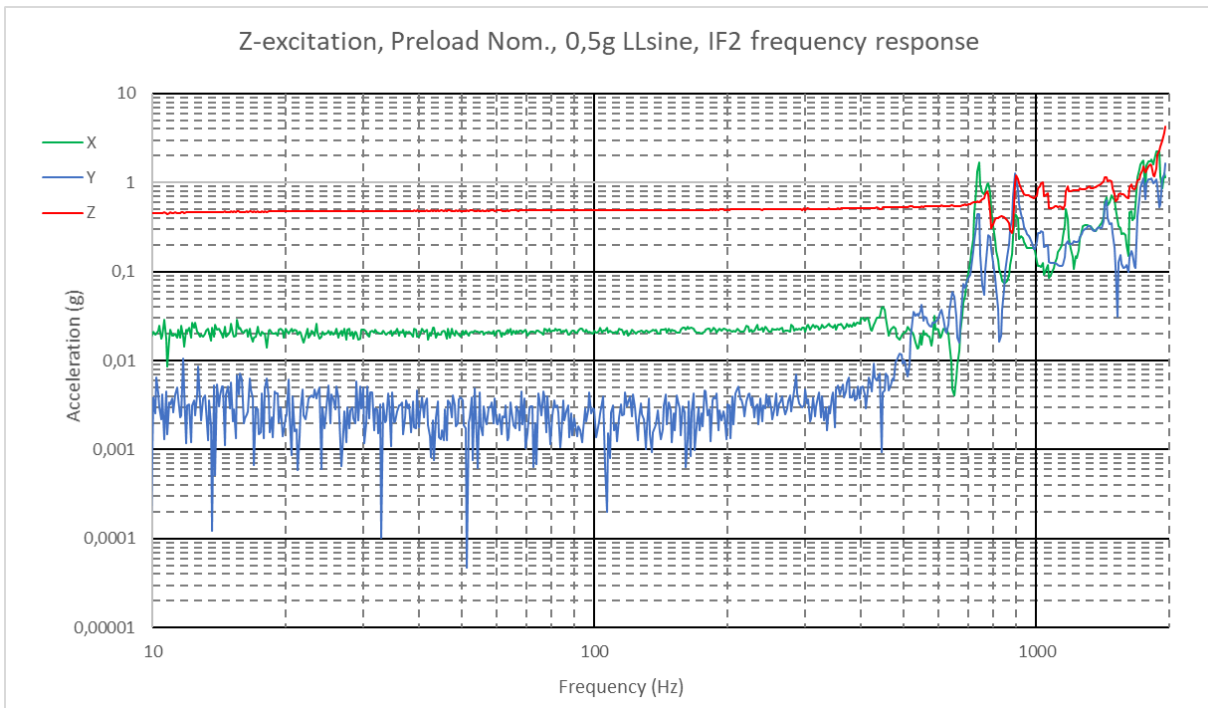
Y-excitation





Z-excitation







Appendix B – Preliminary threaded fasteners forces

Forces in screws from preliminary simulation. X-direction is the axial force.

X-axis excitation

Connected parts		Preload (N)			Random X (N)			Preload + Random X (N)		
Part 1	Part 2	Fx	Fy	Fz	Fx	Fy	Fz	Fx	Fy	Fz
Flange	Tube	551	255	357	768	285	170	1319	540	527
		549	252	348	651	281	170	1199	534	518
Flange	Motor bed	24	252	348	232	281	170	256	534	518
		20	22	58	219	146	48	240	168	106
Flange	Hinge	197	84	39	75	49	29	272	134	68
		194	83	37	47	48	29	241	132	65
Flange	Conn. Box	7	6	24	59	93	57	66	98	81
		6	3	17	52	57	47	58	60	64
Flange	Touch down	128	138	195	81	73	69	209	211	265
		128	137	194	67	51	44	195	188	238
Flange	Pin puller	9	12	36	281	125	22	290	137	59
		7	12	32	255	120	15	262	132	47
Motor bed	Motor	9	5	2	498	127	210	507	131	213
		9	4	1	430	99	159	439	103	160
LID	Lid-arm	123	166	144	18	32	29	141	198	173
		121	157	144	17	28	29	138	184	172
LID	Touch-screw	263	169	248	104	68	145	366	237	392
		263	168	246	75	39	102	338	206	349

Y-axis excitation

Connected parts		Preload (N)			Random Y (N)			Preload + Random Y (N)		
Part 1	Part 2	Fx	Fy	Fz	Fx	Fy	Fz	Fx	Fy	Fz
Flange	Tube	551	255	357	42	99	68	593	353	425
		549	252	348	37	37	37	586	289	385
Flange	Motor bed	24	252	348	40	37	37	64	289	385
		20	22	58	40	14	21	60	36	79
Flange	Hinge	197	84	39	36	20	17	233	104	56
		194	83	37	35	20	17	230	103	54
Flange	Conn. Box	7	6	24	40	12	23	47	18	47
		6	3	17	28	12	22	34	15	39
Flange	Touch down	128	138	195	16	23	16	144	161	211
		128	137	194	16	23	15	143	160	209
Flange	Pin puller	9	12	36	34	14	11	43	26	48
		7	12	32	31	12	10	38	24	42
Motor bed	Motor	9	5	2	94	33	22	103	38	24
		9	4	1	71	24	16	80	28	17
LID	Lid-arm	123	166	144	10	13	13	133	179	157
		121	157	144	10	10	13	131	167	157
LID	Touch-screw	263	169	248	17	34	28	280	203	276
		263	168	246	14	32	28	276	200	275

Z-axis excitation



Connected parts		Preload (N)			Random Z (N)			Preload + Random Z (N)		
Part 1	Part 2	Fx	Fy	Fz	Fx	Fy	Fz	Fx	Fy	Fz
Flange	Tube	551	255	357	46	82	70	597	337	427
		549	252	348	45	49	62	593	301	410
Flange	Motor bed	24	252	348	45	20	33	68	273	381
		20	22	58	31	16	27	51	39	85
Flange	Hinge	197	84	39	19	14	23	216	98	62
		194	83	37	17	14	21	211	97	58
Flange	Conn. Box	7	6	24	22	15	19	29	21	43
		6	3	17	22	11	18	28	14	36
Flange	Touch down	128	138	195	20	26	15	148	164	211
		128	137	194	20	22	14	147	159	208
Flange	Pin puller	9	12	36	33	10	13	42	22	49
		7	12	32	27	8	12	34	20	45
Motor bed	Motor	9	5	2	94	30	25	103	35	27
		9	4	1	60	18	17	69	22	18
LID	Lid-arm	123	166	144	6	10	10	129	176	154
		121	157	144	6	8	9	127	165	153
LID	Touch-screw	263	169	248	15	36	36	278	205	284
		263	168	246	12	25	36	274	192	282



Appendix C – FEM model correlation results

Final tuned parameters

Connected parts		Qty.	Screw	Stiffness	
Part 1	Part 2				
Flange	Tube	8	M4x12	X (N/mm)	180x10 ³
				Y (N/mm)	180x10 ³
				Z (N/mm)	180x10 ³
				XR (N.mm)	90x10 ³
				YR (N.mm)	90x10 ³
				ZR (N.mm)	90x10 ³
Flange	Motor bed	4	M4x10	X (N/mm)	200x10 ⁶
				Y (N/mm)	200x10 ⁶
				Z (N/mm)	200x10 ⁶
				XR (N.mm)	200x10 ⁶
				YR (N.mm)	200x10 ⁶
				ZR (N.mm)	200x10 ⁶
Flange	Hinge	4	M4x8	X (N/mm)	200x10 ⁶
				Y (N/mm)	200x10 ⁶
				Z (N/mm)	200x10 ⁶
				XR (N.mm)	200x10 ⁶
				YR (N.mm)	200x10 ⁶
				ZR (N.mm)	200x10 ⁶
Flange	Conn. box	3	M4x10	X (N/mm)	200x10 ⁶
				Y (N/mm)	200x10 ⁶
				Z (N/mm)	200x10 ⁶
				XR (N.mm)	200x10 ⁶
				YR (N.mm)	200x10 ⁶
				ZR (N.mm)	200x10 ⁶
Flange	Touch	2	M3x8	X (N/mm)	200x10 ⁶
				Y (N/mm)	200x10 ⁶
				Z (N/mm)	200x10 ⁶
				XR (N.mm)	200x10 ⁶
				YR (N.mm)	200x10 ⁶
				ZR (N.mm)	200x10 ⁶
Flange	Pin puller	4	SCREW #6-	X (N/mm)	1000
				Y (N/mm)	1000
				Z (N/mm)	1000
				XR (N.mm)	500

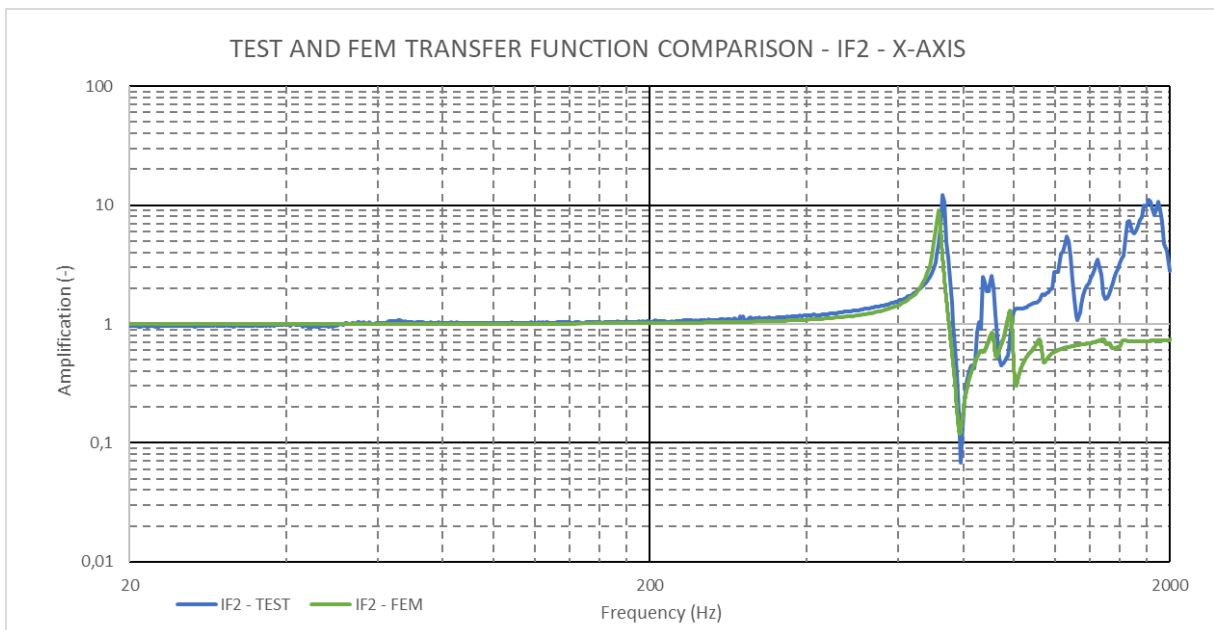
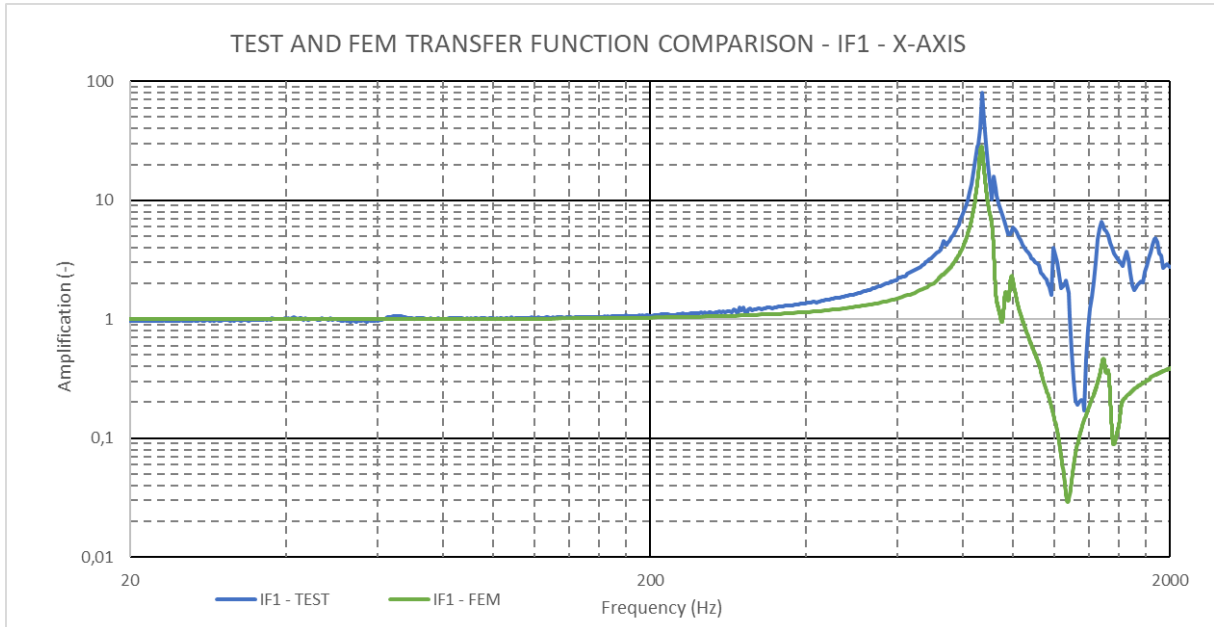


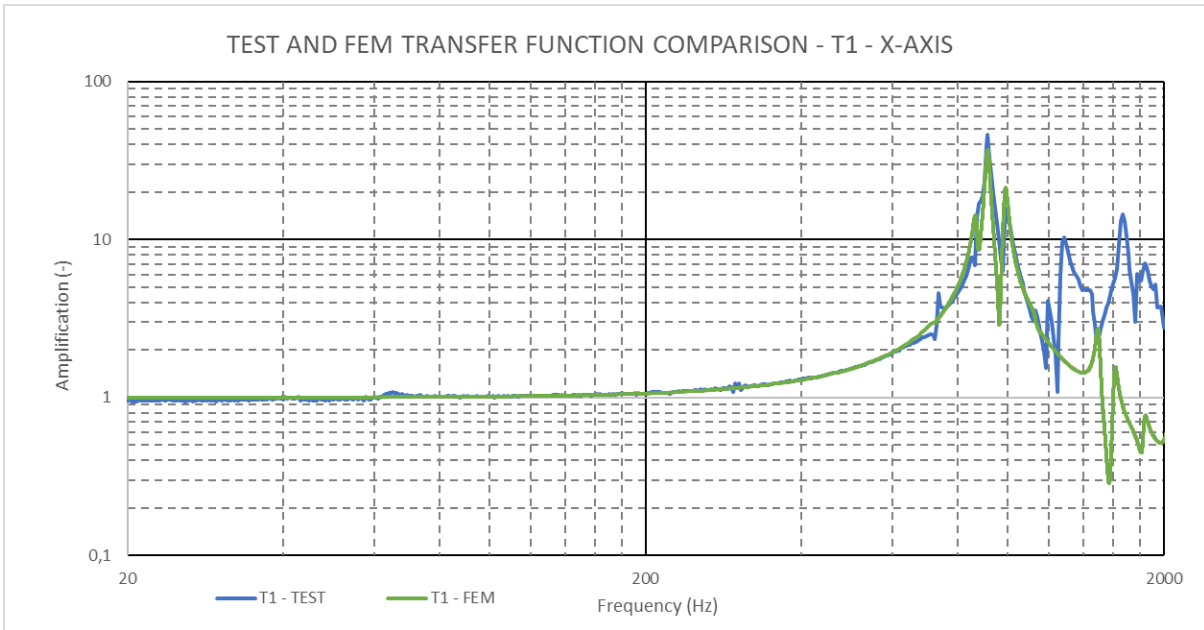
				YR (N.mm)	500
				ZR (N.mm)	500
Motor bed	Motor	4	M2x10	X (N/mm)	40x10 ⁶
				Y (N/mm)	20x10 ⁶
				Z (N/mm)	20x10 ⁶
				XR (N.mm)	200x10 ⁶
				YR (N.mm)	200x10 ⁶
				ZR (N.mm)	200x10 ⁶
Lid	Lid-arm	5	M3x8	X (N/mm)	200x10 ⁶
				Y (N/mm)	200x10 ⁶
				Z (N/mm)	200x10 ⁶
				XR (N.mm)	200x10 ⁶
				YR (N.mm)	200x10 ⁶
				ZR (N.mm)	200x10 ⁶
Hinge	Shaft		Friction	X (N/mm)	2200
				Y (N/mm)	5000
				Z (N/mm)	1200
				XR (N.mm)	200
				YR (N.mm)	200
				ZR (N.mm)	200
Touch-	Touch		Contact	X (N/mm)	100x10 ³
				Y (N/mm)	2x10 ³
				Z (N/mm)	2x10 ³
				XR (N.mm)	200x10 ³
				YR (N.mm)	200x10 ³
				ZR (N.mm)	200x10 ³
Flange	Nose		Contact	X (N/mm)	3x10 ³
				Y (N/mm)	0,5x10 ³
				Z (N/mm)	3x10 ³
				XR (N.mm)	200x10 ³
				YR (N.mm)	200x10 ³
				ZR (N.mm)	200x10 ³



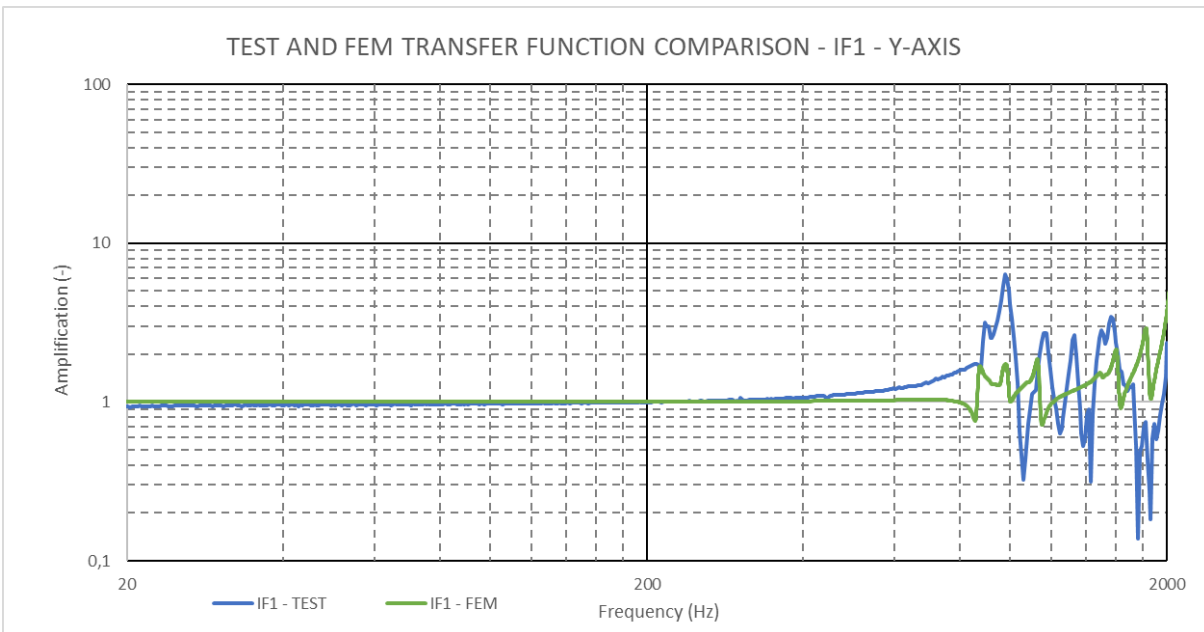
Final tuned transfer functions

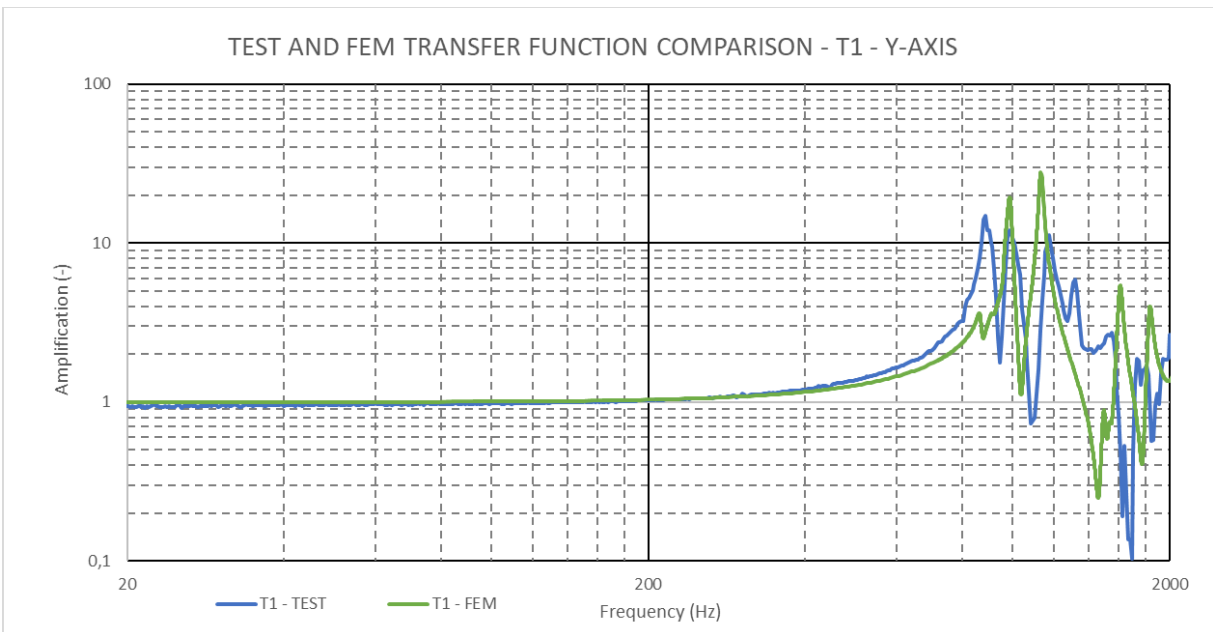
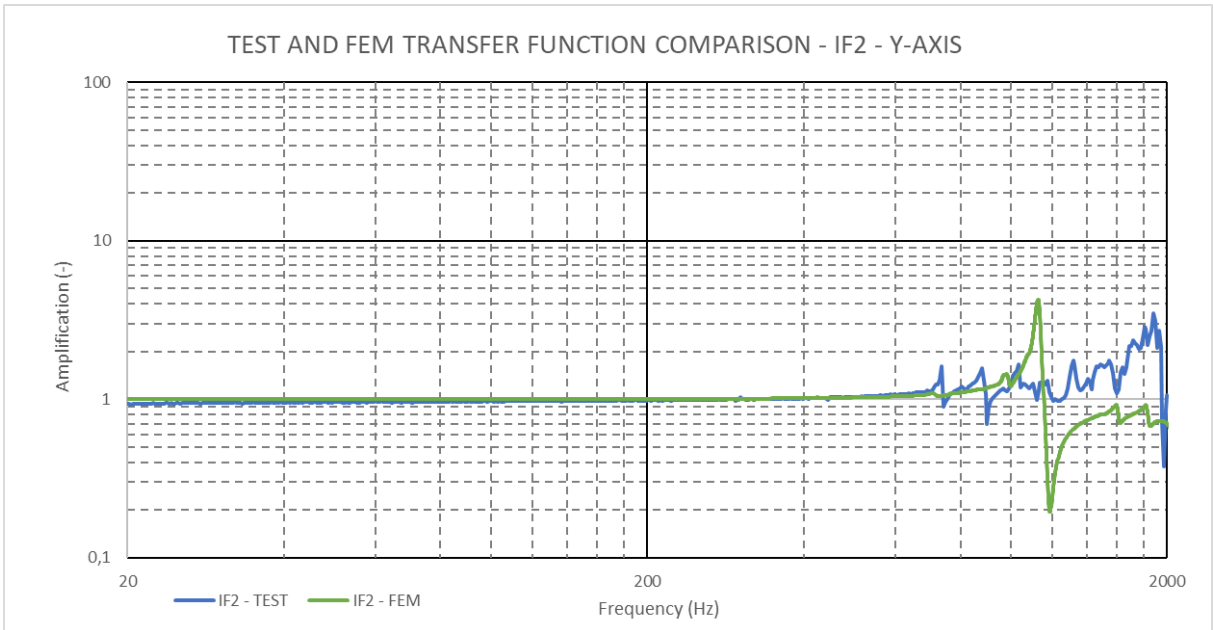
X-axis excitation



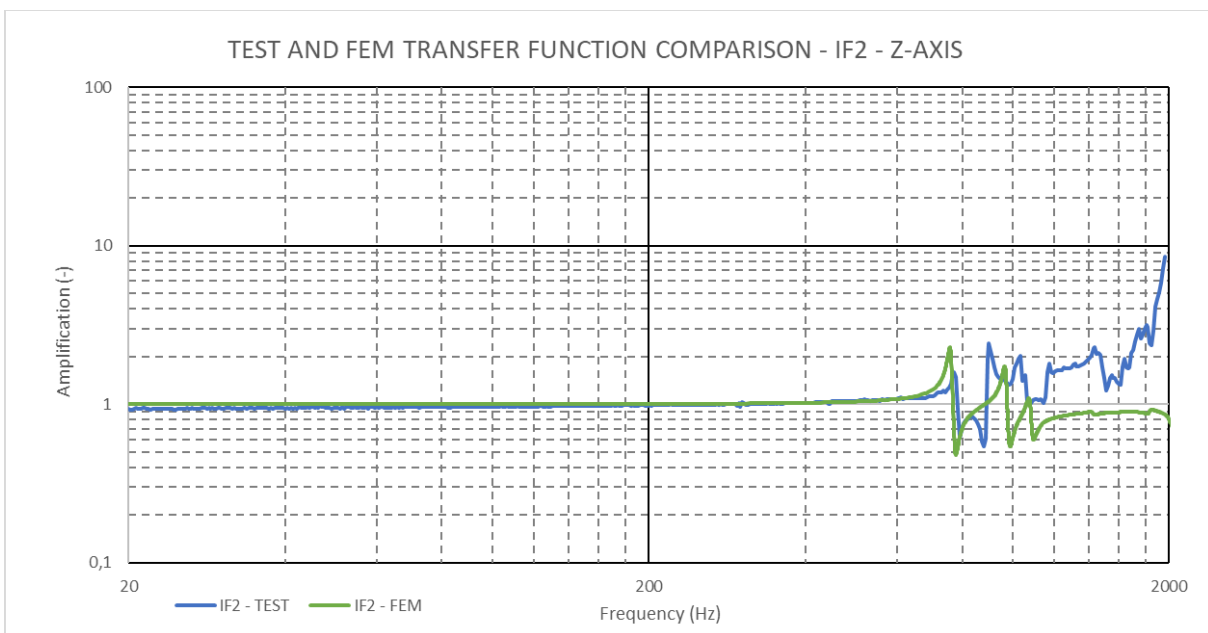
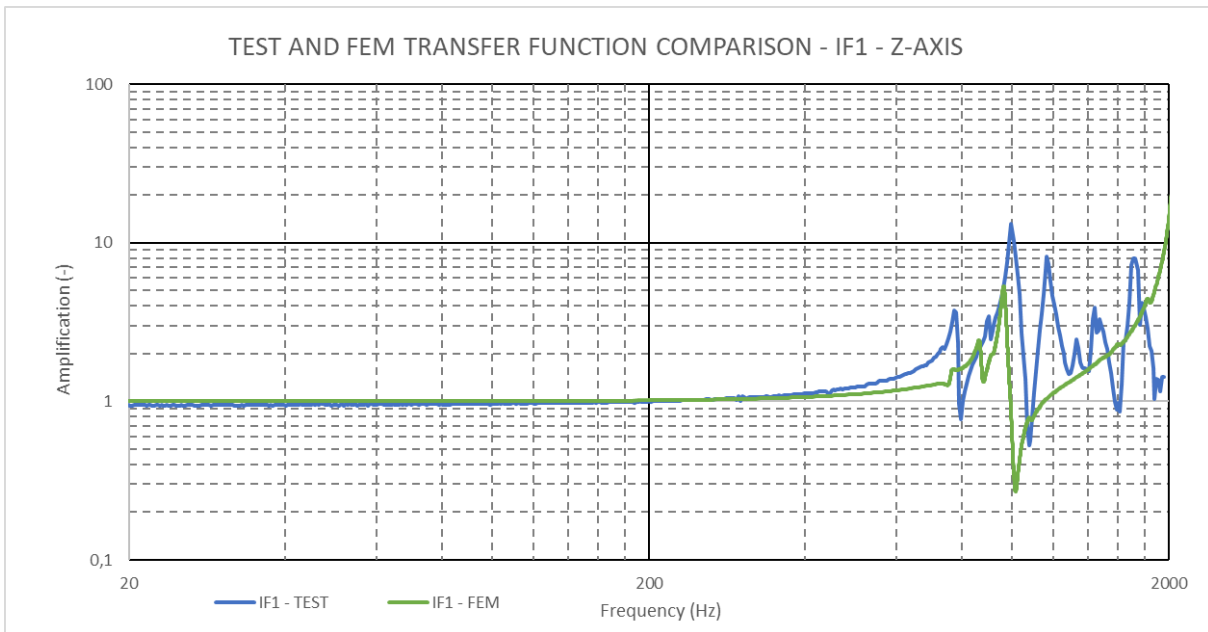


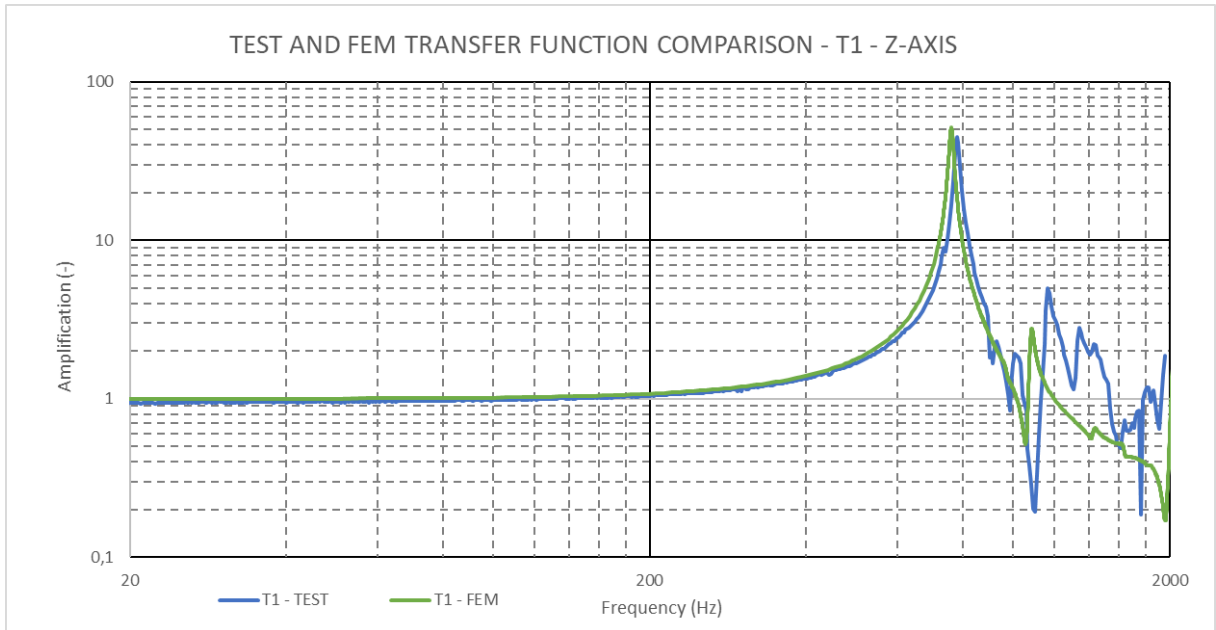
Y-axis excitation





Z-axis excitation

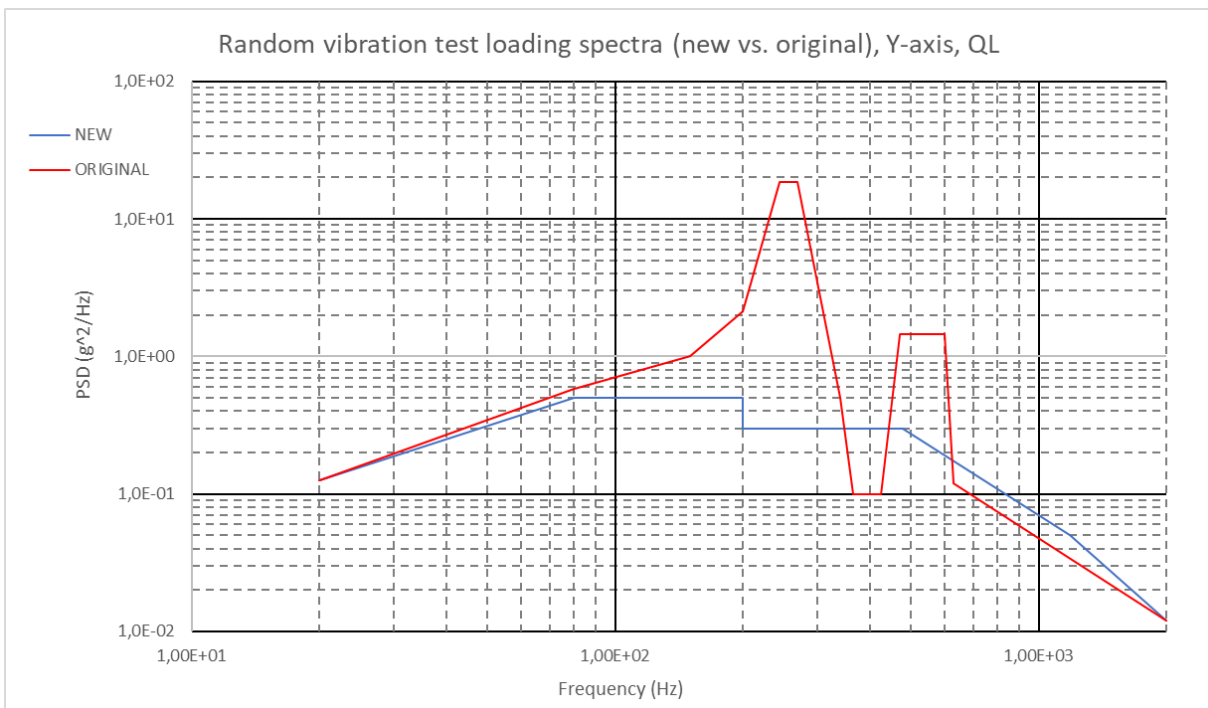
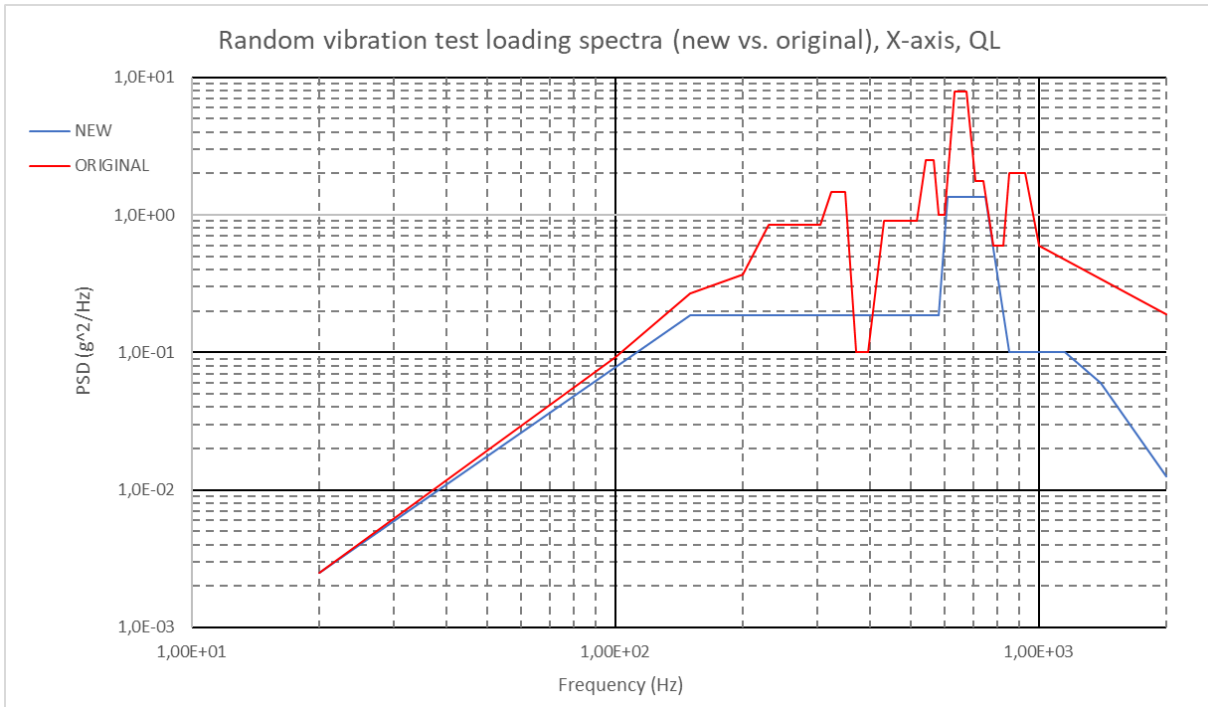


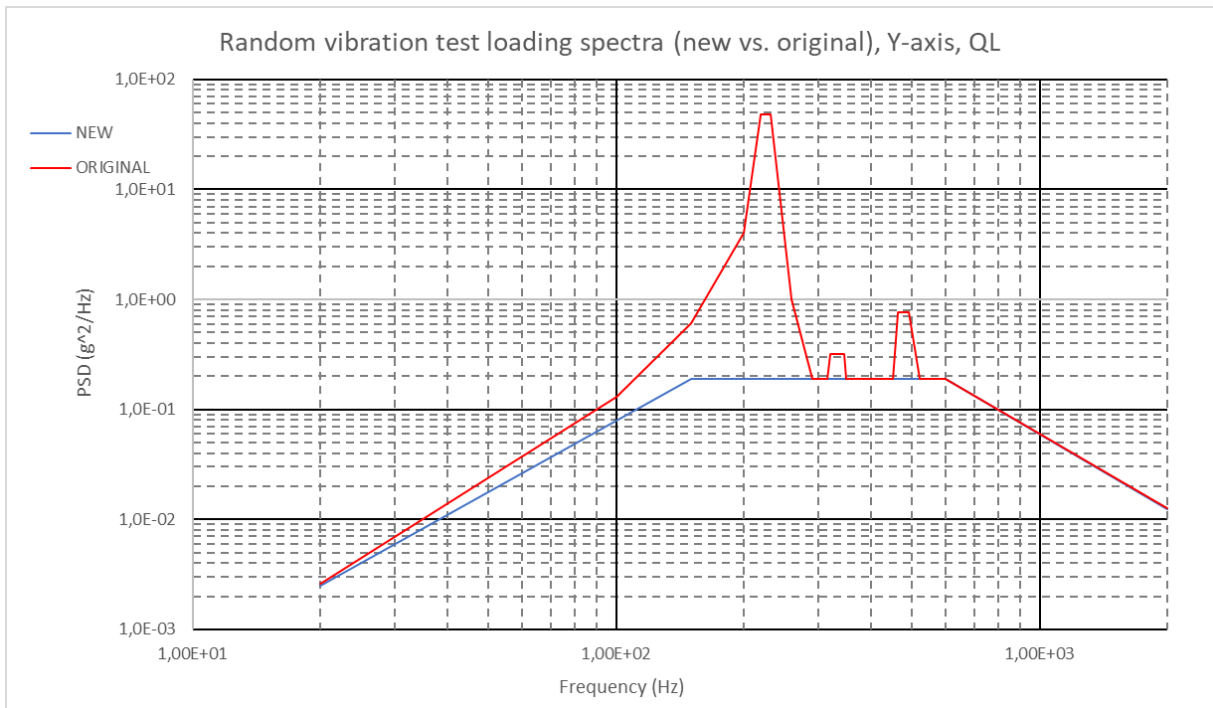




Appendix D – Random vibration loading spectra after coupled analysis

Random vibration loading spectra after the coupled analysis in comparison with the original spectra – Qualification levels







Appendix E – Mechanical analysis stress and threaded fasteners forces results

Random and Quasi-static stress evaluation – X-excitation

Part	Material	Yield Strength		Yield FoS	Ultimate Strength	Ultimate FoS	Random(3σ)+ Preload Stress	Yield MoS	Ultimate MoS	QS+Preload Stress	Yield MoS	Ultimate MoS
		MPa	MPa									
Flange	EN AW 6082 T651	240	295	1,65	295	2,25	47,55	2,06	1,76	29	4,02	3,52
Lid	EN AW 6082 T651	240	295	1,65	295	2,25	96,64	0,51	0,36	54	1,69	1,43
Touch-down	A286 AISI 660	590	900	1,65	900	2,25	46,73	6,65	7,56	15	22,84	25,67
Lid nose	A286 AISI 661	590	900	1,65	900	2,25	130,77	1,73	2,06	70	4,11	4,71
Lid arm	EN AW 6082 T651	240	295	1,65	295	2,25	60,33	1,41	1,17	34	3,28	2,86
Motor bed	EN AW 6082 T652	240	295	1,65	295	2,25	28,48	4,11	3,60	15	8,70	7,74
Hinge	EN AW 6082 T653	240	295	1,65	295	2,25	95,49	0,52	0,37	30	3,85	3,37
Conn. Box	EN AW 6082 T654	240	295	1,65	295	2,25	30,82	3,72	3,25	7	19,78	17,73
Top conn. Box	EN AW 6082 T655	240	295	1,65	295	2,25	1,96	73,21	65,89	2	71,73	64,56
Shaft	AISI 316	290	550	1,65	550	2,25	28,3	5,21	7,64	13	12,52	17,80



Y-excitation

Part	Material	Yield Strength MPa	Yield FoS	Ultimate Strength MPa	Ultimate FoS	Random(3σ)+ Preload Stress MPa	Yield MoS	Ultimate MoS	QS+Preload Stress MPa	Yield MoS	Ultimate MoS
Flange	EN AW 6082 T651	240	1,65	295	2,25	33,87	3,29	2,87	24	5,06	4,46
Lid	EN AW 6082 T651	240	1,65	295	2,25	90,43	0,61	0,45	51	1,85	1,57
Touch-down	A286 AISI 660	590	1,65	900	2,25	38,93	8,19	9,27	28	11,77	13,29
Lid nose	A286 AISI 661	590	1,65	900	2,25	112,56	2,18	2,55	74	3,83	4,41
Lid arm	EN AW 6082 T651	240	1,65	295	2,25	58,65	1,48	1,24	38	2,83	2,45
Motor bed	EN AW 6082 T652	240	1,65	295	2,25	15,29	8,51	7,57	18	7,08	6,28
Hinge	EN AW 6082 T653	240	1,65	295	2,25	70,44	1,06	0,86	47	2,09	1,79
Conn. Box	EN AW 6082 T654	240	1,65	295	2,25	15,83	8,19	7,28	10	13,55	12,11
Top conn. Box	EN AW 6082 T655	240	1,65	295	2,25	4,34	32,51	29,21	6	23,24	20,85
Shaft	AISI 316	290	1,65	550	2,25	20,62	7,52	10,85	13	12,52	17,80



Z-excitation

Part	Material	Yield Strength	Yield FoS	Ultimate Strength	Ultimate FoS	Random(3σ)+ Preload Stress	Yield MoS	Ultimate MoS	QS+Preload Stress	Yield MoS	Ultimate MoS
		MPa	-	MPa	-	MPa	-	MPa	-	MPa	-
Flange	EN AW 6082 T651	240	1,65	295	2,25	46,66	2,12	1,81	22	5,61	4,96
Lid	EN AW 6082 T651	240	1,65	295	2,25	89,74	0,62	0,46	54	1,69	1,43
Touch-down	A286 AISI 660	590	1,65	900	2,25	41,06	7,71	8,74	51	6,01	6,84
Lid nose	A286 AISI 661	590	1,65	900	2,25	107,61	2,32	2,72	66	4,42	5,06
Lid arm	EN AW 6082 T651	240	1,65	295	2,25	55,86	1,60	1,35	32	3,55	3,10
Motor bed	EN AW 6082 T652	240	1,65	295	2,25	17,81	7,17	6,36	7	19,78	17,73
Hinge	EN AW 6082 T653	240	1,65	295	2,25	81,27	0,79	0,61	32	3,55	3,10
Conn. Box	EN AW 6082 T654	240	1,65	295	2,25	3,44	41,28	37,11	11	12,22	10,92
Top conn. Box	EN AW 6082 T655	240	1,65	295	2,25	0,79	183,12	164,96	2	71,73	64,56
Shaft	AISI 316	290	1,65	550	2,25	18,22	8,65	12,42	10	16,58	23,44



Random and Quasi-static threaded fasteners force evaluation – X-excitation

Connected parts		First and second biggest force in the group	Random(3σ) + Preload			Quasi-Static + Preload		
Part 1	Part 2		F _x (N) (axial)	F _y (N) (lateral)	F _z (N) (lateral)	F _x (N) (axial)	F _y (N) (lateral)	F _z (N) (lateral)
Flange	Tube	F ₁	677	232	248	781	108	252
		F ₂	512	202	236	535	92	237
Flange	Motor bed	F ₁	78	158	94	83	48	223
		F ₂	65	75	67	80	31	78
Flange	Hinge	F ₁	142	90	37	129	37	88
		F ₂	129	77	27	127	28	76
Flange	Conn. Box	F ₁	37	17	28	46	16	22
		F ₂	35	11	24	42	10	18
Flange	Touch down	F ₁	94	143	111	62	71	76
		F ₂	90	141	107	61	70	67
Flange	Pin puller	F ₁	59	35	42	43	22	28
		F ₂	56	33	38	43	20	25
Motor bed	Motor	F ₁	64	29	49	48	27	24
		F ₂	30	20	31	31	19	23
Lid	Lid-arm	F ₁	91	89	66	87	85	61
		F ₂	91	89	65	87	83	60
Touch-screw	Lid	F ₁	201	96	172	129	67	119
		F ₂	200	92	172	128	66	117
Motor bed	Motor clamp	F ₁	57	113	35	59	155	9
		F ₂	31	36	6	48	43	3



Y-excitation

Connected parts		First and second biggest force in the group	Random(3σ) + Preload			Quasi-Static + Preload		
Part 1	Part 2		F _x (N) (axial)	F _y (N) (lateral)	F _z (N) (lateral)	F _x (N) (axial)	F _y (N) (lateral)	F _z (N) (lateral)
Flange	Tube	F ₁	506	183	217	524	367	273
		F ₂	439	171	211	462	303	256
Flange	Motor bed	F ₁	52	87	71	126	56	37
		F ₂	45	52	56	90	33	30
Flange	Hinge	F ₁	110	69	26	120	21	55
		F ₂	100	57	20	113	13	48
Flange	Conn. Box	F ₁	30	14	25	31	31	7
		F ₂	28	9	21	26	23	4
Flange	Touch down	F ₁	82	118	98	86	164	65
		F ₂	80	118	96	85	164	60
Flange	Pin puller	F ₁	5	5	26	25	25	6
		F ₂	5	4	24	25	24	6
Motor bed	Motor	F ₁	33	13	24	18	22	36
		F ₂	16	8	11	9	9	12
Lid	Lid-arm	F ₁	84	81	63	78	71	66
		F ₂	84	79	61	78	71	65
Touch-screw	Lid	F ₁	178	79	155	171	16	148
		F ₂	178	78	154	170	15	146
Motor bed	Motor clamp	F ₁	32	61	25	109	78	46
		F ₂	17	22	7	74	62	29



Z-excitation

Connected parts		First and second biggest force in the group	Random(3σ) + Preload			Quasi-Static + Preload		
Part 1	Part 2		F _x (N) (axial)	F _y (N) (lateral)	F _z (N) (lateral)	F _x (N) (axial)	F _y (N) (lateral)	F _z (N) (lateral)
Flange	Tube	F ₁	465	191	230	476	157	251
Flange	Motor bed	F ₂	434	190	224	404	152	217
Flange	Hinge	F ₁	51	62	76	69	104	36
Flange	Conn. Box	F ₂	48	45	52	58	43	31
Flange	Touch down	F ₁	101	59	45	104	51	53
Flange	Pin puller	F ₂	92	47	39	65	12	45
Flange	Motor	F ₁	15	7	17	24	31	2
Flange	Lid-arm	F ₂	14	5	14	20	14	2
Flange	Lid	F ₁	102	122	115	113	113	108
Flange	Touch-screw	F ₂	100	120	114	100	81	67
Flange	Motor clamp	F ₁	27	6	31	46	38	5
Flange	Motor bed	F ₂	27	6	28	46	36	5
Lid	Motor bed	F ₁	32	17	33	74	14	38
Lid	Motor bed	F ₂	14	11	19	28	5	5
Lid	Motor bed	F ₁	83	85	70	81	78	66
Lid	Motor bed	F ₂	83	84	69	77	70	53
Touch-screw	Lid	F ₁	174	81	187	178	73	207
Touch-screw	Lid	F ₂	173	79	187	157	41	89
Motor bed	Motor clamp	F ₁	29	54	26	25	26	39
Motor bed	Motor clamp	F ₂	14	20	10	21	6	17



Appendix F – Threaded fasteners MoS

Threaded fasteners MoS – Random – X-excitation

Connected Parts		TIGHTENING			TENSILE FAILURE			GAPPING		SLIPPING		THREAD PULL-OUT	
Part1	Part2	MoS(ti, y)	MoS(ti, ult)	MoS(tot, y)	MoS(tot, ult)	MoS(tot, y, wc)	MoS(tot, ult, wc)	MoS(sep)	MoS(sep, wc)	MoS(slip)	MoS(slip, wc)	MoS(th, tot)	MoS(th, tot, wc)
Flange	Tube	0,071	1,516	0,585	2,588	0,641	2,856	1,619	1,827	0,219	0,208	14,404	16,544
Flange	Motor bed	0,032	1,425	0,462	2,419	0,468	2,447	8,623	9,239	0,566	0,626	28,220	28,691
Flange	Hinge	0,076	1,527	0,698	2,918	0,715	3,028	11,051	10,603	1,560	1,471	10,571	11,198
Flange	Conn. Box	0,035	1,430	0,453	2,384	0,456	2,421	34,610	29,371	3,385	2,961	28,080	28,694
Flange	Touch down	0,036	1,433	0,682	2,933	0,678	2,942	6,047	3,861	0,482	0,257	18,237	18,324
Flange	Pin puller	0,038	1,439	0,877	3,395	0,881	3,418	10,668	10,130	1,847	1,717	24,580	24,839
Motor bed	Motor	0,112	1,613	0,911	3,433	0,930	3,534	3,315	3,584	0,467	0,453	33,280	34,805
Lid	Lid-arm	0,033	1,427	0,696	2,951	0,705	3,004	6,741	6,741	0,782	0,753	11,958	12,298
Lid	Touch screw	4,482	4,831	8,340	8,924	8,334	8,928	4,181	2,620	0,676	0,323	26,642	26,668
Motor bed	Motor clamp	0,102	1,590	0,854	3,326	0,857	3,361	10,510	8,510	0,706	0,639	13,958	14,198



Random – Y-excitation

Connected Parts		TIGHTENING		TENSILE FAILURE				GAPPING		SLIPPING		THREAD PULL-OUT	
Part1	Part2	MoS(ti, y)	MoS(ti, ult)	MoS(tot, y)	MoS(tot, ult)	MoS(tot, y, wc)	MoS(tot, ult, wc)	MoS(sep)	MoS(sep, wc)	MoS(slip)	MoS(slip, wc)	MoS(th, tot)	MoS(th, tot, wc)
Flange	Tube	0,071	1,516	0,628	2,717	0,671	2,924	2,167	2,410	0,348	0,348	15,400	17,136
Flange	Motor bed	0,032	1,425	0,468	2,439	0,472	2,457	12,935	13,783	0,961	1,044	28,545	28,862
Flange	Hinge	0,076	1,527	0,716	2,976	0,730	3,064	14,265	13,685	2,112	2,019	10,898	11,406
Flange	Conn. Box	0,035	1,430	0,459	2,404	0,462	2,434	42,685	36,380	3,898	3,433	28,413	28,924
Flange	Touch down	0,036	1,433	0,685	2,942	0,681	2,950	6,932	4,386	0,581	0,315	18,322	18,393
Flange	Pin puller	0,038	1,439	0,893	3,445	0,893	3,447	125,884	118,016	4,118	3,932	25,158	25,180
Motor bed	Motor	0,112	1,613	0,943	3,533	0,953	3,587	6,430	6,919	1,142	1,193	34,800	35,636
Lid	Lid-arm	0,033	1,427	0,698	2,960	0,707	3,009	7,303	7,303	0,854	0,829	12,016	12,332
Lid	Touch screw	4,482	4,831	8,344	8,928	8,338	8,933	4,722	2,951	0,786	0,391	26,668	26,691
Motor bed	Motor clamp	0,102	1,590	0,870	3,375	0,871	3,396	18,722	15,283	1,320	1,189	14,295	14,437



Random – Z-excitation

Connected Parts		TIGHTENING		TENSILE FAILURE				GAPPING		SLIPPING		THREAD PULL-OUT	
Part1	Part2	MoS(ti, y)	MoS(ti, ult)	MoS(tot, y)	MoS(tot, ult)	MoS(tot, y, wc)	MoS(tot, ult, wc)	MoS(sep)	MoS(sep, wc)	MoS(slip)	MoS(slip, wc)	MoS(th, tot)	MoS(th, tot, wc)
Flange	Tube	0,071	1,516	0,639	2,749	0,678	2,940	2,358	2,600	0,350	0,351	15,658	17,277
Flange	Motor bed	0,032	1,425	0,469	2,439	0,472	2,457	13,188	13,874	1,102	1,192	28,557	28,864
Flange	Hinge	0,076	1,527	0,722	2,993	0,734	3,074	15,537	14,897	2,114	2,023	10,994	11,466
Flange	Conn. Box	0,035	1,430	0,473	2,448	0,474	2,463	85,371	72,759	6,170	5,452	29,153	29,419
Flange	Touch down	0,036	1,433	0,681	2,928	0,676	2,936	5,572	3,517	0,513	0,266	18,181	18,267
Flange	Pin puller	0,038	1,439	0,887	3,424	0,888	3,435	23,312	21,855	3,349	3,173	24,919	25,038
Motor bed	Motor	0,112	1,613	0,944	3,537	0,954	3,590	6,631	7,234	0,844	0,862	34,851	35,676
Lid	Lid-arm	0,033	1,427	0,699	2,961	0,707	3,010	7,391	7,391	0,797	0,772	12,024	12,337
Lid	Touch screw	4,482	4,831	8,344	8,929	8,339	8,933	4,830	3,028	0,674	0,338	26,673	26,695
Motor bed	Motor clamp	0,102	1,590	0,872	3,381	0,874	3,401	20,658	17,416	1,459	1,298	14,337	14,475



Quasi-static – X-excitation

Connected Parts		TIGHTENING		TENSILE FAILURE			GAPPING		SLIPPING		THREAD PULL-OUT		
Part1	Part2	MoS(ti, y)	MoS(ti, ult)	MoS(tot, y)	MoS(tot, ult)	MoS(tot, y, wc)	MoS(tot, ult, wc)	MoS(sep)	MoS(sep, wc)	MoS(slip)	MoS(slip, wc)	MoS(th, tot)	MoS(th, tot, wc)
Flange	Tube	0,071	1,516	0,561	2,515	0,625	2,816	1,404	1,598	0,217	0,196	13,856	16,213
Flange	Motor bed	0,032	1,425	0,461	2,416	0,466	2,444	8,104	8,492	0,453	0,515	28,159	28,646
Flange	Hinge	0,076	1,527	0,705	2,941	0,720	3,040	12,164	11,448	1,607	1,512	10,701	11,265
Flange	Conn. Box	0,035	1,430	0,445	2,359	0,450	2,405	27,838	23,891	4,037	3,580	27,663	28,424
Flange	Touch down	0,036	1,433	0,690	2,957	0,687	2,962	9,168	5,776	0,886	0,516	18,465	18,518
Flange	Pin puller	0,038	1,439	0,882	3,410	0,884	3,426	14,638	13,723	2,902	2,733	24,749	24,936
Motor bed	Motor	0,112	1,613	0,927	3,484	0,940	3,557	4,421	4,547	0,802	0,744	34,048	35,166
Lid	Lid-arm	0,033	1,427	0,697	2,956	0,706	3,007	7,051	7,051	0,834	0,807	11,991	12,318
Lid	Touch screw	4,482	4,831	8,350	8,938	8,347	8,942	6,515	4,088	1,058	0,573	26,724	26,741
Motor bed	Motor clamp	0,102	1,590	0,853	3,322	0,849	3,344	10,154	6,999	0,536	0,482	13,932	14,084



Quasi-static – Y-excitation

Connected Parts		TIGHTENING		TENSILE FAILURE			GAPPING		SLIPPING		THREAD PULL-OUT		
Part1	Part2	MoS(ti, y)	MoS(ti, ult)	MoS(tot, y)	MoS(tot, ult)	MoS(tot, y, wc)	MoS(tot, ult, wc)	MoS(sep)	MoS(sep, wc)	MoS(slip)	MoS(slip, wc)	MoS(th, tot)	MoS(th, tot, wc)
Flange	Tube	0,071	1,516	0,624	2,703	0,667	2,916	2,092	2,323	0,210	0,211	15,289	17,064
Flange	Motor bed	0,032	1,425	0,451	2,384	0,460	2,430	5,338	5,838	1,444	1,549	27,640	28,394
Flange	Hinge	0,076	1,527	0,710	2,958	0,725	3,051	13,077	12,441	2,624	2,483	10,794	11,334
Flange	Conn. Box	0,035	1,430	0,458	2,401	0,462	2,434	41,308	36,380	3,511	3,166	28,365	28,924
Flange	Touch down	0,036	1,433	0,684	2,939	0,680	2,947	6,609	4,155	0,382	0,295	18,294	18,365
Flange	Pin puller	0,038	1,439	0,887	3,426	0,888	3,436	25,177	23,603	4,125	3,858	24,941	25,051
Motor bed	Motor	0,112	1,613	0,958	3,584	0,964	3,613	11,788	12,630	0,792	0,873	35,584	36,054
Lid	Lid-arm	0,033	1,427	0,701	2,968	0,709	3,013	7,865	7,865	0,913	0,885	12,065	12,361
Lid	Touch screw	4,482	4,831	8,345	8,930	8,340	8,934	4,915	3,081	0,926	0,469	26,676	26,698
Motor bed	Motor clamp	0,102	1,590	0,823	3,226	0,822	3,279	5,496	4,092	0,841	0,517	13,303	13,645



Quasi-static – Z-excitation

Connected Parts		TIGHTENING		TENSILE FAILURE				GAPPING		SLIPPING		THREAD PULL-OUT	
Part1	Part2	MoS(ti, y)	MoS(ti, ult)	MoS(tot, y)	MoS(tot, ult)	MoS(tot, y, wc)	MoS(tot, ult, wc)	MoS(sep)	MoS(sep, wc)	MoS(slip)	MoS(slip, wc)	MoS(th, tot)	MoS(th, tot, wc)
Flange	Tube	0,071	1,516	0,636	2,740	0,676	2,938	2,303	2,568	0,348	0,355	15,588	17,254
Flange	Motor bed	0,032	1,425	0,464	2,426	0,469	2,451	9,748	10,431	0,958	1,074	28,332	28,750
Flange	Hinge	0,076	1,527	0,720	2,987	0,737	3,079	15,088	15,609	2,127	2,158	10,962	11,497
Flange	Conn. Box	0,035	1,430	0,465	2,421	0,468	2,447	53,357	47,079	3,618	3,646	28,705	29,147
Flange	Touch down	0,036	1,433	0,678	2,920	0,674	2,933	5,030	3,336	0,540	0,331	18,104	18,232
Flange	Pin puller	0,038	1,439	0,881	3,407	0,884	3,424	13,683	12,828	2,685	2,493	24,717	24,917
Motor bed	Motor	0,112	1,613	0,900	3,401	0,924	3,520	2,867	3,183	0,620	0,692	32,817	34,594
Lid	Lid-arm	0,033	1,427	0,700	2,964	0,708	3,012	7,574	7,649	0,862	0,859	12,040	12,350
Lid	Touch screw	4,482	4,831	8,344	8,928	8,340	8,934	4,722	3,136	0,625	0,441	26,668	26,701
Motor bed	Motor clamp	0,102	1,590	0,874	3,389	0,873	3,398	23,964	16,280	1,878	1,638	14,392	14,456